INFORMATION TO USERS

This manuscript has been reproduced from the microfilm master. UMI films the text directly from the original or copy submitted. Thus, some thesis and dissertation copies are in typewriter face, while others may be from any type of computer printer.

The quality of this reproduction is dependent upon the quality of the copy submitted. Broken or indistinct print, colored or poor quality illustrations and photographs, print bleedthrough, substandard margins, and improper alignment can adversely affect reproduction.

In the unlikely event that the author did not send UMI a complete manuscript and there are missing pages, these will be noted. Also, if unauthorized copyright material had to be removed, a note will indicate the deletion.

Oversize materials (e.g., maps, drawings, charts) are reproduced by sectioning the original, beginning at the upper left-hand corner and continuing from left to right in equal sections with small overlaps.

Photographs included in the original manuscript have been reproduced xerographically in this copy. Higher quality 6" x 9" black and white photographic prints are available for any photographs or illustrations appearing in this copy for an additional charge. Contact UMI directly to order.

ProQuest Information and Learning
300 North Zeeb Road, Ann Arbor, MI 48106-1346 USA
800-521-0600

Characterization of marine boundary layer aerosol from North Atlantic and European Sources: Physical and chemical properties and climate forcing parameters

Ulrike Dusek

A dissertation submitted in partial fulfillment of
the requirements for the degree of

Doctor of Philosophy

University of Washington

2002

Program Authorized to Offer Degree: Atmospheric Sciences

UMI Number: 3053494

UMI Microform 3053494

ProQuest Information and Learning Company
300 North Zeeb Road
P.O. Box 1346
Ann Arbor, MI 48106-1346

In presenting this dissertation in partial fulfillment of the requirements for the Doctoral degree at the University of Washington, I agree that the Library shall make its copies freely available for inspection. I further agree that extensive copying of this dissertation is allowable only for scholarly purposes, consistent with "fair use" as prescribed in the U.S. Copyright Law. Requests for copying or reproduction of this dissertation may be referred to Bell and Howell Information and Learning, 300 North Zeeb Road, Ann Arbor, MI 48106-1346, to whom the author has granted "the right to reproduce and sell (a) copies of the manuscript in microform and/or (b) printed copies of the manuscript made from microform."

Signature Ulrike Diusr

Date 06/11/02

University of Washington

Graduate School

This is to certify that I have examined this copy of a doctoral dissertation by

Ulrike Dusek

and have found that it is complete and satisfactory in all respects,
and that any and all revisions required by the final
examining committee have been made.

Chair of Supervisory Committee:

David S. Covert

Reading Committee:

Marcia B. Baker

David S. Covert

Dean A. Hegg

Date: 06/11/02

University of Washington

Abstract

Characterization of marine boundary layer aerosol from North Atlantic and European Sources: Physical and chemical properties and climate forcing parameters

by Ulrike Dusek

Chair of Supervisory Committee:

Professor David S. Covert
Department of Atmospheric Sciences

This thesis focuses on aerosol properties measured in Southwestern Portugal during the second Aerosol Characterization Experiment. Fundamental aerosol physical properties such as particle size distribution and hygroscopic properties are related to possible sources and aerosol transformation processes. From these fundamental properties we derive aerosol properties that are important for aerosol forcing of climate. First, a new method for calculating CCN spectra is proposed in this work and tested using sensitivity studies and comparisons to direct measurements. The measured and calculated CCN spectra differ on average by 30%, which at small supersaturations is similar to the measurement uncertainties. Second, aerosol number to volume ratios (R) are calculated and the fact that values of R are relatively constrained is explained based on observed correlations between size distribution parameters. Third, a simple parameterization of the humidity dependence of the submicron aerosol scattering

coefficient has been derived, depending only on a volume weighted average diameter growth factor and the volume mean diameter of the dry size distribution. One set of empirical parameters can be used to parameterize all aerosol types characterized during the ACE-2 measurement period.

Aerosol physical properties and climate forcing parameters in the North-East Atlantic Ocean were clearly affected by pollution outbreaks from Europe. The submicron particle volume increased by a factor of 5 in polluted conditions, the light scattering coefficient of dry particles increased on average by a factor of up to 10. CCN concentrations at supersaturations of 0.2% increased by a factor of 3-5. The aerosol fundamental properties vary often strongly with air mass history, but also show short-term variability that often has a characteristic diurnal scale. The number concentration of fine particles below 50nm and the particle hygroscopic growth factors are mostly dominated by diurnal processes. The variability in the fine particle number concentration can explained by particle nucleation in the morning hours and subsequent particle growth to larger sizes. On the other hand the number concentration of particles in the accumulation mode size range is mostly determined by long range transport.

TABLE OF CONTENTS

LIST OF FIGURES

LIST OF TABLES

ACKNOWLEDGMENTS

I thank my advisor, David Covert, for the guidance, encouragement and support he provided during the work on this project. I am glad I had the opportunity to work with him and benefit from his many insights and original viewpoints.

I also thank my supervisory committee, Marcia Baker, Dean Hegg, and Bob Charlson for interesting discussions and for valuable comments on the dissertation.

I thank my parents and my sisters for being such a wonderful family and for continually encouraging and supporting me in whatever I try to achieve.

And finally I thank all my friends in Seattle who made the five years I spent here a very happy time, especially Darby McDonald, Yaga Bares, and Gretchen Mullendore.

Chapter 1

INTRODUCTION

1.1 Background

1.1.1 Climate forcing of atmospheric aerosols

Aerosols from anthropogenic emissions can disturb the natural radiative balance of the planet and exert a forcing on the climate system (e.g. Charlson et al., 1991; Twomey, 1991). Assessing the impact of aerosols on the climate is complicated because of several issues. First, the residence time of aerosol particles in the troposphere is relatively short: a few hours to a few days depending on their size and chemical composition. As a consequence, aerosols are non uniformly distributed around the globe and their concentration in the atmosphere shows considerable temporal variation. Second, atmospheric aerosols consist of many chemical compounds such as inorganic salts, organic carbon, black carbon and mineral dust. The source locations and source strengths of these aerosol compounds are often poorly known and their abundance varies with geographical location and season. Third, at any given location and time, the physical and chemical properties of the aerosol population are the result of complex processes, which are not yet fully understood. Thus a lot of controlling parameters concerning the impact of aerosols on climate are uncertain or unknown.

Atmospheric aerosols have a so-called direct and indirect effect on the global radiation balance (e.g. Haywood and Boucher, 2000): Directly, aerosol particles impose a

radiative forcing on the climate system by scattering and absorbing radiation in the atmosphere. Indirectly, aerosol particles may modify the cloud radiative forcing by influencing the cloud albedo (first indirect effect) and the global cloud cover (second indirect effect). More recently a 'semi-direct' effect of aerosols on climate has been proposed (Ackermann et al., 2000). This refers to a possible reduction of cloudiness due to atmospheric heating by absorbing aerosol.

The direct aerosol forcing of climate is largely due to the scattering and absorption of solar radiation by aerosol particles. By scattering solar radiation upwards, back to space, aerosols increase the planetary albedo and thus exert a negative forcing on the earth-atmosphere system. By absorbing solar radiation, aerosols increase the overall absorption of the earth-atmosphere system, which results in a positive forcing. The sign and the magnitude of the total forcing are determined by the combined effect of those two opposing forcings. In principle the total direct forcing could be either positive or negative depending on the scattering and absorption characteristics of the aerosol.

The amount of upward scattered and absorbed solar radiation depends on the total optical depth, the upscatter fraction and the single scattering albedo (e.g. Lacis and Mishchenko, 1995). The optical depth is a measure of how much radiation is removed from the original beam in the aerosol layer either by scattering or by absorption. The upscatter fraction is a measure of how much of the total scattered light that is actually scattered upwards back to space and thus contributes to the radiative forcing. The single scattering albedo ω is a measure of the relative importance of light scattering and light absorption. It is defined as the fraction of the total extinct light that was removed from the original beam by means of scattering. $\omega = 1$ indicates purely scattering aerosol (such as sulfates, or sea salt) and $\omega = 0$ indicates the hypothetical case of a purely absorbing aerosol. The single scattering

albedo ω is particularly important because it indicates whether a partially absorbing aerosol will have a cooling or a warming effect on the atmosphere. Haywood and Shine (1995) proposed that there is a critical (spectrally weighted) single scattering albedo ω_c, that separates negative from positive forcing. ω_c is a strong function of the albedo of the underlying surface. Above a strongly absorbing surface such as the ocean the aerosol itself has to be strongly absorbing ($\omega \sim 0.5$) to have a warming effect. Above a highly reflecting surface such as snow or ice even a slightly absorbing aerosol ($\omega \sim 0.97$) will yield a positive forcing. Thus purely scattering aerosols always exert a negative forcing on the climate. The presence of absorbing aerosols results in a positive forcing, which reduces the cooling effect of the purely scattering aerosols. The combined forcing can be either positive or negative depending on the relative amount of absorbing and non-absorbing compounds in the aerosol.

The direct forcing does not necessarily increase linearly with the amount of aerosol present in the atmosphere. This is because the total optical depth δ, the upscatter fraction and the single scattering albedo ω each depend in a complicated way on the aerosol size distribution and the particle refractive index. Particles with diameters comparable to the wavelength of the incident solar radiation contribute most significantly to the direct forcing. Particles that are much smaller scatter very little light and thus have a negligible optical depth. Particles that are much larger are more efficient scatterers but they scatter mostly in the forward direction, and are thus not very efficient in redirecting light back to space. The real part of the refractive index influences the amount and the angular distribution of the light scattered for a given particle size and thus effects both the optical depth and the backscatter fraction. The imaginary part of the refractive index is a measure of light absorption and the single scattering albedo decreases with increasing imaginary part of the refractive index. Thus information on the size distribution and refractive index of the aerosol

are necessary to estimate its direct radiative forcing.

Quantitative estimates of the magnitude of the direct forcing of aerosols are still very uncertain and even the sign of the forcing is not yet clear. Current estimates of the direct forcing of sulfate aerosols range from $-0.3Wm^{-2}$ to $-1Wm^{-2}$ (e.g. Charlson et al., 1991, 1992; Kiehl and Briegleb, 1993; Boucher and Anderson, 1995). Due to the lack of a global coverage of aerosol measurements assumptions must be made about aerosol properties and their global distribution. Differences in those assumptions are mostly responsible for the differences in various estimates. Other anthropogenic species have been studied less, but seem to be equally important for the radiative forcing: Penner et al. (1992); Penner (1995) estimate that the radiative forcing of organic carbon aerosols from biomass burning roughly doubles the sulfate forcing. Tegen et al. (1996) claim that dust aerosols from disturbed soils contribute significantly to the atmospheric heating. The positive forcing of black carbon aerosols amounts to $+0.4\,Wm^{-2}$ with uncertainty of a factor of 3 according to a recent estimate of Haywood and Ramaswany (1998). Most of this uncertainty is due to the poor knowledge of the source strengths and the total burden of black carbon aerosols. At present it is not certain, whether the cooling of the climate due to sulfate and organic aerosols is offset by the warming due to black carbon aerosols (e.g. Hansen et al., 1998).

The indirect effect of aerosols on climate refers to a possible increase in cloud albedo and cloud cover caused by an anthropogenic increase in aerosol number concentrations (e.g. Charlson et al., 1992; Twomey et al., 1987). Cloud droplets form by condensation of water vapor on a subset of preexisting aerosol particles. Cloud condensation nuclei (CCN) are defined as the subset of aerosol particles that are activated to form cloud droplets at supersaturations typical for ambient stratus clouds. An increase in the number concentration of CCN can results in clouds with more, but

smaller droplets and therefore higher albedo (Twomey, 1991). The shift to smaller droplet sizes is moreover likely to suppress drizzle development (Twomey, 1991; Baker and Charlson, 1990) and thus extends cloud lifetime and consequently cloud cover Both effects, the increase in cloud albedo and the increase in global cloud cover, cause an increase in the solar radiation reflected to space. The indirect effect of aerosols on climate could thus lead to a negative forcing of a magnitude comparable to the positive forcing of greenhouse gases, but the uncertainties are still too high to attempt a meaningful quantification.

Aerosol and cloud measurements in ship tracks have provided empirical evidence for the indirect effect. The clouds that form in the narrow lines of polluted air behind ships appear distinctly brighter in satellite images (Coakley et al., 1987). Aerosol measurements in the ship tracks show significantly increased aerosol number concentrations due to emissions from the ship. Simultaneous cloud microphysical measurements find elevated cloud droplet concentrations and a decrease in the mean droplet size (e.g. Ferek et al., 1998). This evidence supports the theory that elevated aerosol concentrations could be responsible for an increase in cloud albedo in certain cloud types and air masses.

1.1.2 The importance of aerosol hygroscopic properties for the aerosol forcing of climate

It has long been known that aerosol particles contain a large fraction of inorganic salts that are hygroscopic in nature. At elevated relative humidities below 100% these salts can absorb water vapor and form stable solution droplets. The resulting increase in particle size or particle mass from dry to hydrated state is called hygroscopic growth. The hygroscopic growth due to inorganic salts has been well documented and investigated in theoretical and experimental studies (e.g. Tang and Munkelwitz, 1994).

Recently empirical evidence has been published that soluble organic compounds can modify the hygroscopic growth of atmospheric aerosols (e.g. Saxena et al., 1995; Dick et al., 2000). This effect of organics is much less understood. The following chapter explains the importance of particle hygroscopic properties for both the direct and the indirect effect of aerosols on climate.

Hygroscopic growth and the direct effect

Due to the hygroscopicity of the aerosol particles the size distribution of the atmospheric aerosol is dependent on the ambient r.h.. Therefore the local radiative forcing changes strongly with r.h. which varies with air mass, time of the day and height. Sensitivity studies of the direct radiative forcing show that 'the single most influential parameter in determining the direct radiative forcing is relative humidity ...' (Pilinis et al., 1995).

The direct aerosol forcing generally increases in magnitude with relative humidity for the following reason. The water uptake associated with hygroscopic growth causes the aerosol particle size to increase nonlinearly with r.h.. The aerosol scattering increases due to an increase in particle surface area. Moreover particles that were too small to contribute significantly to the light scattering in their dry state can grow to sizes where they scatter more efficiently (roughly diameters 0.4-3 μm). Because these small particles are much more abundant than the larger ones, the scattering of the aerosol can increase drastically with r.h.. Current estimates suggest that the forcing can increase by a factor between 1.4 (Boucher and Anderson, 1995) and 2.1 (Pilinis et al., 1995), if the r.h. rises from 40% to 80%. The particle refractive index generally decreases with increasing r.h., which causes a small decrease in the direct aerosol forcing, but this effect is secondary to the increased forcing due to the particle size change.

It has also been noted that the effects of changing humidity on the direct forcing are strongly nonlinear (Haywood and Shine, 1997). The direct forcing is nearly insensitive to relative humidities below 70% but increases strongly between 70% and 80% and even more above 80%. This nonlinear dependence of the forcing on r.h. has important consequences for calculations of the direct forcing in GCMs. For example it seems to be important to calculate the aerosol scattering using the local r.h. instead of a globally averaged r.h. as it was done in early estimates of the direct forcing (e.g. Charlson et al., 1991). Taylor and Penner (1994) report that the global mean forcing decreases from -0.95Wm^{-2} to $-0.6Wm^{-2}$, when the aerosol scattering is calculated using the local relative humidity, instead of using a mean r.h. of 80%. Haywood and Shine (1995) state that taking into account the subgridscale variation of the relative humidity could increase the global mean forcing of sulfate aerosols by a factor of 1.5. This sensitivity of the direct forcing to r.h. shows the importance of a thorough understanding of the hygroscopic growth of aerosol particles and of the humidity dependence of aerosol optical properties and the location of aerosol with respect to r.h. grid variability.

Particle hygroscopic properties and the indirect effect

It has long been known that an increasing fraction of hygroscopic compounds in an aerosol particle reduces the critical supersaturation (S_c) required for activation and subsequent growth as a cloud droplet. (S_c) can be derived from the Koehler equation (e.g. Pruppbacher and Klett, 1997) and is to a good approximation only dependent on the number of ions (N_i) in the particle: $S_c = (2.7 \cdot 10^{-5}/N_i)^{0.5}$ (Hudson and Clarke, 1992). This equation shows that an increasing number of ions (i. e. an increasing hygroscopic fraction) in the particle lowers its critical supersaturation and increases its likelihood of becoming a cloud droplet. The fraction of hygroscopic material in

an aerosol particle is thus important for its ability to form clouds and thus for the indirect effect.

It has been realized that the simple dependence of S_c on N_i might be complicated by the presence of soluble organic compounds or surfactants. Surfactants can lower the critical supersaturation, thus enhancing the cloud droplet concentration (Facchini et al., 1999a). Some slightly soluble organic compounds can even modify the shape of the Koehler curve, so that clouds and fog might be possible without supersaturation (Laaksonen et al., 1998; Shulman et al., 1996; Kulmala et al., 1997). This effect of organics on the Koehler curve has not yet been experimentally verified, but there is increasing empirical evidence, that organic aerosols significantly contribute to the CCN concentrations (e.g. Novakov and Penner, 1993; Novakov and Corrigan, 1996). These studies suggest that the understanding of cloud droplet formation requires not only the knowledge of the hygroscopic properties related to the inorganic fraction of the aerosol, but also insight on how these hygroscopic properties are modified by organic compounds.

1.1.3 Modeling issues

The direct aerosol forcing can, at least in principle, be calculated at any given location if the ambient size distribution, ambient optical properties and the state of mixing of the aerosol are known. However these crucial parameters cannot yet be adequately measured on a regional to global scale or be predicted from global transport models. Due to computational limitations, most of these models and do not treat to treat the aerosol hygroscopic properties as prognostic variables. In these cases the output of the model is limited to the dry aerosol mass concentration and some parameterization of the dry size distribution and to the relative humidity at each grid point. In order to obtain the ambient forcing it is therefore necessary to develop empirical pa-

rameterizations of the hygroscopic growth and of the humidity dependence of aerosol radiative properties based on measurements from key locations on the globe.

1.2 The ACE-2 field experiment

The aerosol measurements used in this thesis were made as a part of the second Aerosol Characterization Experiment (ACE-2) (Raes et al., 2000; Verver et al., 2000). ACE-2 was one of several large-scale aerosol characterization experiments designed to understand aerosol radiative forcing in key areas of the globe. The first experiment (ACE-1) was held in the southwest Pacific ocean to characterize the natural background aerosol in a region, that is rarely influenced by anthropogenic emissions (Bates et al., 1998). ACE-2 was held in the more polluted sub-tropical North Atlantic region during June and July 1997.

The general ACE-2 measurement area is shown in Figure 1.1. In this area marine background air mass is frequently disturbed by pollution outbreaks from the European continent, which happen when the Azores high extends over western Europe after the passage of mid-latitude cyclone. One main goal of the ACE-2 experiment was to characterize how the European pollution outbreaks change the physical properties of the background aerosol and as a consequence the direct and indirect aerosol forcing in North Eastern Atlantic. Another goal was to investigate how the continental pollution aerosol is modified during its transport from the European continent into the ACE-2 measurement area. During the ACE-2 intensive measurement phase from June 16 to July 25 1997 aerosol properties were measured on several field stations on land as well as on board of ships and several airplanes. The main land-based stations were on the island Tenerife (Spain) and in Sagres, situated on the south-west tip of Portugal as shown in Figure ??.

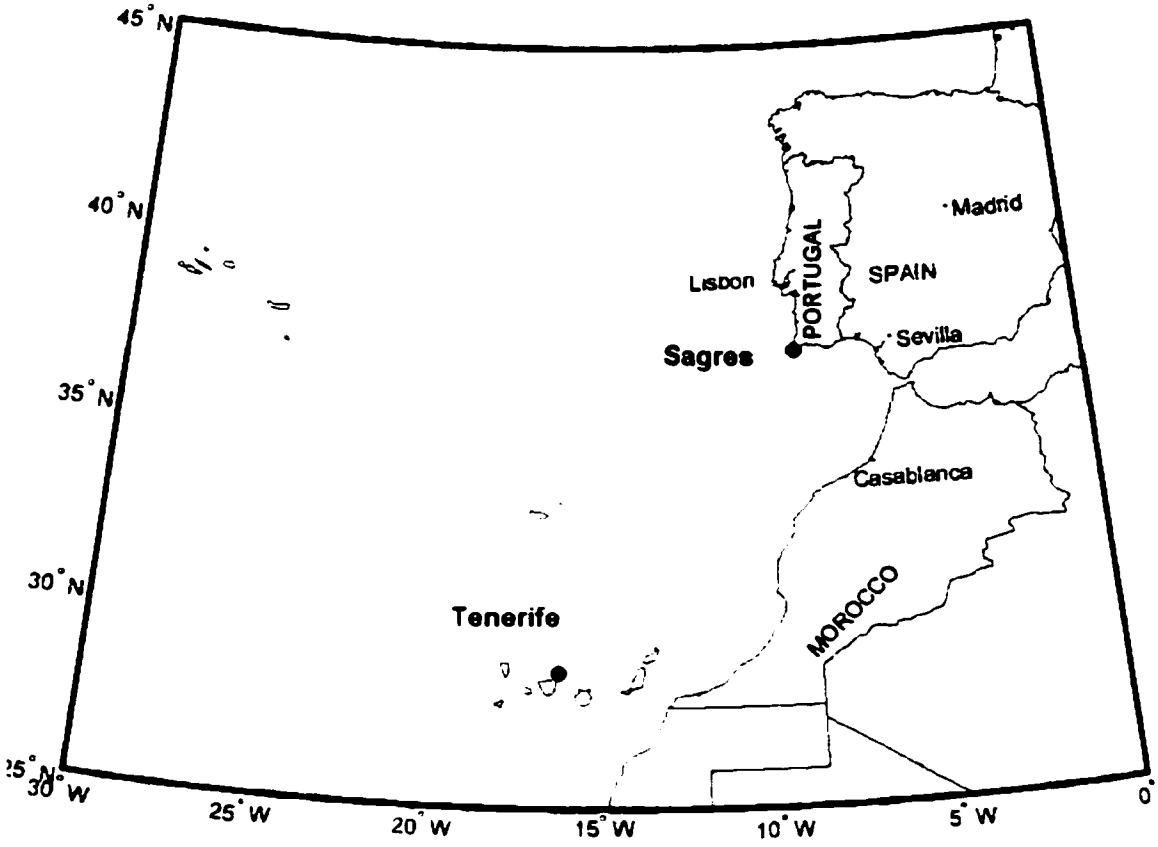

Figure 1.1: The ACE-2 measurement area

1.3 Thesis goals and methods

Most of the work presented in this thesis is based on measurements of the aerosol size distribution and hygroscopic growth in Sagres. These aerosol properties are compared in different air mass conditions and subsequently used to derive aerosol properties more closely related to the direct and indirect effect of aerosols on climate.

A special focus of this thesis are aerosol hygroscopic properties and the influence of those hygroscopic properties on cloud condensation nuclei and aerosol scattering at different relative humidities.

In principle two basic approaches can be used to achieve information on aerosol properties that are important for the direct and indirect effect of aerosols on climate, such as concentration of cloud condensation nuclei or aerosol scattering efficiencies. The approach used in the context of this thesis is to measure fundamental aerosol properties such as the particle size distribution and chemical composition and calculate the properties relevant for the aerosol forcing of climate using current theoretical understanding of aerosol radiative and cloud nucleation properties. Another approach is to measure the radiative or cloud nucleation properties of the aerosol directly using instruments such as integrating nephelometers (e.g. Heintzenberg and Charlson, 1996) or cloud condensation nuclei counters. Both approaches have certain advantages and disadvantages, since both aerosol measurement methods and theoretical understanding have still considerable uncertainties.

Aerosol measurements are in general quite difficult to make. Since it is inefficient to visually to count aerosol particles under a microscope, indirect methods have to be used to count and size the particles. Many of the more complex measurement methods have been recently developed and are still being improved. These measurement methods are more susceptible to errors and the measurement uncertainties under field conditions are often not well characterized. It can be an advantage to only use simple and established measurement methods and infer other aerosol properties using theoretical considerations. However, many simplifying assumptions have to be made to be able to treat the system of individual particles with different shapes and chemical compositions theoretically and there are still considerable gaps in our current understanding of the atmospheric aerosol. At the current stage of aerosol research

both measurement methods and the theoretical understanding can be advanced by rigorous comparisons of measured and derived aerosol properties. Therefore a significant part of this thesis is devoted to consistency studies between directly measured aerosol properties and the same aerosol properties derived from more fundamental measurements using current theory. These consistency studies allow to rigorously test the current understanding of the theory as well as to evaluate errors in current established or recently developed measurement methods.

Three major consistency studies are presented in this thesis. The first is a test if measured hygroscopic growth factors are consistent with particle chemical composition. This study is important since it shows if the particle hygroscopic growth can be predicted from the particle composition. Two previous hygroscopic consistency studies have shown that in the Po Valley (Italy) (Berg et al., 1998a) and in Northern England (Swietlicki et al., 1999) the measured aerosol hygroscopic growth is generally consistent with the water uptake from the inorganic fraction of the aerosol. The second consistency study is a comparison of directly measured CCN spectra with CCN spectra derived from hygroscopic growth factors and the particle size distribution. Several comparisons between measured and derived CCN concentrations have been attempted in different areas of the globe (e.g. Covert et al., 1998; Chuang et al., 2000, and references therein). In most of these studies the measured CCN concentrations are significantly lower than the calculated CCN concentrations. Low mass fractions of soluble material or the presence of organic compounds, that hinder or slow down the water uptake have often been hypothesized to explain these observations. Since many supporting observations are available in this work, these issues can be discussed in some detail. The third consistency study is a comparison of dry and humidified aerosol scattering coefficients measured by a nephelometer with calculated scattering coefficients. These calculated scattering coefficients are derived from size

distribution, hygroscopic growth factors and particle chemical composition. Integrating nephelometers have been evaluated, tested and calibrated in laboratory settings (e.g. Anderson et al., 1996) and under field conditions (e.g. Quinn and Coffmann, 1998). One previous consistency study of humidified scattering coefficients (Malm et al., 2000) has been able to model the measured increase in scattering with relative humidity relatively well.

A second important focus of this thesis is to characterize the aerosol properties in south-western Portugal during the ACE-2 measurement period. The characterization of the aerosol at a certain location is difficult to do in a meaningful way. The aerosol properties in a location like Sagres are dependent on the history of the air mass arriving at this location, alternating between relatively clean and polluted conditions. However even within each air mass type the aerosol properties show considerable variability that in some cases can be larger than the change in those aerosol properties with air mass types. The diurnal variability of particle concentrations in different size classes and the diurnal variability of hygroscopic growth factors are investigated as an example for these fluctuations on short time scales.

The more fundamental aerosol properties, namely particle size distributions and hygroscopic growth factors are summarized in Chapter 3. These aerosol properties are related to possible sources and processes that acted on the aerosol during transport to Sagres. Aerosol properties that are more directly related to the direct and indirect effect of aerosols on climate such as cloud condensation nuclei and scattering coefficients are derived in the following chapters based on the aerosol size distribution, hygroscopic growth and chemical composition.

A third focus of this thesis is to derive parameterizations of aerosol properties that cannot yet be treated as prognostic variables in global transport models, but are nevertheless needed to calculate the radiative forcing of aerosols. It is important to

find empirical formulas that depend on parameters predicted in those global transport models such as the total particle mass or volume and potentially a mean particle diameter. Such parameterizations are presented in the Chapter 4 that focuses on number to volume ratios of the aerosol and in Chapter 6, where a parameterization of the humidity dependence of the aerosol scattering coefficient is derived. Number to volume ratios over the Atlantic ocean have been measured in the past (e.g. Hegg and Jonsson, 2000; Hegg and Kaufman, 1998, and references therein) and have been found surprisingly constant. The number to volume ratios derived in this thesis are compared to numbers found by other authors and reasons for the constancy of the number to volume ratios are proposed based on theoretical considerations.

Chapter 2

INSTRUMENTATION AND DATA EVALUATION

The work presented in this thesis is mainly based on measurements of the aerosol number-size distribution and hygroscopic growth factors. This section gives detailed descriptions of the instruments used during ACE-2 to measure these aerosol properties and of the first steps of data correction and analysis.

Measurements of both the number size distribution and the hygroscopic growth factors require particle sizing. In both cases the same type of instrument namely the Differential Mobility Analyzer (DMA) was used to the determine particle size. This instrument is described in in section 2.1. The next two sections explain how the DMA is used to measure aerosol number-size distributions and hygroscopic growth factors.

2.1 The Differential Mobility Analyzer

The differential mobility analyzer determines particle size by subjecting charged particles to an electrostatic field and sorting them according to their terminal velocity which depends on their size. Generally aerosol particles have a variety of particle shapes and it is not trivial to assign a diameter to each particle. Commonly effective diameter are defined depending on the specific measurement method used to size the particles. In the case of electrostatic measurements the effective diameter is the so-called Stokes diameter defined as the diameter of a spherical particle with the same terminal velocity in the electromagnetic field. In the case of impactor measurements the effective diameter is the so-called aerodynamic diameter, the diameter of a spher-

ical particle of density of 1 g cm^{-3}, that has the same terminal settling velocity as the particle in question. Particles with the same Stokes and aerodynamic diameters can have quite different actual particle sizes, depending on the particle density.

A schematic design of the DMA is shown in Figure 2.1.

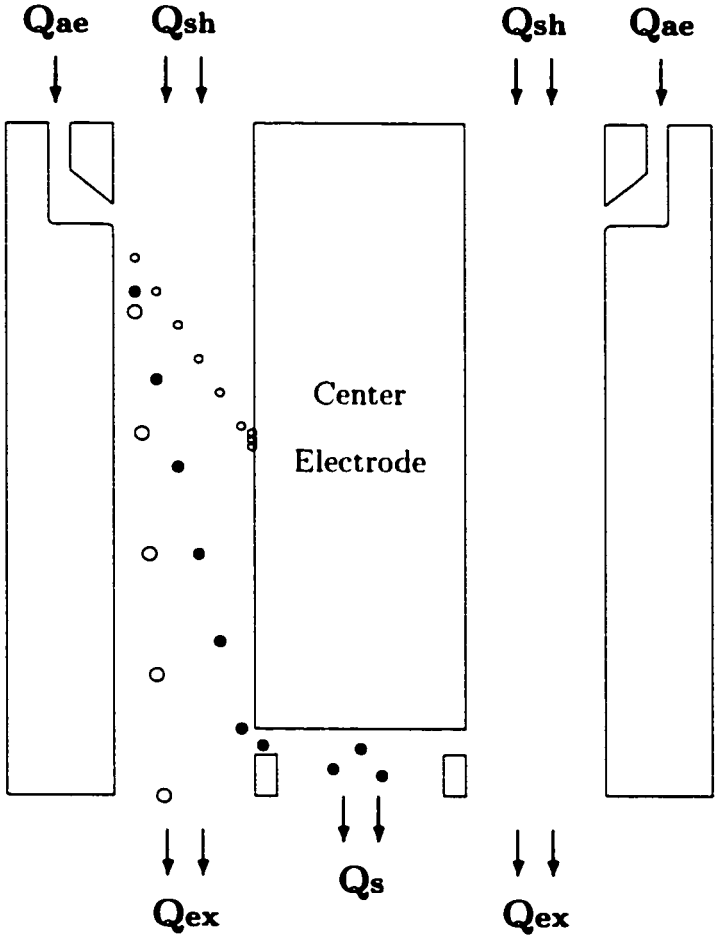

Figure 2.1: The differential Mobility Analyzer

The differential mobility analyzer has cylindrical shape and consists of a center electrode and an outer grounded cylinder. In the space between the cylinder and the center electrode a layer of particle free 'sheath' air (Q_{sh}) flows along the center

electrode. The air stream containing aerosol particles (Q_{ae}) is forced to flow in a thin, laminar layer along the outer cylinder walls. At the lower end of the instrument a small sample stream (Q_s) is withdrawn through a narrow opening in the bottom of the center rod. The excess air (Q_{ex}) exits through the bottom of the instrument. A voltage U is applied to the center electrode creating an electric field in the space between the center electrode and the outer cylinder.

As the charged particles enter the electric field a fraction with either positive or negative charge begins to drift towards the center electrode with a velocity that is proportional to their electrical mobility Z_p.

$$Z_p = \frac{n \cdot e \cdot C_c}{3\pi \cdot \eta \cdot d_p}. \tag{2.1}$$

where d_p is the particle diameter, n is the number of charges, e the elementary charge, η the air viscosity and C_c the Cunningham slip correction factor. The time to achieve terminal velocity must be much smaller than the transit time through the column. The drift velocity decreases with increasing particle size. For each voltage U applied to the center rod of the DMA only particles within a very narrow mobility fraction can exit through the opening into the sample air stream. Particles with higher mobility (smaller diameters) are deposited on the center rod walls upstream and particles with lower mobility (larger diameters) remain in the excess air stream.

Although the actual particle trajectories in the instrument are complicated, the probability of a particle entering the sample flow is independent of the detailed structure of the flow field (Knutson and Whitby, 1975). This probability is called the transfer function. If the aerosol flow Q_{ae} equals the sample flow Q_s and the sheath flow Q_{sh} equals the excess flow Q_{ex} then the transfer function is ideally triangular as shown in figure 2.2.

For a voltage U applied to the central electrode the fraction of selected particles

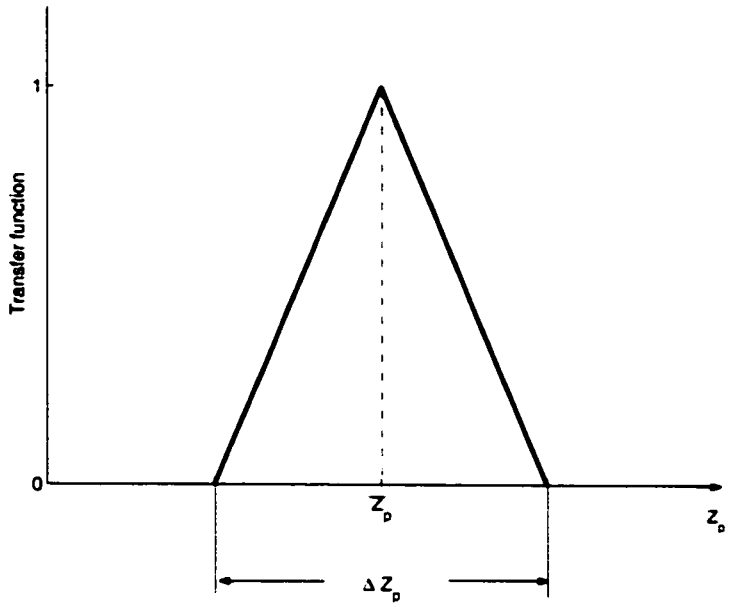

Figure 2.2: Schematic diagram of an idealized DMA transfer function

have a mean electrical mobility of

$$\bar{Z}_p = \frac{Q_{sh} \cdot ln(r_2/r_1)}{2\pi \cdot U \cdot L} \tag{2.2}$$

and span a range of mobilities of

$$\Delta Z_p = 2 \cdot \frac{Q_a}{Q_{sh}} \cdot Z_p. \tag{2.3}$$

In reality the width of the transfer function is somewhat broadened by diffusion and its area is decreased due to losses (e.g. Martinsson et al., 2001).

2.2 Measurement of the Number-Size Distribution

2.2.1 Measurement principle: The TDMPS system

The DMA combined with a bipolar charger and a particle counter can be used to infer the particle size distribution. The bipolar charger imposes a known charge distribution on the aerosol. The voltage on the center rod of the DMA is increased stepwise and particles that enter the sample flow at each voltage are counted by a condensational particle counter (CPC). An inversion program converts the measured voltage-number pairs to the actual size distribution using the known charge distribution of the aerosol and the known transfer function of the instrument.

Aerosol number-size distributions in Sagres during ACE-2 were measured using a Twin Differential Mobility Particle Sizer (TDMPS) (Birmili et al., 1999). Two Vienna type DMAs (Winklmayr et al., 1991) of different lengths, a DMA and an ultrafine DMA (UDMA), are used to measure aerosol particles from 20-800nm and from 3-20nm respectively. The instrument setup is schematically shown in figure 2.3.

Polydisperse aerosol enters the bipolar charger and the air stream is then split. A volume flow of 0.5l/min enters the DMA and a volume flow of 2l/min enters the UDMA. At the beginning of each size distribution measurement both DMAs select the common particle size of 20nm. Subsequently the voltage is decreased stepwise in the UDMA to reduce the size of particles in the sample stream and increased in the DMA to increase the particle size. At each voltage the particles are counted using a CPC and an ultrafine CPC respectively and the final number-size distributions are derived by the inversion routine of Stratmann and Wiedensohler (1996).

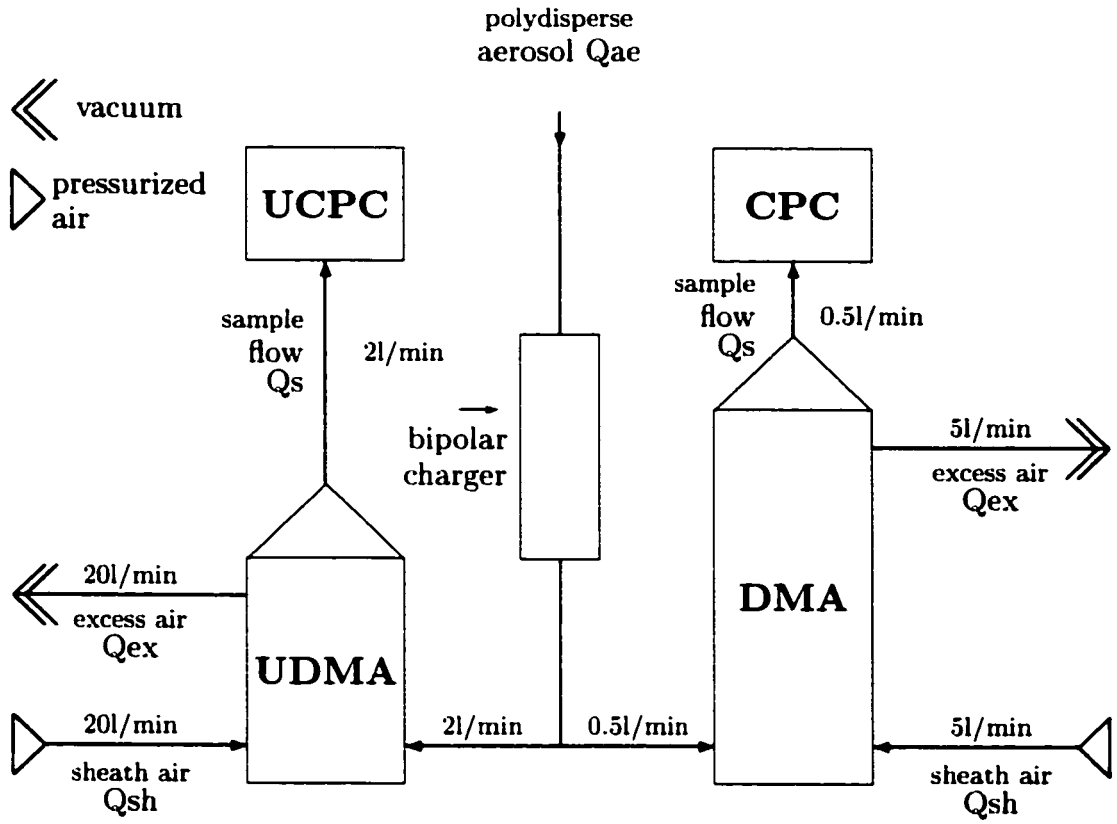

Figure 2.3: The TDMPS System

2.2.2 Parameterizing the number-size distribution using lognormal distributions

The size distributions measured in Sagres during ACE-2 can usually be well approximated using a linear combination of several lognormal distributions:

$$\frac{dN_{fit}}{d\log d_p} = \sum_{i=1}^{n} \frac{N_i}{\sqrt{2\pi}\cdot\log\sigma_{g,i}} \cdot \exp\left(-\frac{(\log d_p - \log d_{g,i})^2}{2\cdot\log^2\sigma_{g,i}}\right), \tag{2.4}$$

where N_i is the total number concentration in mode i, $\sigma_{g,i}$ its geometric standard deviation, and d_{gi} the mean geometric diameter. Size distributions are usually parameterized to reduce the number of parameters used to describe a size distribution.

However in this work some physical significance is attached to the individual lognormal modes fitted to the size distribution and the goodness of the fit is not always the only criterium in determining how the modes should be fitted to the size distribution.

The fitting is done using a labVIEW routine written by Birmili (1998), which minimizes the deviations between the measurement points $dN/dlog(d_p)$ and the fitted values $dN_{fit}/dlog(d_p)$ by adjusting the parameters N_i, $d_{g,i}$, and $\sigma_{g,i}$. In general more than one lognormal distribution is necessary to represent the measured distributions. Usually three lognormal modes are necessary to capture the dominant features of the size distribution, but sometimes up to five different modes can be clearly distinguished in the measured size distribution. These five modes are classified according to the size range in which their mean diameter occurs as shown in Table 2.1. The size ranges of the modes show enough independence that each mode can be identified separately.

Table 2.1: Classification of the main lognormal modes of the aerosol size distribution in Sagres during ACE-2

Mode	**Range of mean diameter d_g**
Ultra Fine	0 - 18 nm
Small Aitken	10 - 40 nm
Aitken	30 - 120 nm
Accumulation	80 - 250 nm
Sea salt	200 - 800 nm

The Aitken mode, the Accumulation mode and the Sea salt mode are the dominant and most persistent modes. The small Aitken and the Ultra fine mode are only intermittently present and are associated with regional and local particle production.

2.2.3 Quality control

Figure 2.4 shows an example of a size distribution when all five modes were present at the same time. The data points are marked with stars and the fits of the different

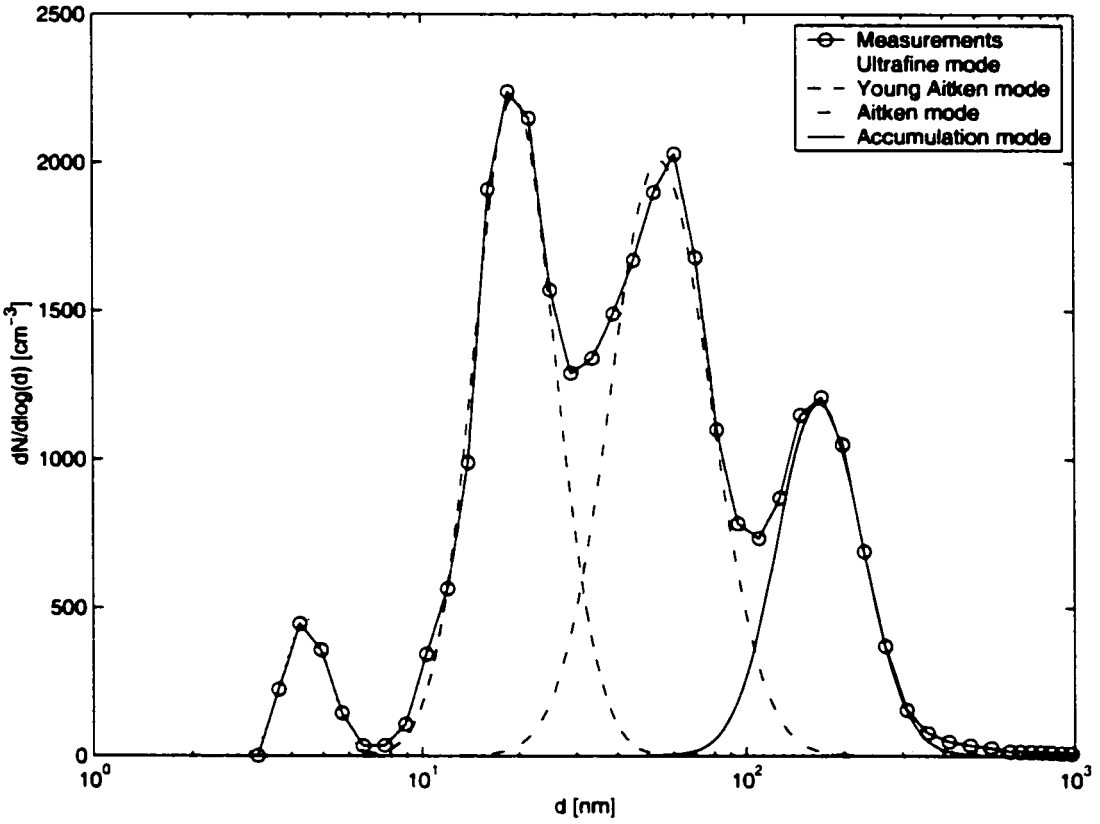

Figure 2.4: Example of a particle size distribution with five clearly separated modes

modes are shown as lines of various styles. In this example all the modes are clearly separated and show lognormal shape. If all the modes are clearly separated they are usually well captured by the fitting routine.

There are occasions however when some of the modes are not as clearly separated and one mode appears only as a shoulder on another mode. In this case the question

can be raised if there are really two overlapping lognormal modes or if there is only one mode that simply deviates from the lognormal shape. In this situation it is often helpful to look at the higher moments of the number-size distribution such as the surface or the volume size distribution. If any mode is lognormal in the number-size distribution it will also be lognormal in the higher moments of the size distribution. Figure 2.5(a) shows one example of a questionable number-size distribution.

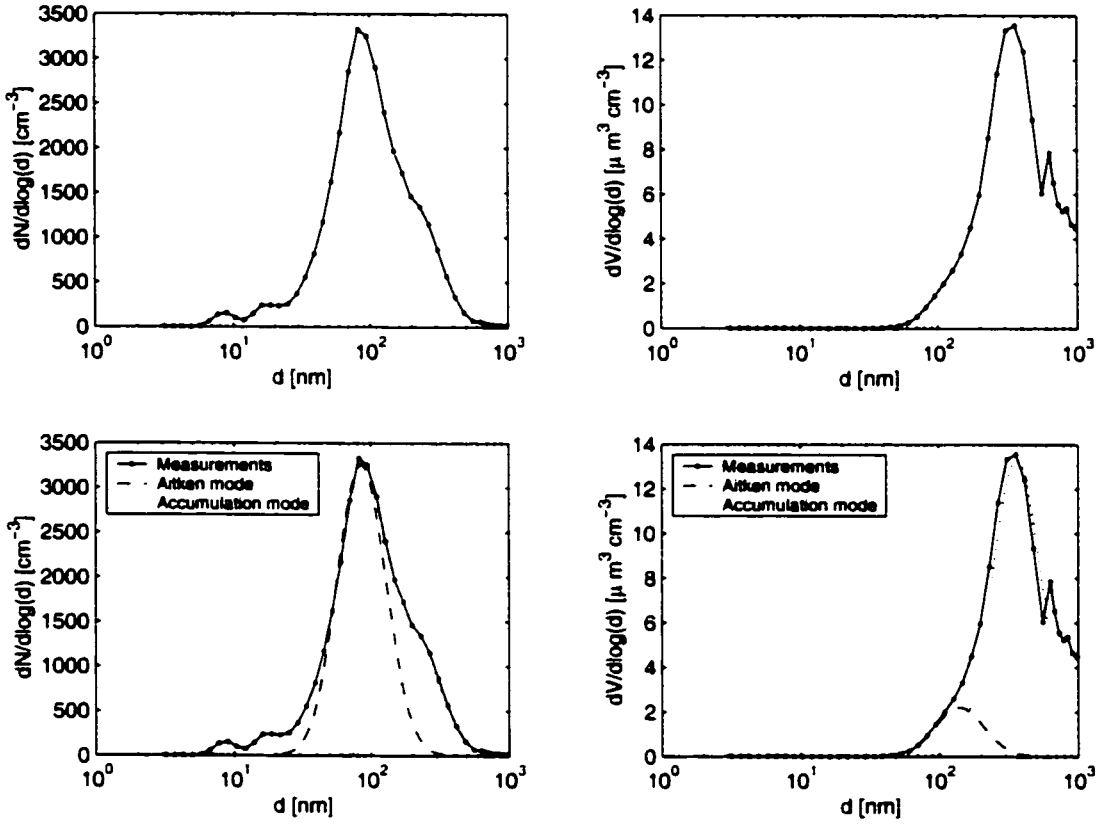

Figure 2.5: Number and volume size distribution with overlapping modes

In the number-size distribution the main peak in the Aitken mode size range is asymmetric, with a shoulder towards larger sizes. It is unclear if this shoulder is a second lognormal mode or if the distribution deviates from lognormal shape. The

corresponding volume size distribution

$$\frac{dV}{d\log d_p} = \frac{\pi \cdot d_p^3}{6} \cdot \frac{dN}{d\log d_p} \tag{2.5}$$

shown in Figure 2.5(b). This representation of the size distribution emphasizes the larger particle sizes. It can be seen clearly that the shoulder shows as a separate, larger mode that now is the dominant mode and that it has lognormal shape. Thus it seems it is justified to fit two lognormal modes to the main peak of the number-size distribution. What might have appeared as an asymmetric mode in the number-size distribution is actually composed of two overlapping lognormal distributions. This conclusion can be drawn for almost all asymmetric distributions in Sagres during ACE-2.

While clearly separated modes are usually unambiguously fitted, the fitting of overlapping modes is more prone to inaccuracies. The first problem is to decide at which point two instead of one lognormal distribution should be fitted to a slightly asymmetric mode. Slight asymmetries in the measured distribution are often present and if the goodness of fit is the only criterium two modes always provide a better fit in such a situation. However sometimes there is no physical reason to split a mode or add additional modes just to improve the goodness of the fit, which could result in misleading physical interpretations. Considering how well the modes approximate higher moments of the distribution can be helpful in this case as well. Since the lognormal modes are calculated to provide a best fit to the number-size distribution only, the examination of higher moments of the size distribution is an independent test if the fit is physically meaningful. An example of this is shown in Figure 2.6. It can be seen that the main mode can be fitted well with one and with two modes. Quantitatively two modes provide a somewhat better fit both to the number and to the volume size distribution. However there is no indication that two modes are necessary to provide an adequate fit. To exclude most cases of artificial mode splitting

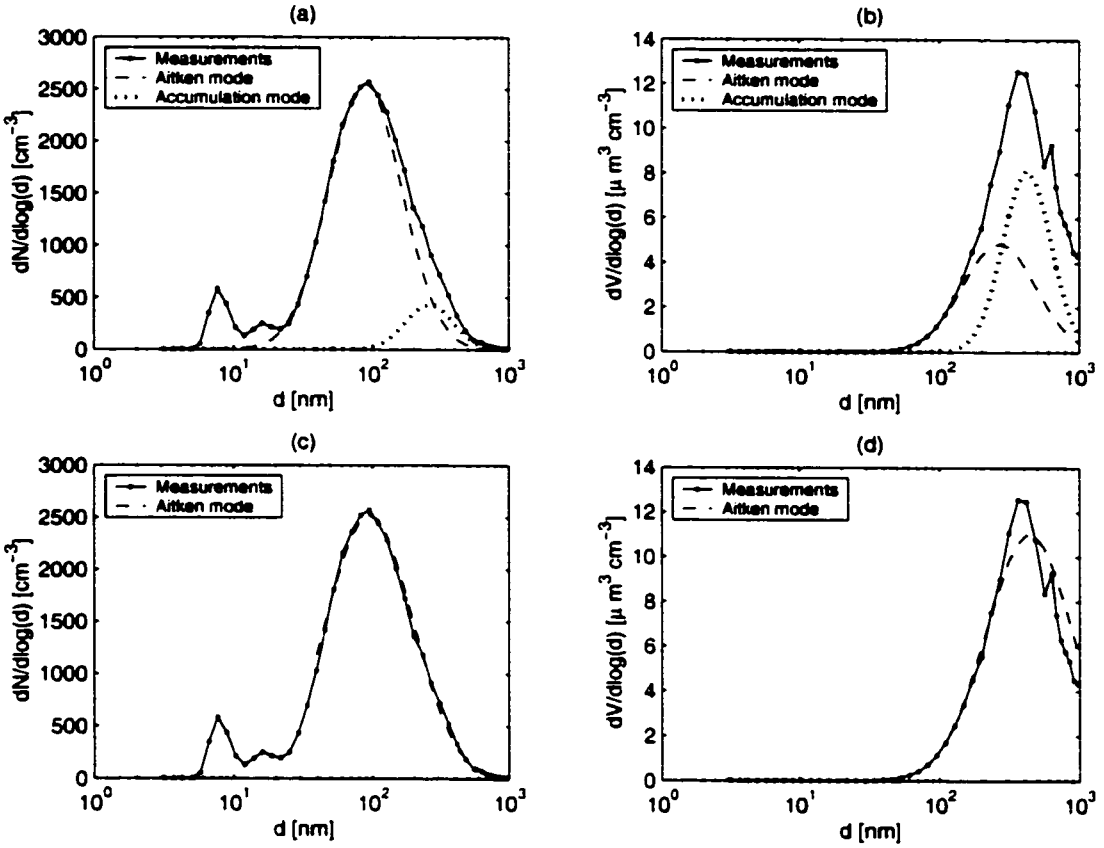

Figure 2.6: Example for artificial split of a monomodal size distribution into two modes

all distributions are re-fitted using one mode. If the ratio of the sum of squared deviations (ssd) using a single mode to ssd using two modes is greater than 0.02 for the number-size distribution and the greater than 0.2 for the volume size distribution then the two modes are replaced by the single mode. The cut-off ssd were determined by visual inspection and are a somewhat arbitrary, but at least consistent criterium whether one or two modes should be fitted.

The same technique can be used to see how well the mode parameters are captured when fitting overlapping modes. The number-size distribution in Figure 2.7(a) has

again two overlapping modes, that seem to be reasonably well resolved by the fits. In the volume size distribution shown in Figure 2.7(b) however there is one tight and

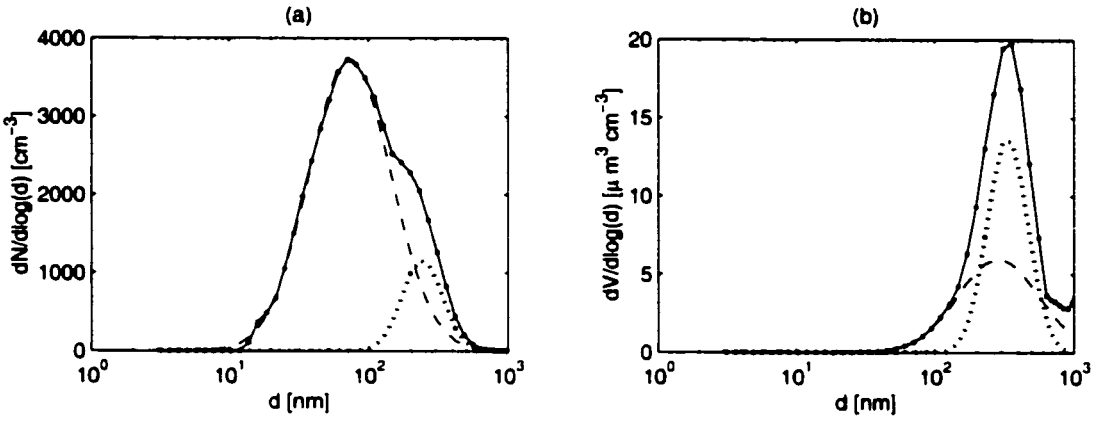

Figure 2.7: Example for a problematic fit of overlapping modes

clearly lognormal mode that is quite obviously a single lognormal mode. However the fits are suggest that it is composed of two overlapping modes, which does not seem very plausible physically. Therefore, it can be concluded that in the fitting process the number concentration of the accumulation mode has been underestimated and the standard deviation as well as the number concentration of the Aitken mode have been overestimated.

2.3 Measurements of particle hygroscopic properties

2.3.1 Measurement principle - the TDMA

During ACE-2 the particle hygroscopic properties were measured using a Tandem Differential Mobility Analyzer (TDMA). This instrument was first used for the study of aerosol hygroscopic properties by Rader and McMurry (1986); Stolzenburg and McMurry (1988). Since then it has been widely used in both laboratory and field

studies (e.g. Covert and Heintzenberg, 1993; Swietlicki et al., 2000).

A schematic diagram of a TDMA is shown in Figure 2.8(a). It consists of two identical Differential Mobility Analyzers (DMA1 and DMA2) that are in series and a humidifying system that conditions the aerosol between DMA1 and DMA2. The

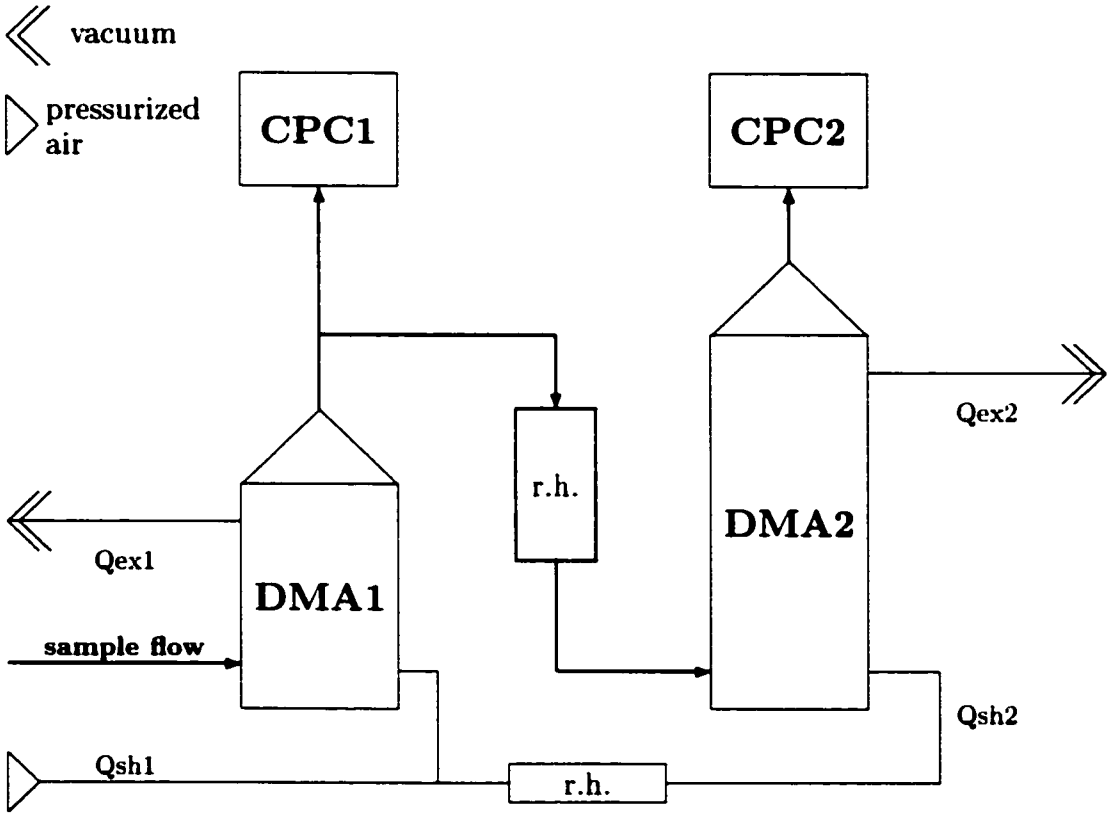

Figure 2.8: The Tandem Differential Mobility Analyzer (TDMA)

aerosol is first passed through a drier and dried to a r.h. below 10%. DMA1 is operated at this low r.h. and selects dry aerosol particles within a narrow size range. This size range is determined by the transfer function of DMA1 which is ideally

triangular with a diameter range of ±10% or less of the mean dry diameter (d_0) depending on the DMA1 flow rates. This quasi-monodisperse aerosol is then subjected to a specified, higher r.h. in a humidifier. The humidifier consists of a micro-porous Teflon tube inside a larger tube, that is continually circulated with water. The aerosol flows in the inner Teflon tube, and gets humidified by water vapor passing through the pores of the Teflon. The relative humidity of the aerosol sample flow changes according to the temperature of the surrounding water which is controlled by a r.h. sensor at the inlet to the DMA column. The r.h. of the sheath flown in DMA 2 is matched to the r.h. of the aerosol sample flow. In the humidifier hygroscopic aerosol particles grow by hydration to an equilibrium size that depends on the r.h. and the amount and chemical nature of the hygroscopic material in the particles. Since there are differences in the hygroscopic growth of individual particles, the nearly monodisperse size fractions broadens during this process. The resulting growth distribution is analyzed by DMA2. This distribution shows an increase in size and breadth compared to the dry diameter d_0 and can have one or more modes if the aerosol consists of particle fractions with distinctly different hygroscopic behavior.

2.3.2 Fitting of the growth distributions

Similarly to the size distribution measurements, the scans of the wet size distribution have to be inverted taking into account the transfer function of the DMAs. The inversion routine used for the ACE-2 dataset was developed by Stolzenburg and McMurry (1988) and adapted for LABView by Zhou (2001). This program obtains the mean growth factor (Gf), standard deviation σ, and relative number fraction Nf for each growth mode by fitting theoretical TDMA transfer functions to the measured aerosol distribution using a least squares fit routine.

The parameters Gf, σ and Nf were originally calculated by minimizing a Chi-

square function defined as the sum of normalized residuals:

$$\hat{\chi}^2 \equiv \frac{1}{f} \cdot \sum_{k=1}^{ns} R_i = \sum_{k=1}^{ns} \frac{2 \cdot \left(N_k - \hat{N}_k\right)^2}{w_k \cdot \left(N_k + \hat{N}_k\right)}, \tag{2.6}$$

where N_k are the measured particle number concentrations at various diameters d_k, $\hat{N}_k$ are the particles calculated by the theoretical growth distribution, f are the degrees of freedom and the ns are the number of measurement points. The weighting factor w_k is defined as

$$w_i \equiv \frac{1}{\Delta t_k \cdot Q_{cnc}}. \tag{2.7}$$

where Δt_k is the sample time for the N_k measurement and Q_{cnc} the effective CNC2 sample flow. Since the sample flow rate is constant the weighting factor puts more emphasis on the data points that were sampled for a longer time. In the TDMA measurements during ACE-2 the sampling time was increased for the diameter channels on the fringes of the growth distribution that had low aerosol concentrations. Thus these data points were emphasized resulting in worse fitting of the peaks. An example of this is shown in Figure 2.9. The measured data are shown as dark circles and the theoretical distribution obtained by varying the parameters Gf, σ, and Nf are shown as open circles. The fits in Figure 2.9(a) and (b) have the same Chi-square value although visually the peak is much better captured in 2.9(a). Moreover the best fit determined by the minimal Chi-square value (Figure 2.9(c)) visually deviates more from the measurements than the fit in 2.9(a).

Therefore the residual function R_k in the sum to be minimized is replaced by:

$$\hat{R}_k \equiv \frac{\left(N_k - \hat{N}_k\right)^2}{w_k \cdot \left(N_k + \hat{N}_k\right)} \cdot \frac{C_{2k}}{C_{1k}}. \tag{2.8}$$

where C_{2k} and C_{1k} are the absolute counts in channel k of DMA2 and DMA1 respectively.

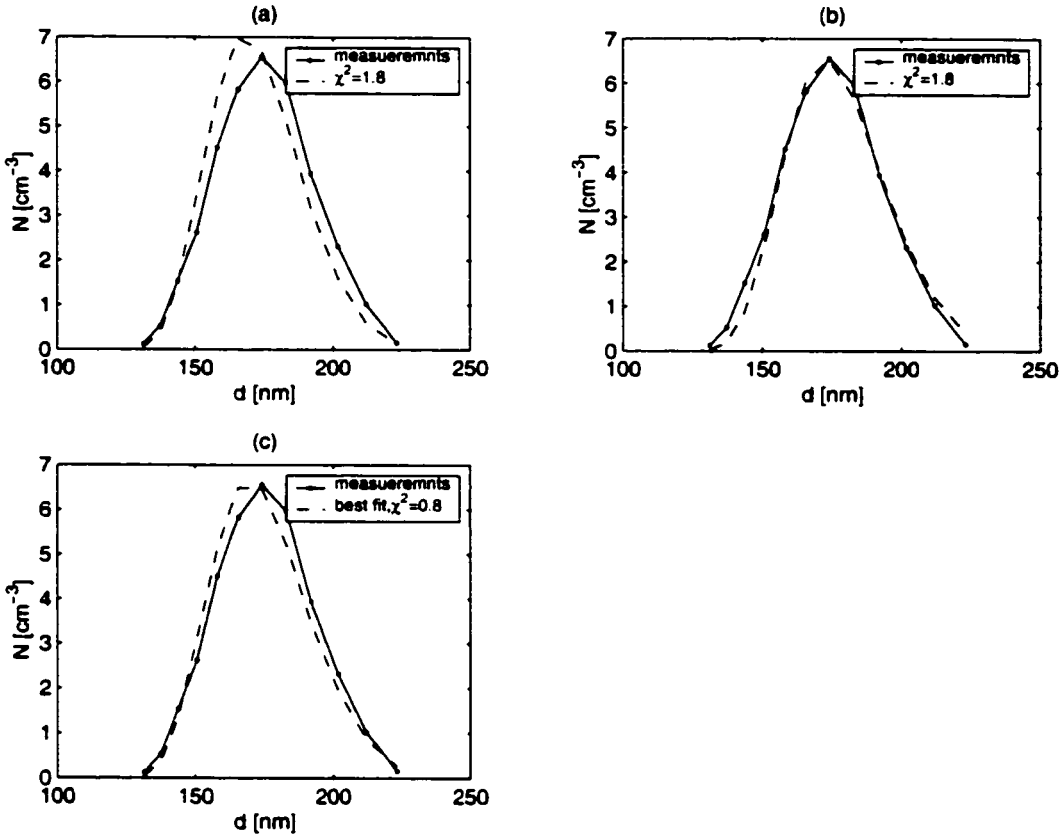

Figure 2.9: Example for a problems in the fitting of peaks

This is a function that is more representative the absolute differences between measured and calculated data points instead of the normalized residuals and thus places higher emphasis fitting the data points near the peak. The growth factors change only slightly, when they are derived by the new fitting function, but the number fraction and standard deviations of the growth modes can change between 5 and 15%.

2.3.3 Fit evaluation

The fitting is done semi-manually. Every fit is visually inspected and the user of the fitting routine decides how many modes to fit to each growth distribution. In Sagres the growth distribution usually had one and occasionally two modes, a more and a less hygroscopic mode. The more hygroscopic mode with a mean growth factor ranging from 1.5 to 1.8 is virtually always present, but a less hygroscopic mode appeared only occasionally. The manual fitting introduces a certain arbitrary element, but it has also some advantages to completely automated fitting routines. Comparison between the hygroscopic properties calculated by two different fitting routines for the same data set can give an idea of the magnitude of uncertainties introduced by the data inversion. Therefor an arbitrary subset of the TDMA data has been inverted by both the fitting routine of Stolzenburg and McMurry (1988) and an automated fitting routine written by ?.

Figure 2.10 shows the results of this comparison for a dry particle size of 50nm and of 250nm. It can be seen in Figure 2.10(a) and (d) that the more hygroscopic growth factors determined by both programs are in quite good agreement on average, although there is slight scatter among the individual data points. The less hygroscopic growth factors however show much more scatter and also some systematic difference between the two fitting routines as is shown in Figure 2.10(b) and (e). The automated fitting routine calculates on average lower growth factors for the less hygroscopic fraction. The uncertainties in the less hygroscopic growth factors introduced by the fitting routines probably overwhelm the measurement uncertainties introduced by sizing and counting errors. The fraction of particles in the more hygroscopic mode still shows considerable scatter. This analysis shows that we can place more confidence in the accuracy of the more hygroscopic growth factors than in that of less hygroscopic growth factor or in the number fraction in each growth mode.

2.3.4 Correction of growth factors to 90% r.h.

The relative humidity in the TDMA system usually is subject to minor fluctuations from approximately 87%-92%. The measured growth factors are corrected from the measurement r.h. to a relative humidity of 90% using a method developed by Swietlicki et al. (1999). The method can be summarized as follows:

A soluble volume fraction (ϵ) can be derived at the instrument relative humidity r.h.$_m$ (which is usually different from 90%) by relating the measured hygroscopic growth factor Gf to a hypothetical growth factor of a completely soluble particle consisting of a single model salt Gf$_{sol}$:

$$\epsilon = \frac{Gf^3 - 1}{Gf_{sol}^3 - 1} \tag{2.9}$$

Gf$_{sol}$ can be estimated by calculating the molality η_{sol} and the density rho_{sol} of the model salt solution at the water activity of the solution droplet at r.h.$_m$. This water activity (a$_w$) can be estimated as:

$$a_w = r.h. \cdot exp\left(\frac{4\sigma M_w}{\rho_w RT \cdot Gf \cdot d_0}\right), \tag{2.10}$$

where σ is the surface tension of water, M$_w$ is the molecular weight of water, R the universal gas constant, T the temperature, Gf the measured hygroscopic growth factor, and d$_0$ the dry particle diameter. η_{sol} and ρ_{sol} can be calculated using parameterizations available in the literature for various salts of atmospheric importance (e.g. Tang and Munkelwitz, 1994). Once η_{sol} and ρ_{sol} are estimated, Gf$_{sol}$ can be calculated as:

$$Gf_{sol} = \sqrt[3]{1 + \frac{\rho_s}{\rho_w \cdot \eta \cdot M_s}}. \tag{2.11}$$

Once the soluble volume fraction ϵ is calculated (by combining Equations 2.9,

2.10, and 2.11), the growth factor at any water activity can be calculated as:

$$Gf(a_w, \epsilon) = \sqrt[3]{1 + \epsilon \cdot \left(\frac{\rho_s}{\rho_{sol}} \cdot \left(1 + \frac{1}{\eta_{sol} \cdot M_s} \right) - 1 \right)}, \tag{2.12}$$

, where ρ_s is the density of the dry salt. For the purpose of correcting the growth factor to a chosen relative humidity instead of a water activity, it must be noted that a_w in Equation 2.12 is dependent on the (unknown) growth factor at that chosen humidity. It is recommended to start at a water activity a_w=r.h. and then iterate Equations 2.10 and 2.12 until the $Gf(a_w,\epsilon)$ converges.

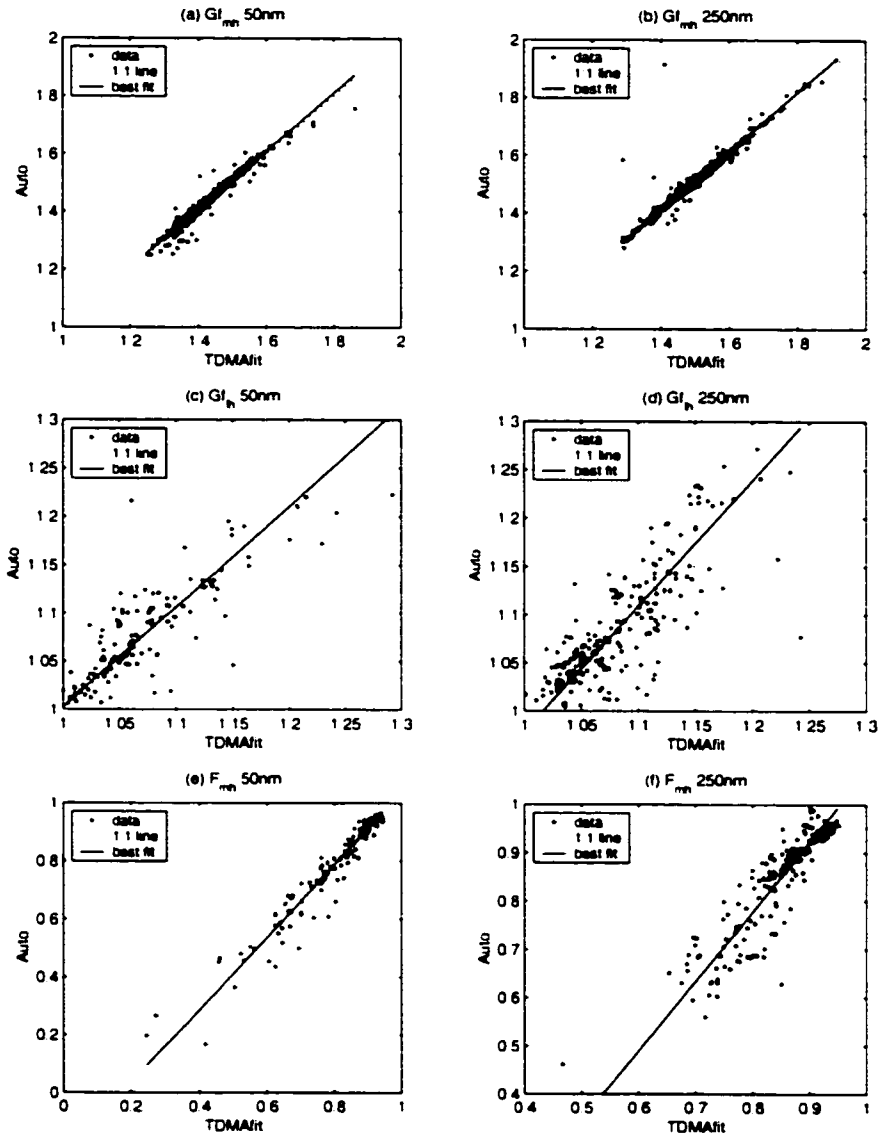

Figure 2.10: Evaluation of the fitting routines: (a) Comparison of more hygroscopic factors at a dry particle size of 50nm. (b) Comparison of less hygroscopic factors at a dry particle size of 50nm. (c) Comparison of the more hygroscopic number fraction at a dry particle size of 50nm. (d) Comparison of more hygroscopic factors at a dry particle size of 250nm, (e) Comparison of less hygroscopic factors at a dry particle size of 250nm, (f) Comparison of the more hygroscopic number fraction at a dry particle size of 250nm.

Chapter 3

AEROSOL PROPERTIES IN SAGRES, SW PORTUGAL DURING ACE-2

This chapter characterizes fundamental physical properties of the aerosol in Sagres on the SW coast of Portugal: the size distribution and hygroscopic properties. These aerosol properties are the basis for deriving aerosol properties other aerosol properties that can be linked to the direct and indirect forcing of aerosols on climate in later chapters of this thesis. In this chapter the variability in the size distribution and the hygroscopic properties is analyzed in terms of variations that have time scales of the order of several days and shorter-term variations that often occur with a characteristic diurnal scale. The longer term variabilities can be linked to changes in air mass back trajectories, that transport aerosol formed in different areas (e.g. the Arctic, or N. Atlantic ocean, Northern Europe, etc.) to Sagres. The long term variabilities thus seem to correspond to changes in the long range transport to Sagres. Variations on shorter time scales are characteristic of regional aerosol processes, i.e. processes that occur on the Iberian Peninsula or near the coast of Portugal. Variations from local sources in the immediate vicinity of the Sagres measurement site (such as road traffic to or from the site) are considered contamination of the data set and data affected are removed whenever possible.

Properties of the atmospheric aerosol are a result of processes that have acted on the aerosol over a period of several days. Aerosol properties measured at any location and point in time are therefore dependent on the history of the air mass

arriving at that location and can only be understood by considering two factors, long range transport and regional sources and processes. This is especially important for a location like southwestern Portugal, where long range transport of air from the Atlantic can result in very clean conditions and transport of air from northern Europe or the Iberian peninsula can result in polluted conditions that are not caused by any local sources. A change in air mass history changes the aerosol properties at the ACE-2 measurement site in Sagres dramatically. On the other hand ship traffic near Sagres and point sources along the coast of Portugal emit aerosol particles and aerosol precursors that mix into the background air mass. These sources can impose a regional signature on the aerosol transported to Sagres. As an example emissions of sulfur dioxide (SO_2), a main aerosol precursor are shown in Figure 3.1. Emissions of SO_2 are highest over Northern Germany and several eastern European states, such as Poland. However emissions of SO_2 are significant over the Iberian Peninsula as well: There are several point sources (most likely power plants) along the coast, as well as the city of Lisbon directly to the North of Sagres. The area around Lisbon emits 10,000-50,000 tons of SO_2 per year and thus constitutes a significant source of pollution. Figure 3.1 shows that emissions from ship traffic off the coast of Portugal raise the SO_2 concentrations above background concentrations. The emissions from ships are of the order of 1000-5000 tons per km^2 per year, which is lower than emissions by the power plants and Lisbon but covers a larger area.

In this chapter the aerosol in Sagres is characterized with respect to two aspects, the air mass history and characteristic regional processes that result in diurnal variations in aerosol properties. The first section summarizes aerosol properties according to air mass back trajectories. The second section describes characteristic diurnal variations in the aerosol that are driven by local atmospheric dynamics independently of air mass history.

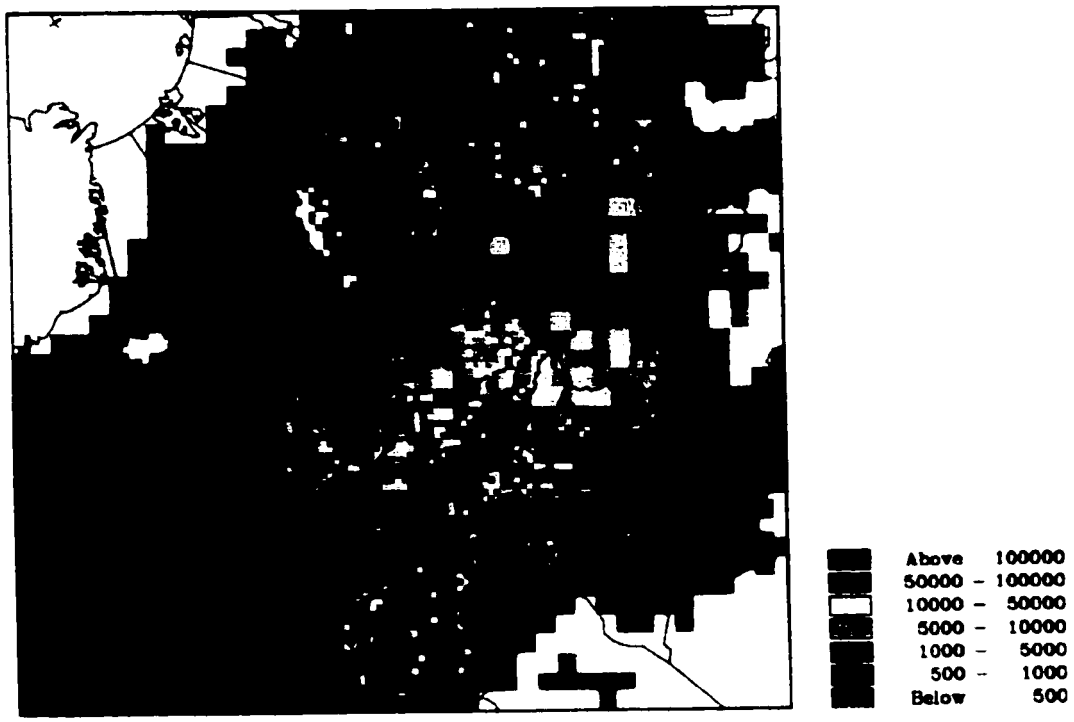

Figure 3.1: Emissions of SO_2 in Europe

3.1 *Aerosol properties in different air mass conditions*

3.1.1 Main air mass conditions

During the ACE-2 field experiment the measurement site at Sagres was influenced by several different air mass types. For the first half of the experiment cleaner air coming from the North Atlantic Ocean prevailed, whereas during the second half of the experiment polluted air masses originating over the European continent reached Sagres more frequently. Trajectories for cleaner time periods originate over the North Atlantic or the Arctic ocean. In many cases, air masses approach the Iberian Peninsula to the north of Sagres and the boundary layer flows down the coast to the Sagres

measurement site. These cases are not included in the marine data set to avoid contamination from local sources along the coast. Trajectories for the polluted time periods are subdivided according to the distance, time and pathway from the source region. Air masses containing aged pollution originate over France or Great Britain and flow out over the Atlantic, where they spend several days before reaching Sagres. Air masses containing more recent pollution cross the Iberian Peninsula immediately before arriving at Sagres from inland.

6-day air mass back trajectories were calculated 4 times a day: at midnight, 6 am, noon and 6PM. At each time 4 air mass back trajectories were calculated. The endpoints of the air mass back trajectories form a square centered around Sagres with a side length of 1/2 degree. Calculating 4 air mass back trajectories at any given time period can be used as quality control for the data. If all air mass back trajectories originate at a similar location and height it is very likely that the history of the air mass arriving at Sagres is described well by the air mass back trajectories. Time periods when the air mass back trajectories originate at very different locations (e.g. 2 trajectories originate over the Atlantic ocean and 2 trajectories originate over the Mediterranean sea) are excluded from analysis, since it is not clear which air mass type prevailed in Sagres.

Figure 3.2 shows typical 6-day air mass back trajectories associated with the four main air mass types encountered in Sagres: Marine Arctic, marine Atlantic, aged pollution and recent pollution. The location of the air mass 1, 2, and 3 days before reaching Sagres are indicated along the trajectory. The time periods for each air mass type are given in table 3.1.

Arctic air mass trajectories (Figure 3.2(a)) originate above the Arctic Circle and the air mass is rapidly transported southward to the measurement site at Sagres. The air mass travels from latitudes of above 65 degrees N to Sagres in only three

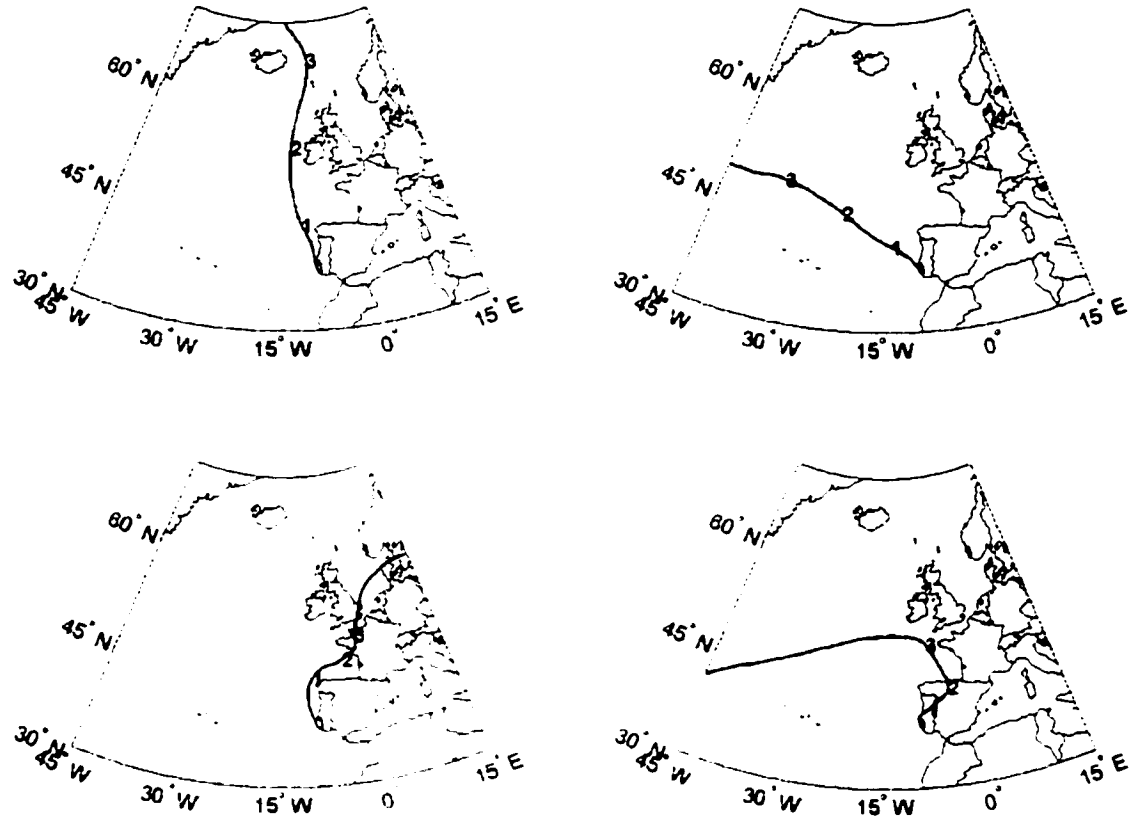

Figure 3.2: Typical air mass back trajectories associated with the 4 main air mass types during ACE-2: (a) Marine Arctic conditions, (b) marine Atlantic conditions, (c) aged pollution and (d) recent pollution

days. Subsidence is evident during that transport towards Sagres. Atlantic air mass trajectories (Figure 3.2(b)) originate over the Atlantic and usually spend more time in the marine boundary layer, before reaching Sagres. On some occasions the air travels for some distance close to the coast, where it might be influenced by pollution from regional sources or ships. Air masses back trajectories typical for aged pollution are shown in Figure 3.2(c). The air mass leaves the continent approximately two days before arriving at Sagres. The typical aging time of the aerosol in European outflow

conditions is thus approximately 2 days. Figure 3.2(d) shows typical air mass back trajectories for recent pollution. The trajectory originates over the ocean, but spends approximately two days over land before reaching Sagres.

The change in concentration of pollutants with air mass history can be demonstrated by averaging the concentrations of SO_2 and of aerosol particles for the time periods characterized by the four different air mass conditions defined above. However, the classification according to air mass back trajectories is somewhat crude. The air mass back trajectories are calculated every 6 hours and do not take into account changes in the mesoscale wind direction on shorter time scales. Moreover, fluctuations in the local wind direction can transport pollutants to Sagres that are not representative of the air mass that is characterized. This problem can be addressed by sorting the data according to local wind direction to assess if any particular wind direction is associated with elevated pollutant concentrations and possibly contaminates that data set.

Figure 3.3 shows a summary of the prevailing wind directions and concentration of pollutants during Arctic air mass conditions. The frequency of occurrence of local wind direction is shown in Figure 3.3 (a). The wind rose is divided into 12 segments of 30 degrees each. The length of the segments in radial direction outward is equal to the fraction of time the wind was coming from directions enclosed in this segment. Figure 3.3 (b) shows the concentration of SO_2 averaged over time periods in which wind directions within each segment were measured. Figure 3.3(c) shows averages of total particle number concentration plotted according to wind direction and Figure 3.3(d) shows average number concentrations of particles with diameters larger than 100 nm. Segments which contain less than 4 hours of data were not plotted to avoid showing outliers with little statistical significance.

During marine Arctic air mass conditions the winds were mainly northwest to

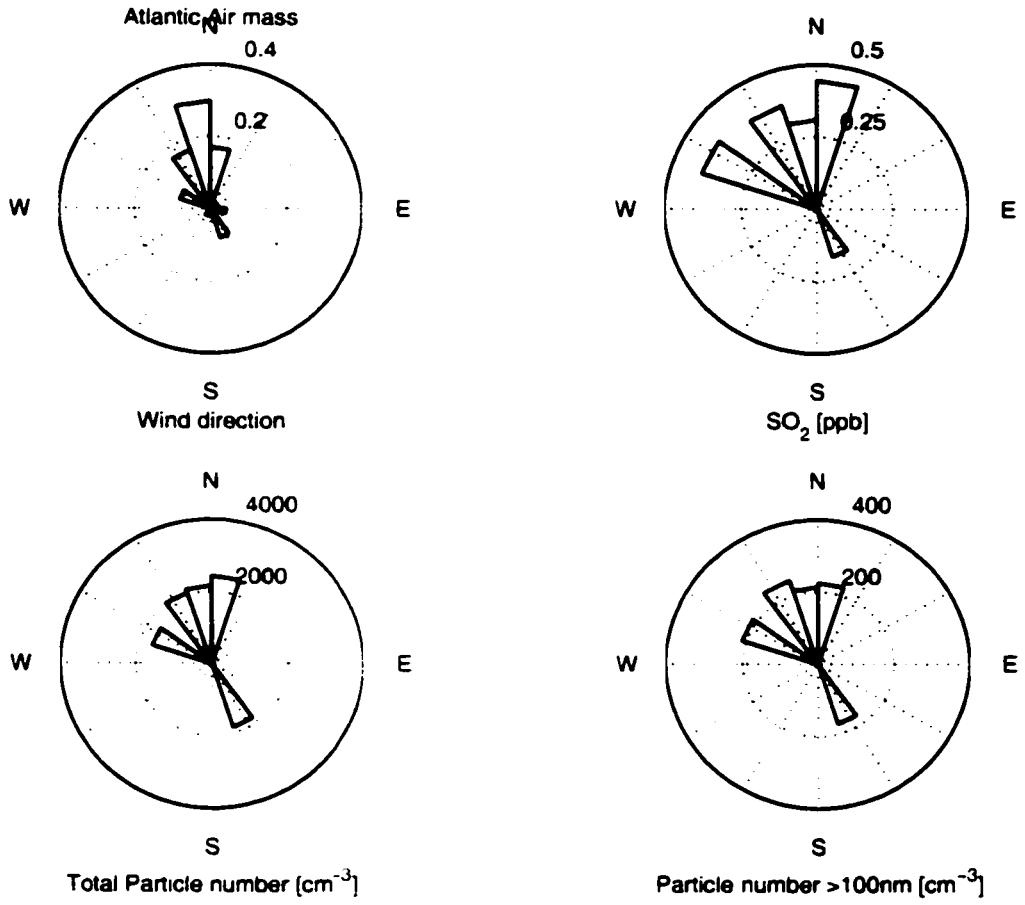

Figure 3.3: Wind directions and concentration of pollutants at Sagres during Arctic air mass conditions: (a) Frequency of occurrence of local wind direction, (b) SO_2 concentration according to wind direction, (c) total particle number concentration according to wind direction, (d) number concentration of particles larger than 100 nm

northerly (350 deg), consistent with the orientation of the air mass back trajectory. Only on a few occasions other wind directions were measured. On those occasions neither SO_2 nor particle concentrations were elevated compared to the dominant wind direction as can be seen in Figure 3.3(b)-(d) even though the town and harbor

of Sagres are to the SSE of the measurement site. SO_2 concentrations generally lie between 0.25 and 0.5 ppb, the lowest average measured in Sagres during the ACE-2 field campaign. Total particle concentrations were around 2000 cm^{-3}, but only 10% of those particles are larger than 100 nm resulting in a low aerosol volume during Arctic air mass conditions. Particle number concentrations are nearly independent of wind direction which shows that little contamination from local sources was present.

Figure 3.4 shows a summary of the prevailing wind directions and concentration of pollutants during marine Atlantic air mass conditions. During this time period the predominant wind direction was from the North (central value 360 deg). Average SO_2 concentrations were approximately twice as high as in Arctic air mass conditions. The total particle number concentration shows a very strong increase when the wind arrives just east of North (15 deg), while the number concentration of particles larger than 100nm increases only slightly. A large number of fine particles must be produced upwind to the North of Sagres. A closer examination of the data set shows that the elevated average is mainly due to a strong increase in the number concentration of fine particles smaller than 50 nm on one occasion that lasts only for a few hours. The source of these particles is probably recent particle nucleation in the plume of the Sinas power plant or the Lisbon urban area north of Sagres. If the time period influenced by emissions from the power plant is removed from the data set, then the average particle number concentration in this segment is comparable to particle number concentrations measured in more westerly wind directions. In addition to the one nucleation event there are a few occasions where the size distribution loses its marine appearance and is dominated by local influences. These time periods are excluded from further analysis as well.

Figure 3.5 shows a summary of SO_2 and particle number concentrations for time periods of aged pollution. During these time periods the local wind direction is

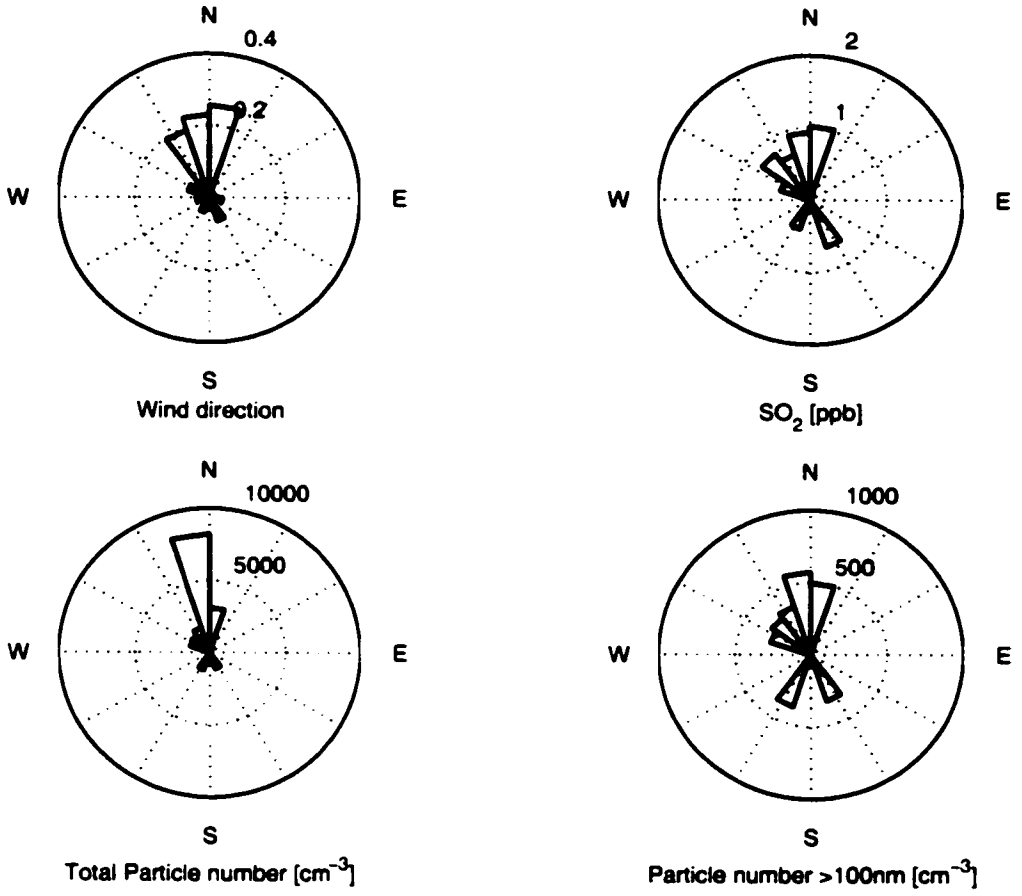

Figure 3.4: Wind directions and concentration of pollutants at Sagres during Atlantic air mass conditions: (a) Frequency of occurrence of local wind direction, (b) SO_2 concentration according to wind direction, (c) total particle number concentration according to wind direction, (d) Number concentration of particles larger than 100 nm

more westerly and land based coastal pollution is less likely to contaminate the data. Mean SO_2 concentrations are comparable to SO_2 concentrations in Atlantic conditions, which indicates that the SO_2 emitted over northern Europe has been depleted during the two days the air mass spent over the ocean. SO_2 concentrations are high-

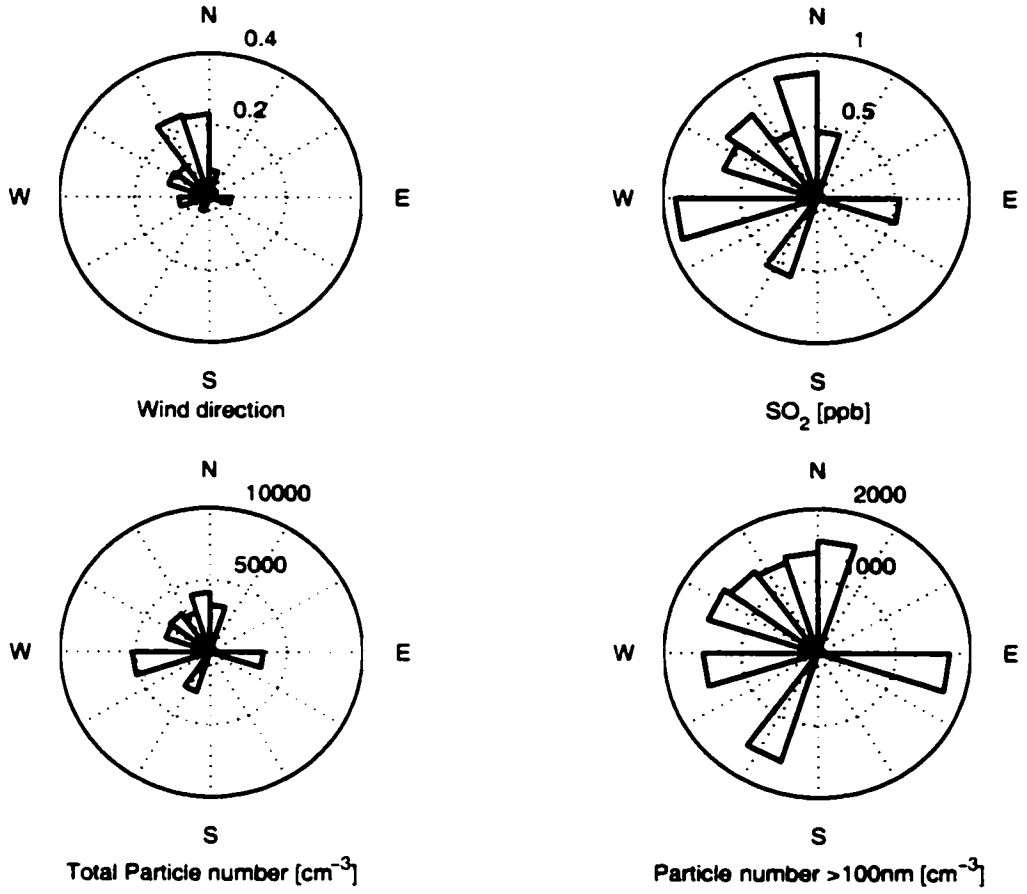

Figure 3.5: Wind directions and concentration of pollutants at Sagres during aged pollution episodes: (a) Frequency of occurrence of local wind direction, (b) SO_2 concentration according to wind direction, (c) total particle number concentration according to wind direction, (d) Particles larger than 100 nm

est when the local wind direction is from the north and the west. Northerly winds might transport some pollution from the area around Lisbon to Sagres. To the west of the measurement site lies a small,less traveled road which might explain the elevated fine particle concentrations measured during time periods of westerly wind directions. However westerly winds occurred less than 5% of the time and the local

contamination does not influence overall averages noticeably. In all other cases particle concentrations are independent of local wind direction. Approximately 40-50% of all particles are larger than 100nm, a much higher percentage than during marine air mass conditions. Air masses originating over the continent contain higher concentrations of primary particles and aerosol precursor gases. High particle concentrations promote efficient coagulation and high concentrations of precursor gases promote condensational particle growth, both processes that increase the average particle. After enough time for aerosol processing has has passed, a high percentage of the particles can be found at larger sizes.

Figure 3.6 shows wind directions and pollutant concentrations when recent pollution is carried to Sagres from the Iberian Peninsula. The local winds during this time period are almost exclusively northerly (350 degrees). In Figure 3.6 it can be seen that the wind direction of 350 degrees is consistent with the last hours of typical air mass back trajectories, which cross the Iberian Peninsula and turn sharply upon reaching the coast and arrive in Sagres from the North. Due to this northerly direction of the air mass back trajectories prior to arriving at Sagres, there might be some influence from the Lisbon urban area in the recent pollution aerosol. SO_2 concentrations are higher than during time periods of marine air or aged pollution. Particle concentrations are also higher than during the other air mass conditions, and approximately a third of the total particle population is larger than 100 nm. This is lower than in aged pollution as might be expected after less aging time.

3.1.2 Aerosol size distributions and hygroscopic properties in different air mass conditions

The following two tables show a summary of size distribution parameters and hygroscopic properties in the four main air mass conditions defined above. The geometric

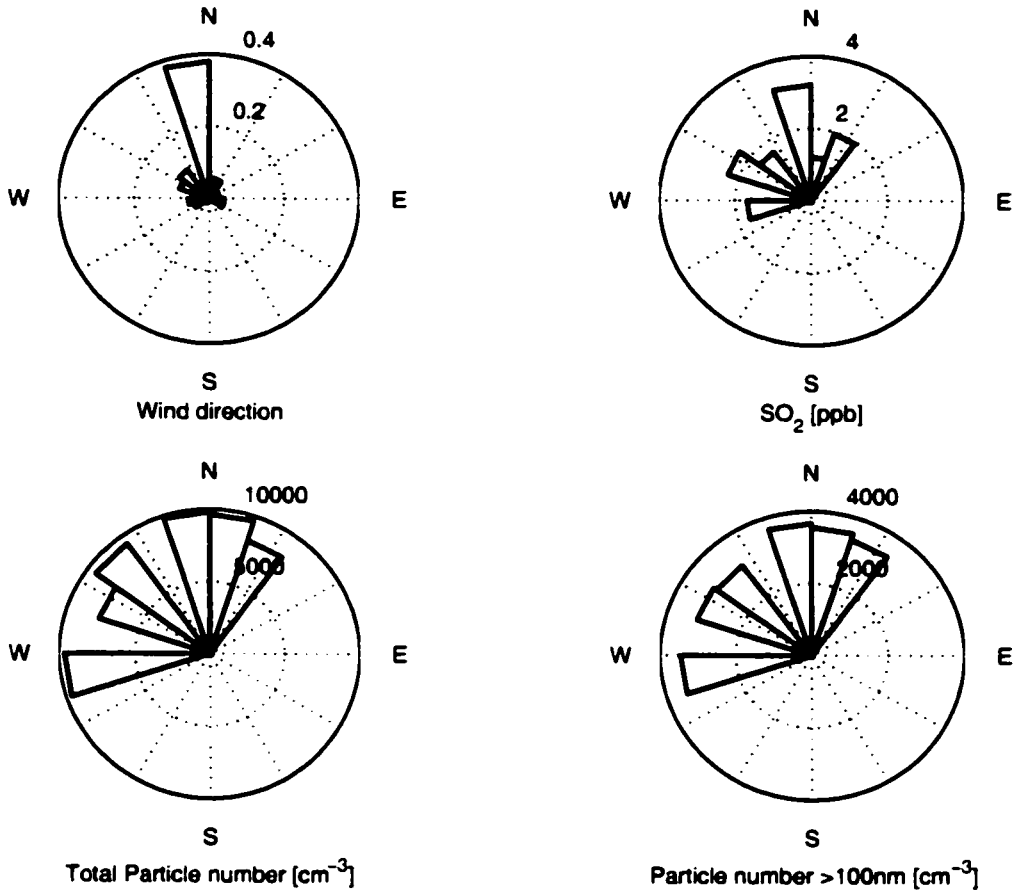

Figure 3.6: Wind directions and concentration of pollutants at Sagres during a recent pollution episode: (a) Frequency of occurrence of local wind direction, (b) SO_2 concentration according to wind direction, (c) total particle number concentration according to wind direction, (d) Number concentration of particles larger than 100 nm

mean diameter (d_g), the total number concentration (N), and the standard deviations (σ_g) of the lognormal distributions that were fitted to the size distribution are given in Table 3.1. The fitting methods and the definitions of the distinct lognormal modes are given in Section 2.2.2. Not all five modes were present all the time and the fre-

quency of occurrence of the individual modes are shown as freq. [%]. The mean data for each air mass type are presented. The value of ± 1 standard deviation is given as a measure of variability in the data set, except for the number concentrations of each mode. Since N is not normally distributed, but skewed to larger values a few outliers often give a unrealistically large standard deviation. Instead the number concentrations at the 16th and 84th percentile are given, which corresponds to the interval defined by ± 1 standard deviation of a normal distribution.

The ultrafine mode was present in only about 35% of the observations. The mean diameter, the number concentration and the standard deviation of the Ultrafine mode are similar in all air mass conditions ($250cm^{-3} < N < 533\ cm^{-3}$, d_g =8nm, $1.2 < \sigma_g < 1.3$). The small mean diameters of this mode suggests that it must have been formed recently. The fact that N, d_g, and σ_g of the Ultrafine mode are relatively independent of air mass history suggests it has been formed by regional (100km, 2hrs) processes that do not change significantly in different air mass conditions.

The Aitken mode was more prevalent, being present in about 80% of the observations. The parameters of the small Aitken mode are also similar in different air mass conditions ($480cm^{-3} < N < 1000cm^{-3}$, 20nm < d_g <28nm, $1.3 < \sigma_g < 1.4$). The only exception is that its mean diameter, which is larger in recent pollution. Since the small Aitken mode is most probably formed by growth of ultrafine particles through coagulation and condensation, it can grow to larger sizes in recently polluted air masses, where condensible gas phase precursors are more concentrated. It can be concluded that both the ultrafine and the small Aitken mode are formed in the region of southern Portugal. The only reason that the Ultrafine and small Aitken mode are distinct is that the particles contained in each mode probably nucleated at different times and locations upwind from Sagres and/or grew at a different rates during the transport to the measurement site.

Table 3.1: Summary of size distribution parameters: Freq [%] gives the percent of cases in which each mode was present, d_g is the geometric diameter of the mode, σ_g the geometric standard deviation, and N the number concentration of the mode

	Arctic	**Atlantic**	**Aged Poll.**	**Recent Poll.**
		Ultrafine Mode		
Freq [%]	39	29	35	44
d_g [nm]	8 ± 3	8 ± 2	8 ± 3	8 ± 2
N [cm^{-3}]	390 [30, 390]	250 [20, 260]	533 [30, 840]	340 [30, 390]
σ_g	1.2 ± 0.1	1.2 ± 0.1	1.3 ± 0.1	1.3 ± 0.1
		Small Aitken Mode		
Freq [%]	61	91	88	73
d_g [nm]	20 ± 5	20 ± 4	23 ± 8	28 ± 9
N [cm^{-3}]	860 [160,1500]	640 [90,1400]	480 [50,500]	1110 [180,1900]
σ_g	1.3 ± 0.1	1.4 ± 0.1	1.3 ± 0.1	1.4 ± 0.1
		Aitken Mode		
Freq [%]	100	100	100	98
d_g [nm]	40 ± 11	49 ± 10	77 ± 22	78 ± 16
N [cm^{-3}]	1500 [790,2100]	1100 [510,1700]	2400 [1500,3200]	7110 [5000,9000]
σ_g	1.5 ± 0.1	1.6 ± 0.2	1.7 ± 0.2	1.6 ± 0.1
		Accumulation Mode		
Freq [%]	100	100	88	100
d_g [nm]	149 ± 24	172 ± 24	213 ± 57	221 ± 67
N [cm^{-3}]	180 [110,240]	253 [120,370]	670 [340,1000]	1070 [200,1300]
σ_g	1.47 ± 0.09	1.44 ± 0.09	1.49 ± 0.11	1.47 ± 0.11
		Sea Salt Mode		
Freq [%]	100	86	100	100
d_g [nm]	570 ± 70	490 ± 60	630 ± 90	580 ± 80
N [cm^{-3}]	6 [4,8]	16 [10,22]	10 [7,12]	15 [11,20]
σ_g	2.2 ± 0.1	2.2 ± 0.1	2.3 ± 0.2	2.1± 0.1

The mean diameter and the number concentration of Aitken mode particles increases significantly from clean to polluted conditions. The formation of particles in the Aitken mode size range occurs on longer time scales than the formation of smaller particles, and a significant fraction of these particles has probably been formed along the trajectory before the air mass reached southwest Portugal. The parameters of the Aitken mode thus reflect more strongly the history of the air mass than regional processes.

The differences between air masses in accumulation mode mean diameter and number concentration is even more pronounced and the trends in Accumulation mode mean diameters and number concentrations are similar to the trends in the Aitken mode. The sea salt mode that has a natural source, does not vary consistently with air mass history.

Table 3.2 shows a summary of the hygroscopic properties in different air mass conditions. The hygroscopic growth of the particles is often bimodal and two fractions of particles a more-hygroscopic (mh) fraction with higher growth factors and a less-hygroscopic (lh) fraction with lower growth factors can be distinguished. A more- and a less-hygroscopic growth mode are often detected in the continental aerosol (e.g. Zhang et al., 1993), but are largely absent over the ocean. More hygroscopic and less hygroscopic growth factors (Gf_{mh} and Gf_{lh}) measured at different particle sizes are averaged for the four air mass conditions. More hygroscopic particles were always present, whereas less hygroscopic particles were present only intermittedly. The frequency of occurrence of less hygroscopic particles is shown as a percentage of the total number of growth factor measurements (Freq. [%]). Nf_{lh} is the average number fraction of less hygroscopic particles in cases where two growth modes are present.

The more hygroscopic growth factors increase with particle diameter in all air

Table 3.2: Summary of the hygroscopic properties of the aerosol in Sagres during ACE-2: Gf_{mh} and Gf_{lh} are the more and less hygroscopic growth factors,Freq [%] gives the percent of growth factor measurements where a less hygroscopic mode was present, and Nf_lh is the number fraction of less hygroscopic particles when present

	35nm	50nm	100nm	150nm	250nm
			Arctic Air Masses		
Gf_{mh}	1.55±0.07	1.56±0.07	1.6±0.08	1.65±0.08	1.65±0.08
Gf_{lh}	1.13±0.10	1.21±0.14	1.14±0.10	1.14±0.15	1.18±0.13
Freq.[%]	13	11	19	11	7
Nf_{lh}[%]	19±23	23±28	12±18	11±10	5±2
			Atlantic Air Masses		
Gf_{mh}	1.54±0.09	1.57±0.08	1.62±0.09	1.68±0.08	1.67±0.07
Gf_{lh}	1.17±0.05	1.15±0.09	1.19±0.1	1.27±0.09	1.21±0.11
Freq.[%]	35	13	19	33	35
Nf_{lh}[%]	24±22	22±9	16±8	20±12	18±9
			Aged Pollution		
Gf_{mh}	1.54±0.06	1.57±0.05	1.61±0.06	1.63±0.07	1.67±0.09
Gf_{lh}	1.14±0.08	1.10±0.05	1.12±0.07	1.17±0.08	1.13±0.05
Freq.[%]	39	17	5	9	6
Nf_{lh}[%]	21±17	12±9	10±5	9±7	7±3
			Recent Pollution		
Gf_{mh}	1.52±0.06	1.54±0.08	1.56±0.08	1.56±0.08	1.59±0.08
Gf_{lh}	1.18±0.06	1.15±0.05	1.05±0.07	1.14±0.08	1.21±0.05
Freq.[%]	33	13	2	9	70
Nf_{lh}[%]	21±17	7±5	5±2	4±1	24±11

mass conditions consistent with the Kelvin effect. This effect describes the increase of the water vapor pressure over a small particle due to the surface curvature. As a result smaller particles have to take up a smaller fraction of water than larger particles to be in equilibrium with the same ambient relative humidity. This effect of surface curvature on the hygroscopic growth factor is most important for particles sizes below 100nm.

The more hygroscopic growth factors are similar at each particle size in aged pollution, Atlantic, and Arctic air masses (e.g. between 1.65 and 1.67 at 250nm), but lower in recent pollution (e.g. 1.59 at 250nm). Less hygroscopic particles appear relatively frequently at the smallest particle size of 35nm, but in recent pollution and in Atlantic air masses the Accumulation mode contains a significant fraction of less hygroscopic particles as well.

Less hygroscopic particles are usually produced by combustion processes and are initially nearly hydrophobic (Weingartner et al., 1997) with growth factors close to 1. They acquire water soluble material through aging in the atmosphere and their growth factors start to increase. Of the several sites where hygroscopic growth factors were measured during ACE-2, Sagres was the only location where less hygroscopic particles appeared in the absence of local pollution (Swietlicki et al., 2000). Less hygroscopic particles in the size range below 100nm might be produced by ships off the Portuguese coast. Measurements in ship tracks have shown that primary particles produced by ships are usually composed of organic substances and contain only about 10% water-soluble material (Hobbs et al., 2000). Less hygroscopic particles can also form in urban areas along the coast of Portugal, which is the most likely source of the larger less hygroscopic particles found in recent pollution and Atlantic air mass types. The fact that the less hygroscopic growth factors are significantly larger than 1 suggests that they are slightly aged particles that were not produced locally or in

the close vicinity of Sagres.

Aerosol size distribution and hygroscopic growth in air masses transported from the Arctic

Figure 3.7 shows an aerosol size distribution typical for arctic trajectories. The number size distribution is displayed in Figure 3.7(a) and the corresponding volume size distribution in Figure 3.7(b). The one or more lognormal distributions fitted to the

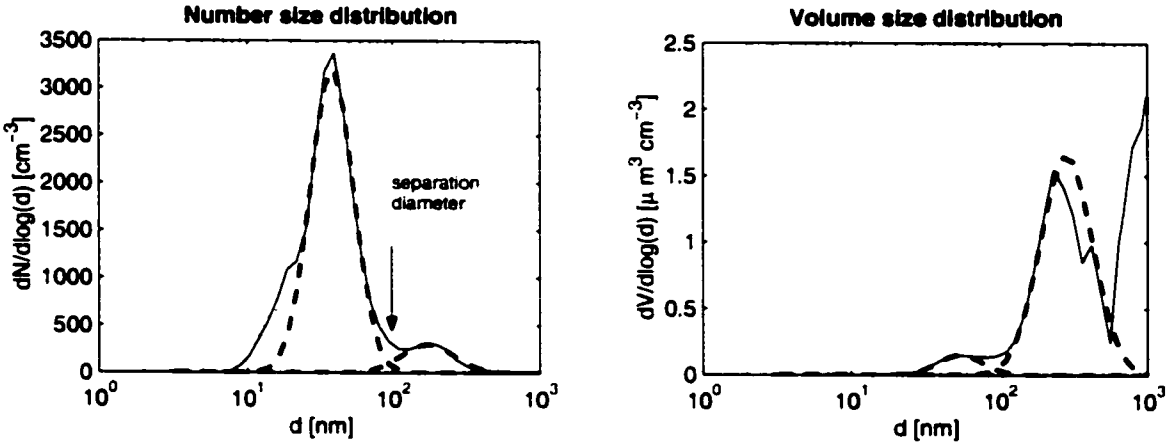

Figure 3.7: Aerosol size distribution typical for Arctic air mass conditions: (a) Number size distribution (b) corresponding volume size distribution

individual modes are shown as dashed lines. In both the number and the volume size distribution the Aitken and accumulation mode are clearly separated. Such bimodal distributions are a common feature of aerosol in the marine environment (e.g. Covert et al., 996a). There is strong evidence that this separation results from repeated cloud processing of the aerosol in stratus and stratocumulus clouds with low supersaturations (e.g. Hoppel et al., 1994). If the aerosol particles have uniform chemical composition each value of water vapor supersaturation in a clouds corresponds to

a critical particle diameter. Particles whose diameters exceed this critical diameter serve as nucleation sites for cloud droplets whereas smaller particles form the interstitial aerosol. The cloud droplets take up most of the water and are thus more diluted and have a larger surface area than the interstitial particles. This large surface area allows cloud droplets to take up SO_2 and convert it to sulfate by aqueous phase reactions. Upon evaporation the size of the cloud droplet nuclei is increased, depending on the amount of sulfate produced in the droplets, whereas the size of the interstitial aerosol particles does not increase nearly as much. After several cloud cycles the cloud nuclei form a separate mode, the accumulation mode.

In reality the separation between cloud and interstitial aerosol does not always occur at the same diameter, due to variations in particle chemical composition and in the supersaturations in the cloud. However in marine environments the range of critical diameters is narrow enough to result in a well defined minimum between Aitken and Accumulation mode. The location of the minimum that separates accumulation and Aitken mode is an indication of the maximum supersaturations experienced by the air parcel during its passage through clouds (e.g. Cantrell et al., 1999). We define the location of this minimum quantitatively as the diameter at which the lognormal fits to Aitken and Accumulation mode intersect (indicated by a vertical arrow in Figure 3.7 (a)). In Arctic air mass conditions the separation of Aitken and accumulation mode occurs on average at a diameter of 95nm.

Figure 3.7(b) shows that the accumulation mode and the tail of a mode of coarser particles account for most of the submicron particle volume. These coarse particles are most likely wind generated sea salt particles. Although most of the sea salt mass occurs at supermicron sizes, sea salt particles have been detected at submicron sizes before (e.g. Berg et al., 1998b; Quinn et al., 1998). The average mass-size distribution of Na and Cl (Neusüß et al., 2000) in clean marine air masses (shown in Figure 3.7(c))

shows that sea salt contributes to the submicron mass in those clean conditions.

Figure 3.8(a) shows a statistical summary of Aitken and Accumulation mode parameters in Arctic air mass conditions. The mean diameter of the mode is plotted on x-axis and the total number concentration in the mode on the y-axis. Each point in the diagram corresponds to a lognormal distribution with a certain mean diameter and a certain number concentration. The color contouring shows the frequency of occurrence of certain combinations of mean diameters and number concentrations. The Aitken mode mean diameters are narrowly clustered around 40nm whereas the Aitken mode number concentrations is quite variable. In contrast the number concentration of the accumulation mode is much more stable than the number concentration of the Aitken mode. The size distribution parameters measured in Arctic air mass types in Sagres can be compared to size distribution parameters measured directly in the Arctic marine boundary layer by Covert et al. (996b). The mean diameters of the Aitken and accumulation mode were 45 and 170 nm, which is similar to the mean diameters found in Sagres. However in the Arctic marine boundary layer the total number concentration was on average around 100 cm^{-3}, and the accumulation mode contained about 40% of the total number, which indicates a well processed aerosol. Apparently a high number of Aitken mode particles are added or formed in that air mass during the transport to Sagres. Entrainment of free tropospheric aerosol (e.g. Raes, 1995; Raes et al., 1997) and emissions from ships are a likely source of particles in that size range.

The frequency distribution of the parameters of the accumulation mode is tilted so that the number concentration decreases with increasing mean diameter. The mean diameter and the number concentration of the accumulation mode are not statistically independent. The inverse relationship between the parameters must be a result of the process that forms the accumulation mode. As explained above, this mechanism is

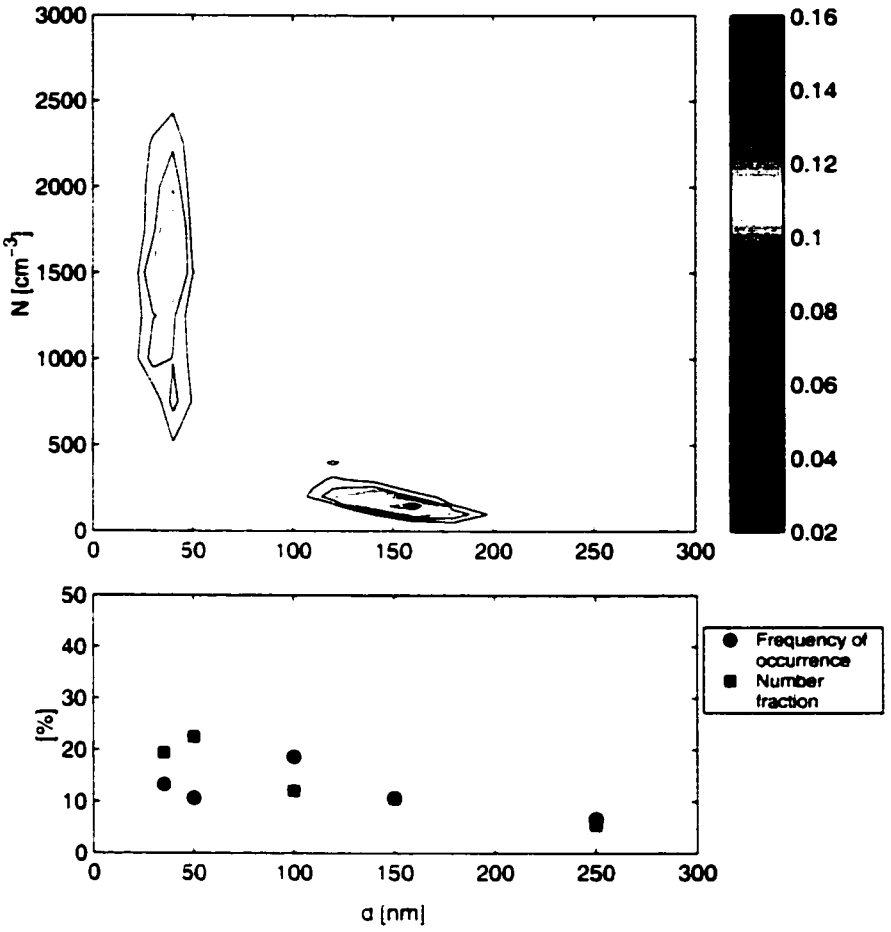

Figure 3.8: (a) Frequency distribution of the size distribution modal parameters in Arctic air mass conditions. The contours show frequency of occurrence of certain combinations of mode mean diameter and number concentration. Contours on the left correspond to the Aitken mode, contours on the right to the Accumulation mode. (b) Frequency of occurrence and number fraction of less hygroscopic particles in Arctic air mass conditions

commonly thought to be cloud processing. The mean diameter of the accumulation mode thus depends on the amount of sulfate accumulated on the particles during their lifetime as cloud droplets. The SO_2 concentration in the Arctic air mass is low

and relatively stable and the volume of the accumulation mode is relatively constant around $0.5\mu m^3 cm^{-3}$. This indicates that during air mass transport from the Arctic approximately the same total amount of SO_2 was converted to sulfate in all cases independent of particle number concentration. If few cloud droplets were present, each droplet could scavenge more SO_2 and the particles could grow to larger sizes than if more cloud droplets present. High droplet number concentrations prevent the accumulation particles from achieving large sizes and as a consequence the particle number decreases with increasing mean diameter.

Figure 3.8(b) summarizes the hygroscopic properties during Arctic air mass conditions. Since more and less hygroscopic growth factors do not differ significantly from two of the other air mass types, only the frequency of occurrence and number fraction of less hygroscopic particles are shown as a function of particle size. The frequency of occurrence of less hygroscopic particles in Arctic Air masses is lower than in all other air mass conditions. Comparing Figure 3.8(a) and (b) shows that the hygroscopic properties measured at particle diameters of 35 and 50nm are representative of Aitken mode particles and hygroscopic properties at 150 and 250 nm are representative of accumulation mode particles. Less hygroscopic particles were present around 10% of the time at all sizes and when present, accounted for approximately 20% of the Aitken mode particles and 12% of the accumulation mode particles.

Aerosol size distribution and hygroscopic growth in air masses from the Atlantic

Figure 3.9(a) shows the frequency distribution of size-distribution parameters for time periods when air masses from the Atlantic were reaching Sagres. Air mass back trajectories during that time period were often closer to the Portuguese coast and the aerosol properties presented here are sometimes not characteristic of marine background conditions but rather of the anthropogenically modified aerosol near the Por-

tuguese coast. Whenever local pollution episodes were detected, the locally influenced measurements were eliminated from the following calculations. The size distribution

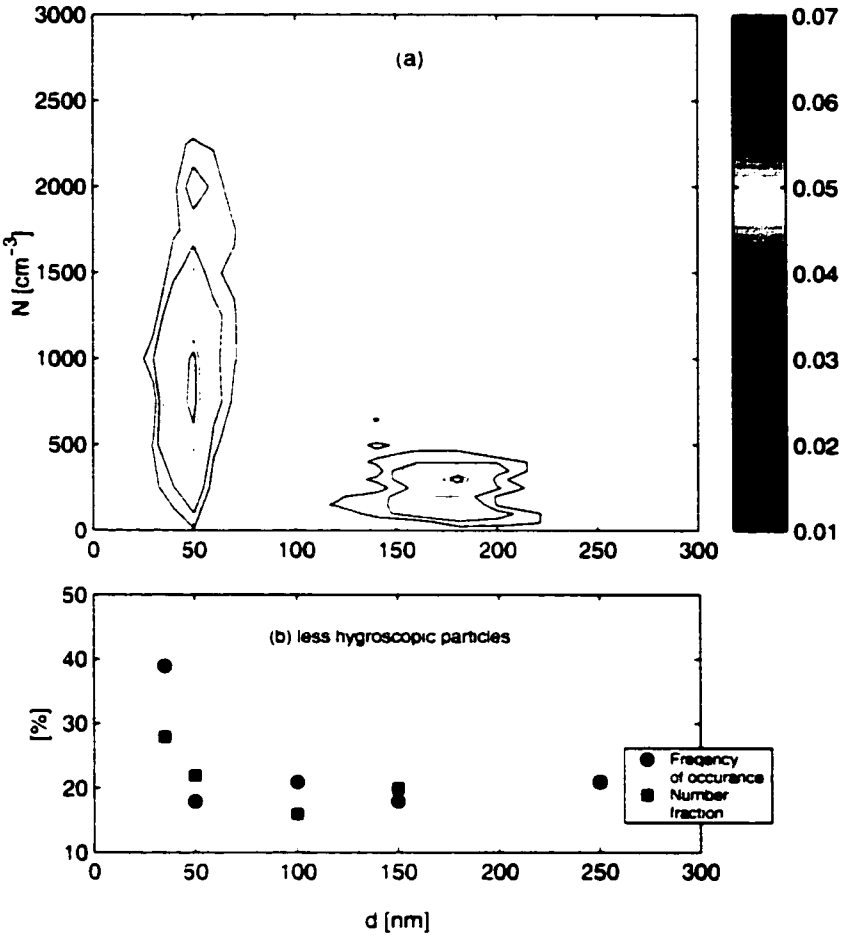

Figure 3.9: (a) Frequency distribution of the size distribution modal parameters in Arctic air mass conditions. (b) Frequency of occurrence and number fraction of less hygroscopic particles in Arctic air mass conditions

in Atlantic Air masses show the bimodality typical of marine distributions, consisting of an Aitken and an accumulation mode separated by a minimum. This minimum occurs usually at diameters near 100 nm. The mean separation diameter is slightly

larger than in Arctic air masses. The Aitken mode number concentration is lower than in the Arctic air mass and the mean Aitken mode diameter is larger. Air mass back trajectories show that usually the marine air spends more time in the boundary layer and also more time near the coast before reaching Sagres than the Arctic air. Enhanced particle growth by condensation due to SO_2 sources along the coast and more time for coagulation might explain the lower Aitken mode number concentration and the larger mean diameter in marine air masses. The mean accumulation mode diameter lies around 170 nm and accumulation mode number concentration does not decrease with increasing mean diameter. The levels of SO_2 are higher in the Atlantic than in Arctic air masses and it is likely that SO_2 is not a limiting factor for particle growth in the marine aerosol near the Portuguese coast. Moreover SO_2 concentration and particle number concentration are somewhat correlated. Both are higher when the air mass spends more time along the coast prior to reaching Sagres, which allows the accumulation mode particles to grow to larger diameters even if their number concentration is high.

Figure 3.9(b) shows that in Atlantic air mass conditions less hygroscopic particles appear more frequently than in Arctic air mass conditions. The less hygroscopic particles are largely absent in the cleanest Atlantic conditions, when the air flow reaches Sagres from the southeast. This is further evidence that less hygroscopic particles are produced by regional pollution sources on land or by ship traffic along the coast.

Aerosol size distribution and hygroscopic growth during aged pollution

Figure 3.10 shows typical examples of the two types of size distributions encountered during the two episodes of pollution outbreaks from Europe that reached Sagres after approximately two days of aging over the marine coastal region west of France and the

Iberian Peninsula. Figure 3.10(a) and (c) show the number-size distributions along

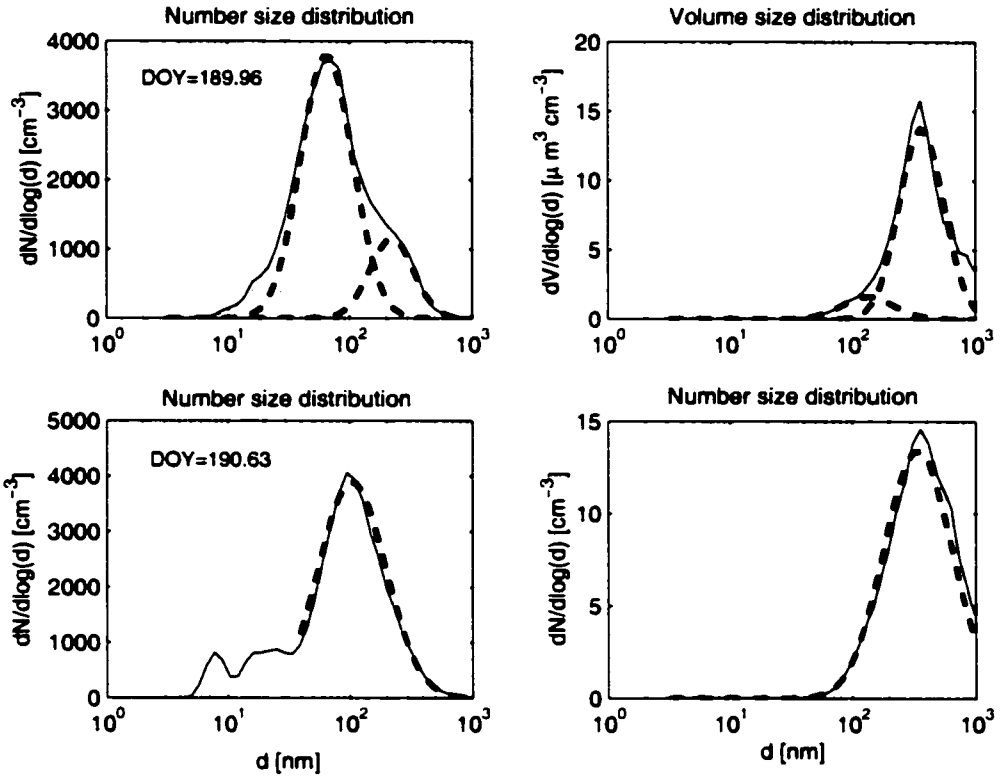

Figure 3.10: Aerosol size distributions typical for Aged pollution episodes: (a)and (b) Bimodal number and volume distribution. (c) and (d) Monomodal number and volume distribution

with the lognormal fits. Figure 3.10 (b) and (d) show the corresponding volume size distributions. The first type of distribution (Figure 3.10 (a) and (b)) is clearly bimodal even though the modes are not as well separated as in more marine air masses. Despite the fact that the accumulation mode only appears as a shoulder on the Aitken mode in the number size distribution, the fitting program captures the standard deviation and mean diameter of the accumulation mode very well as can be seen in the volume size distribution. Unfortunately the fitting program does not always perform this well,

and sometimes the number concentration in the accumulation mode is underestimated by the fitting routine. The second type of distribution (Figure 3.10(c) and (d)) is not bimodal and is often better fitted with just one lognormal mode. The differences in the two types of size distributions might be due to the amount of cloud processing that the aerosol experiences during its transport over the ocean. If few clouds are present the size distribution might be just slightly broadened, while repeated and extensive cloud processing might result in a more well defined accumulation mode. Intermediate stages between those cases can also be observed during time periods characterized by aged pollution.

Figure 3.11 shows the frequency distributions of the aerosol modal parameters and the occurrence of less hygroscopic particles in aged pollution. It can be seen that the modal parameters in this case are not as well separated as in the marine case. The frequency of occurrence of Aitken mode mean diameter shows two maxima. One maximum lies around 100 nm and is mainly due to the mono-modal size distributions of the type presented in Figure 3.10(c) and (d). The second maximum lies around 70 nm and is representative of bimodal size distributions. When an accumulation mode is developed during transport the Aitken mode mean diameter stays smaller, because sulfate mass is selectively added to the larger particles during cloud processing. If the particles mainly grow by condensation, then the sulfate acquired during transport is more equally distributed among particle sizes and the Aitken mode can grow to a larger mean diameter. The frequency distribution of the accumulation mode is tilted so that larger particle concentrations correspond to smaller mean diameters, very similar to the frequency distribution in Arctic air mass types.

The hygroscopic growth measurements show very few occasions of less hygroscopic particles during aged pollution. The less hygroscopic particles that might have been part of the aerosol over the European continent have been converted to more hygro-

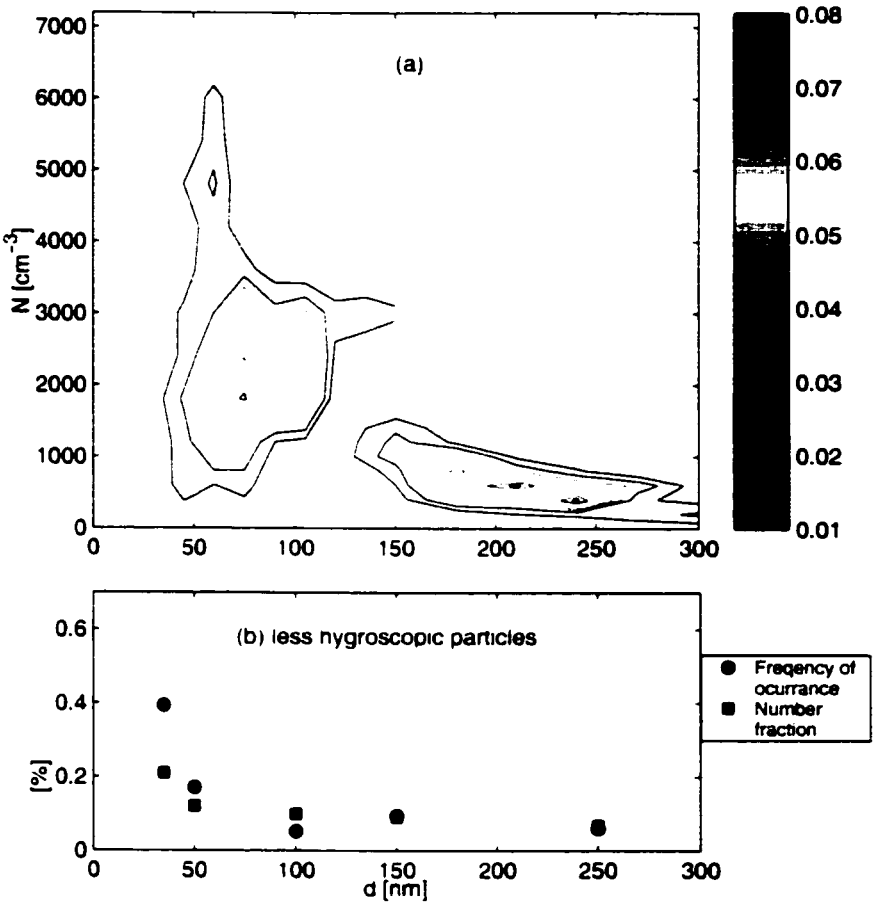

Figure 3.11: (a) Frequency distribution of the size distribution modal parameters in aged pollution episodes. (b) Frequency of occurrence and number fraction of less hygroscopic particles in aged pollution

scopic particles by the time the air mass reaches Sagres. Less hygroscopic particles emitted by regional pollution along the coast of Sagres obviously do not play an important role in the aged pollution aerosol and are mostly absent in the accumulation mode size range. The trajectories and local wind directions during that time period indicates that the air masses are not near the coast before reaching Sagres. Therefore

regional pollution might not be as noticeable during those time periods.

Aerosol size distribution and hygroscopic properties during recent pollution

Figure 3.12(a) shows the frequency distributions of aerosol modal diameters and the occurrence of less hygroscopic particles during recent pollution.

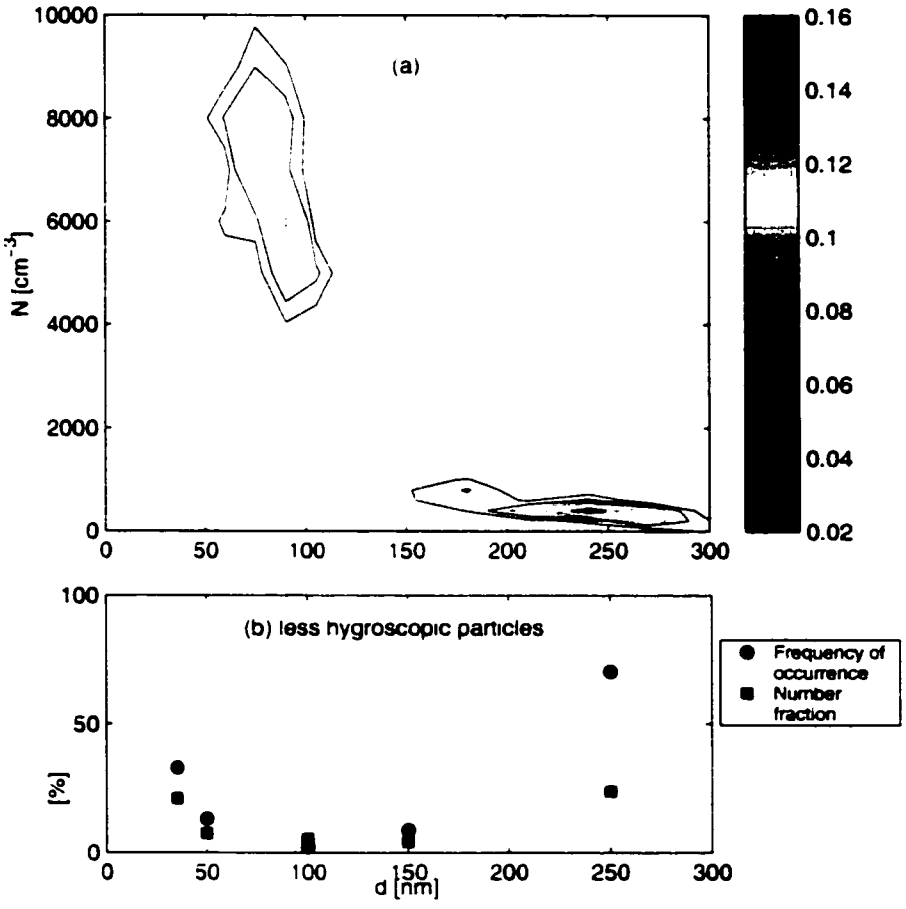

Figure 3.12: (a) Frequency distribution of the size distribution modal parameters in a recent pollution episode. (b) Frequency of occurrence and number fraction of less hygroscopic particles in a recent pollution episode

The Aitken mode is the dominant mode in terms of number concentration. The number of Aitken mode particles decreases with increasing Aitken mode diameter which indicates that coagulation plays a significant role in particle growth. A small and stable accumulation mode is present with a mean diameter of 250nm. It is not likely that this mode is produced by cloud processing, since few clouds were present over land during the ACE-2 measurement period. This conclusion is supported by the fact that the hygroscopic properties of particles at 250 nm differ from those of smaller particles. Less hygroscopic particles in this size range are present most of the time and account for approximately 25% of the particles, while they are virtually absent at diameters typical of the Aitken mode. This indicates that accumulation mode particles are probably directly emitted into the atmosphere and that combustion plays an important part in producing these particles.

3.1.3 Summary and implications for aerosol processes

This section gives a summary of important aerosol physical properties for the four air mass types introduced in section 3.1.1. Most of these aerosol properties have been discussed in some depth in the previous sections and are now compared more directly. Some additional aerosol properties are considered which are helpful to interpret the data.

Figure 3.13 shows a comparison of several important aerosol properties related to the size distribution: the total aerosol volume concentration, the geometric mean diameters of Aitken and accumulation mode, and the diameter that separates Aitken and Accumulation mode. The total aerosol volume concentration increases by a factor of 5 in the more polluted air masses from about 2 $\mu m^3 cm^{-3}$ to 10 $\mu m^3 cm^{-3}$. The total volume (shown in Figure 3.13(a)) concentration is similar in aged and recent pollution. The volume concentration shows the signature of pollution more strongly

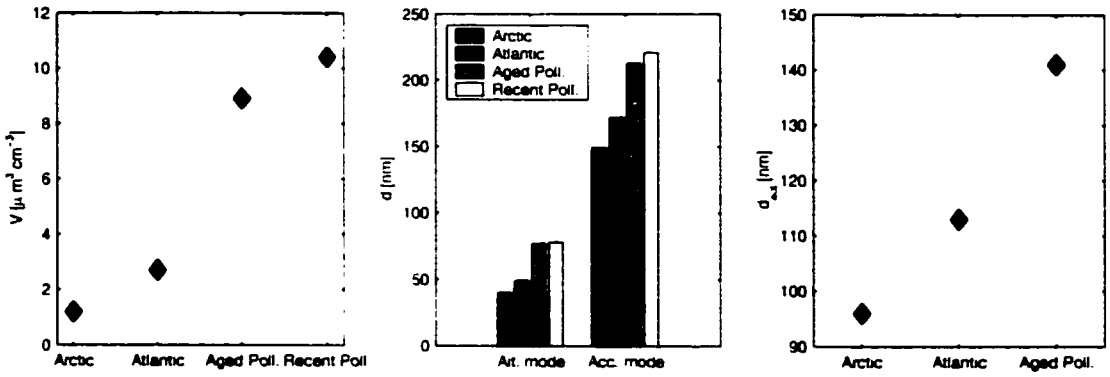

Figure 3.13: (a) Comparison of total volume concentration in different air mass types, (b) mean diameters of Aitken and accumulation mode, (c) mean diameter separating Aitken and Accumulation mode

than the total number concentration, which is often dominated by small particles that are mostly regional in origin. Figure 3.13(b) shows that the geometric mean diameters of both the Aitken mode and the Accumulation mode increase with the level of the pollution. The two main processes that increase the mean diameter of the aerosol particles are gas to particle conversion (in and out of cloud) and coagulation. Higher primary particle emissions in the industrial areas on the continent promote coagulation and the higher concentration of condensible gases in continental air masses makes gas to particle conversion more efficient. This explains the increase of accumulation and Aitken mode mean diameters with pollution observed in Sagres.

Figure 3.13(c) shows the diameter that separates the Aitken and Accumulation mode only for the Arctic and North Atlantic marine conditions and aged pollution, since it is unlikely that the accumulation mode in recent pollution is produced by cloud processing. The mean separation diameter increases from the very clean conditions in the Arctic air mass to the more polluted conditions. This could be an indication that the maximum supersaturation in cloud is reduced if a large number of particles is

available for activation. An increase in the activated dry particle diameter from 95 to 140 nm corresponds to decrease in the critical supersaturation from 0.15% to 0.09%, if the particle is composed of pure ammonium sulfate. However a crucial assumption in this estimate is that the large scale characteristics of the clouds and the structure of the marine boundary layer are similar in marine conditions and in cases of European outflow. The maximum critical supersaturation could be reduced by cloud processes that are independent of particle concentration, if for example the average updraft velocity in the stratus cloud deck were diminished in the European outflow air masses. Data of Snider and Brenguier (2000) do not suggest that updraft velocities in clean and polluted conditions are systematically different, but those measurements were taken only occasionally and usually not near the Portuguese coast. Chemical and growth factor measurements indicate that the fraction of soluble material is similar in clean conditions and aged pollution, which suggest that the increase in activation diameter is not caused by a change in particle chemical composition. The differences in the separation diameter indicate that the supersaturation in stratus clouds might be decreased by large particle concentrations, but do not provide conclusive evidence.

Figure 3.14 shows a summary of particle hygroscopic properties in different air mass types. In Figure 3.14(a) the more hygroscopic growth factors in recent pollution are compared to the more hygroscopic growth factors averaged over the three other air mass types, which are not significantly different. The fact that particle hygroscopic properties are similar in all air masses except in recent pollution suggests that they are indicative of the more recent history of the air mass and reflect regional characteristics of the aerosol. At small particle sizes of 35 and 50 nm the more hygroscopic growth factors are similar in all air mass types. In recently polluted air mass types the growth factors increase less with size than growth factors in the other air masses.

To eliminate the influence of the surface tension on the hygroscopic growth and to

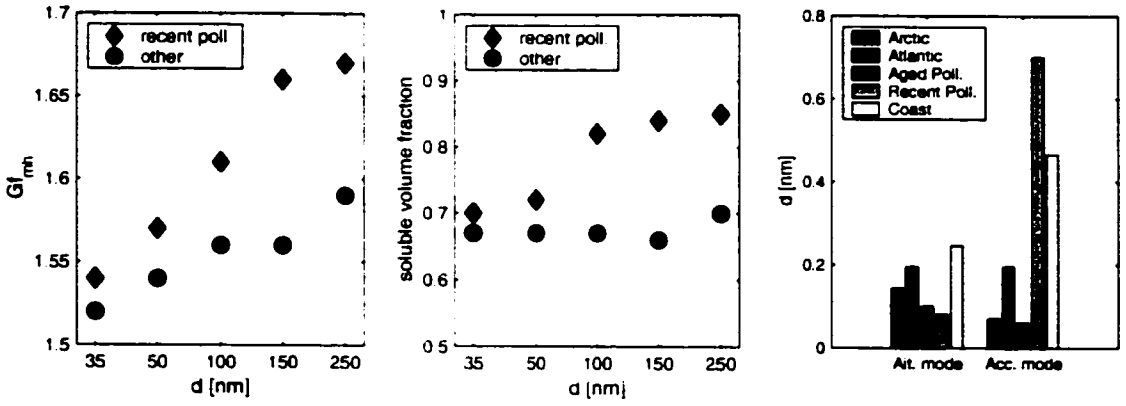

Figure 3.14: Particle hygroscopic properties in different air mass conditions: (a) More hygroscopic growth factors in Atlantic air mass conditions, Arctic air mass conditions and aged pollution (squares) vs. recent pollution (circles), (b) Soluble volume fractions in Atlantic air mass conditions, Arctic air mass conditions and aged pollution (squares) vs. recent pollution (circles), (c) Occurrence of less hygroscopic particles in different air mass conditions

compare the chemical nature of the particles more directly, soluble volume fractions are calculated using the procedure described in section 2.3.4. The hygroscopically active material is assumed to be ammonium sulfate. The soluble volume fractions are shown in Figure 3.14(b) as a function of particle diameter. Even in clean conditions none of the particles are completely soluble. On average their soluble volume fraction ranges from 0.7 to 0.85, which is lower than particles in Tenerife or over the Atlantic ocean measured by a ship (Swietlicki et al., 2000). The soluble volume fractions of the more hygroscopic particles in Sagres are probably lowered by the coagulation with less hygroscopic particles emitted by ships and other regional pollutants. These less hygroscopic particles are never found in measurements in Tenerife or on the ship. Particles in recent pollution have a soluble volume fraction that is almost independent of particle size, whereas in other air mass types the soluble volume fractions are increasing with size.

Figure 3.14(c) shows the abundance of less hygroscopic particles defined as the frequency of occurrence of lh particles multiplied by the number fraction of lh particles when present. The data are averaged over the Aitken and Accumulation mode size range for each of the four air mass types. To isolate the role of coastal pollution sources data that were previously eliminated from the Atlantic data set, because the air mass flows down the coast are now shown as an extra data point. The sizes included in each each mode were determined from the frequency distributions of the size distribution parameters presented in Section 3.1.2. The size range of the accumulation mode includes 150 and 250nm for marine air mass types, aged and coastal pollution and only 250nm for recent pollution. The size rage of the Aitken mode includes 35-100nm for Arctic air mass types, 50-150 nm for recent pollution and 50-100nm for other air mass types.

Less hygroscopic particles occur most frequently in recently polluted air masses types in the accumulation mode size range. This points to particle sources over the Iberian Peninsula that emit less hygroscopic particles preferentially at larger sizes around 250nm. Atlantic air masses and air masses characterized by coastal influence show similar levels of less hygroscopic particles at all sizes. Air mass back trajectories indicate that both air mass types spend an extended amount of time in the boundary layer near or at the coast which is contaminated by combustion emissions from the shipping lane. The two air mass types that spend the least amount of time near the shipping lane (aged and recent pollution) show very few less-hygroscopic particle in the Aitken mode size range. Less hygroscopic particles of all sizes are virtually absent in aged pollution, which is a strong indication that these air masses have not been in contact with land or any combustion sources for an extended time period before reaching Sagres.

3.2 Diurnal variations in the aerosol properties in Sagres

Section 3.1 shows that long range transport is one of the important factors that determine the physical properties of the aerosol in Sagres. This section focuses on the modification of the aerosol transported to Sagres by regional aerosol processes that have a characteristic diurnal time scale.

There are several factors that could cause diurnal variations in aerosol properties. A first factor is a diurnal variation in aerosol formation precesses. Photochemical reactions are important in atmospheric chemistry and many reaction that create aerosol particles including the formation of condensible precursor gases are driven by sunlight (e.g. Seinfeld and Pandis, 1998). Solar radiation has also been shown to promote particle nucleation in the planetary boundary layer Boy and Kulmala (2001). A second factor is a possible diurnal change in primary particle emissions from anthropogenic sources. This must be considered since the measurement site in Sagres is not in a remote location and can on occasion be influenced by sources along the coast. A third factor might be a land-sea breeze effect due to the location of Sagres on the coast. However the local wind direction never changes very strongly at Sagres coming mostly from the North and there are no drastic changes in the total aerosol size distribution that are correlated to a change in wind direction. During clean conditions the land breeze never gets strong enough to replace the marine aerosol with aerosol from inland and during recent pollution episodes the continental aerosol is never swept away by the sea breeze and replaced clean marine aerosol. If land sea-breeze changes have effects on the aerosol those are definitely secondary effects compared to the long range transport. A fourth factor might be vertical mixing driven by daytime heating.

Diurnal variations are found both in the size distribution and in hygroscopic properties of the aerosol and are especially pronounced in the aerosol properties that do

not vary strongly with long range transport: the number concentration of particles in the ultrafine and small Aitken mode and the hygroscopic growth factors. The diurnal variations in the aerosol size distribution are discussed in section 3.2.1, the diurnal variations of aerosol hygroscopic properties in section 3.2.2.

3.2.1 Diurnal variations in the size distribution

Diurnal variations in particle number concentration are most pronounced at the smallest particle sizes. This result can be expected since the production as well as the removal of particles with sizes smaller than 50 nm occurs on much shorter time scales than of particles in the Aitken and accumulation size range.

Figure 3.15 shows a time series of particle number concentration in the ultrafine, small Aitken, Aitken, and accumulation mode. The time series is shown for 5 consecutive days. The first two days (DOY 175 - 176) are characteristic of moderately polluted conditions. The remaining days of time period shown in Figure 3.15 (DOY 177-179) are more typical of marine air masses conditions with air mass back trajectories that originate over the Atlantic and the Arctic ocean.

Ultrafine particles (shown in Figure 3.15(a)) are present only sporadically during the day and are mostly absent during the night. On the two more polluted days a burst of ultrafine particles of limited duration appears during midday. On the later days ultrafine particles appear more irregularly and have much smaller number concentrations. Ultrafine particles are indicative of recent particle formation (nucleation events) in the atmosphere (e.g Boy and Kulmala, 2001; Birmili et al., 2000). These particles could be produced by binary nucleation involving sulfuric acid and water vapor, when the sulfuric acid concentrations are very high ($\sim$ 100 ppt) or by ternary nucleation involving sulfuric acid, ammonia, and water, when sulfuric acid concentrations are typical of marine or continental background conditions. Kulmala et al.

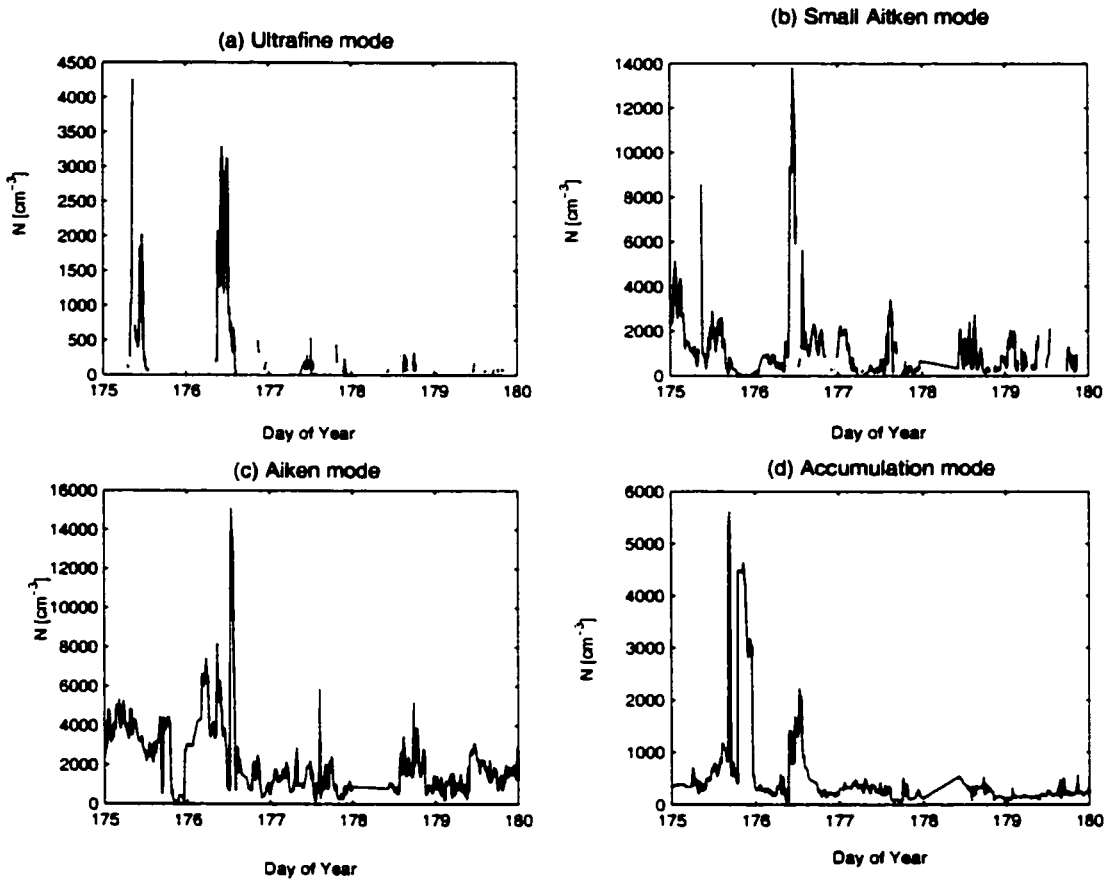

Figure 3.15: Time series of particle number concentration: (a) Ultrafine mode, (b) small Aitken mode, (c) Aitken mode, (d) Accumulation mode

(2000) suggest that ternary nucleation occurs continually during daytime and leads to a reservoir of of thermodynamically stable clusters with diameters smaller than 3nm. These clusters can grow to measurable sizes greater than 3nm when they are transported into an environment where additional condensible gases are available.

The diurnal variations at larger particle sizes are not as apparent as the diurnal variations of the number concentration of the ultrafine mode. Small Aitken mode particles appear more continuously than ultrafine particles. On DOY 176 both the small

Aitken mode and the ultrafine mode show a strong increase in number concentration during the same time interval, suggesting a similar source. The number concentration of Aitken mode particles seems more dominated by changes in air mass conditions than by diurnal variations. The number concentrations are clearly higher during polluted (DOY 175-176) than during clean (DOY 177-179) conditions. The accumulation mode number concentration shows a strong increase on DOY 176, whenever the Aitken mode almost disappears, indicating that on these occasions there is one dominant mode, whose mean diameter lies between typical Aitken and Accumulation mode mean diameters. This shows that the classification scheme presented in section 2.2.1 is not ideal for all possible size distributions. However cases like this one are rather infrequent.

The nucleation events in Sagres fall into three categories. A typical evolution of the particle size distribution for each category is shown in Figure 3.16 (a)-(c). The time of day is shown on the x-axis, particle diameter on the y-axis and the shaded contours show isolines of dN/dlog(d). A nucleation event of the first category is shown in Figure 3.16(a). An ultrafine mode with high number concentrations and a small mean diameter appears in the early morning. This mode subsequently grows to a mean diameter of about 50 nm within a few hours. A nucleation event of the second category is shown in Figure 3.16(b). The ultrafine mode is present for a few consecutive hours during daytime with no consistent growth in the mean diameter. A nucleation event of the third category is shown in Figure 3.16(c). Ultrafine particles appear sporadically in low number concentrations throughout the day. From the gas phase and meteorological parameters available for the Sagres measurement site, it is difficult to assess what causes the different kinds of particle nucleation. Events of the first kind are not necessarily tied to abnormally high SO_2 concentrations, and measurements of more direct particle precursors such as H_2SO_4 and ammonium are

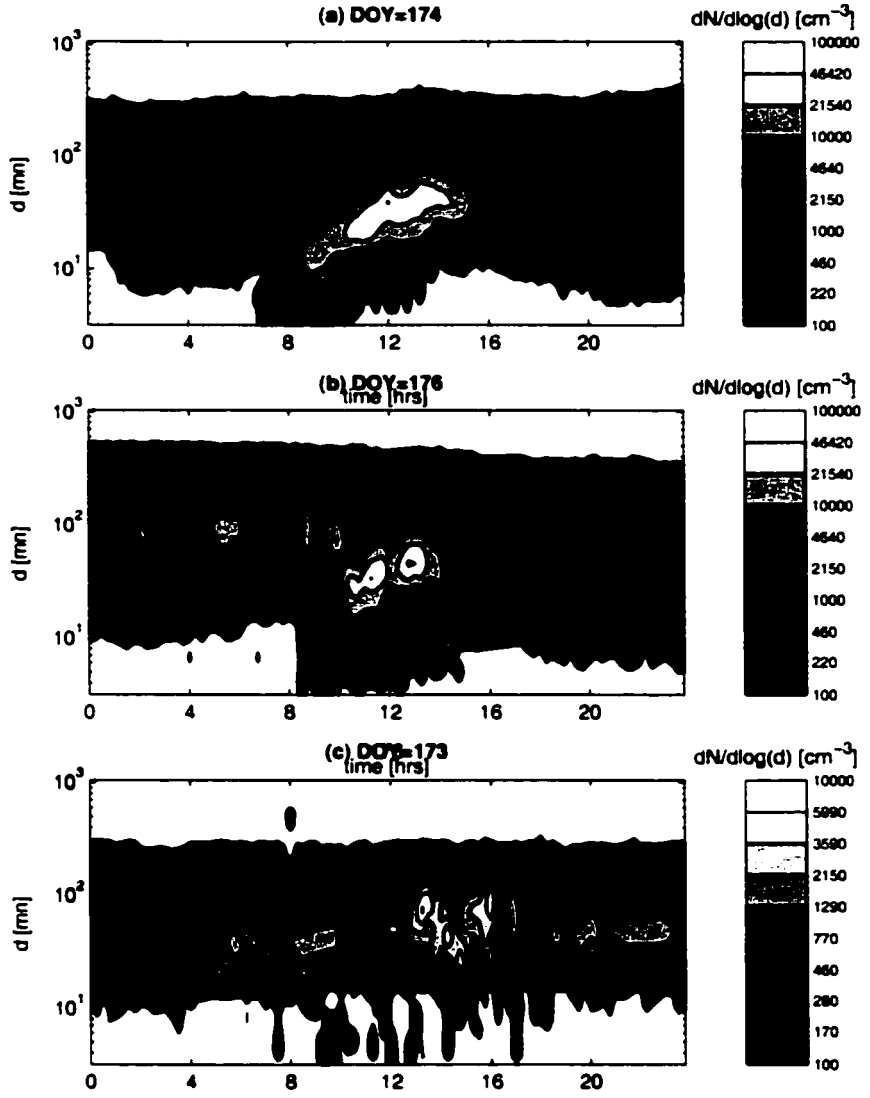

Figure 3.16: Typical cases of fine particle nucleation. The particle size distribution on three different days is shown as it changes with time of the day. (a) Case 1: burst of particle nucleation with subsequent growth of the particles to larger sizes, (b) Case 2: Particle nucleation over an extended time period without visible particle growth, (d) Case 3: Sporadic appearance of ultrafine particles

not available. However, the fact that ultrafine particle appear at least to some extent on almost every day of the ACE-2 measurement period, seems to support the theory by Kulmala et al. (2000) that particle nucleation occurs almost continuously in the atmosphere and that particle growth to detectable sizes under favorable conditions. Since not enough supporting measurement were made in Sagres during ACE-2 it is not clear how to define those 'favorable' conditions.

Figure 3.17 shows a daily composite of particle number concentrations in the ultrafine, small Aitken, Aitken, and accumulation mode. The day is divided into 2 hour time periods and the particle number concentrations measured during each time period are averaged for all days of the ACE-2 measurement period. These averages are shown with uncertainty bars that represent the 95% confidence intervals of the mean. If the particle number concentration was not influenced by diurnal processes, the data would lie on a horizontal line in the daily composite. However both the Ultrafine mode, the small Aitken mode and the Aitken most show a distinct peak in particle number concentration during several hours of the day. The number concentration of ultrafine particles is small during most of the day except during the time period between 6am and noon. The first ultrafine particles appear between 6 and 8am in the morning shortly after sunrise, which suggests that they grow quite rapidly from the size of small stable clusters less that 3nm to detectable sizes. On average the number concentration of ultrafine particles reaches a maximum between 8 and 10 am and then declines to low values in the afternoon. Particles in the ultrafine size range below 10 nm are formed preferably in the morning hours and slowly disappear in the afternoon. They either grow to sizes lager than 10nm by vapor deposition or self-coagulation or they simply are removed by coagulation with larger particles. No significant new particle formation takes place in the afternoon.

The small Aitken mode particles show a similar pattern, their average concen-

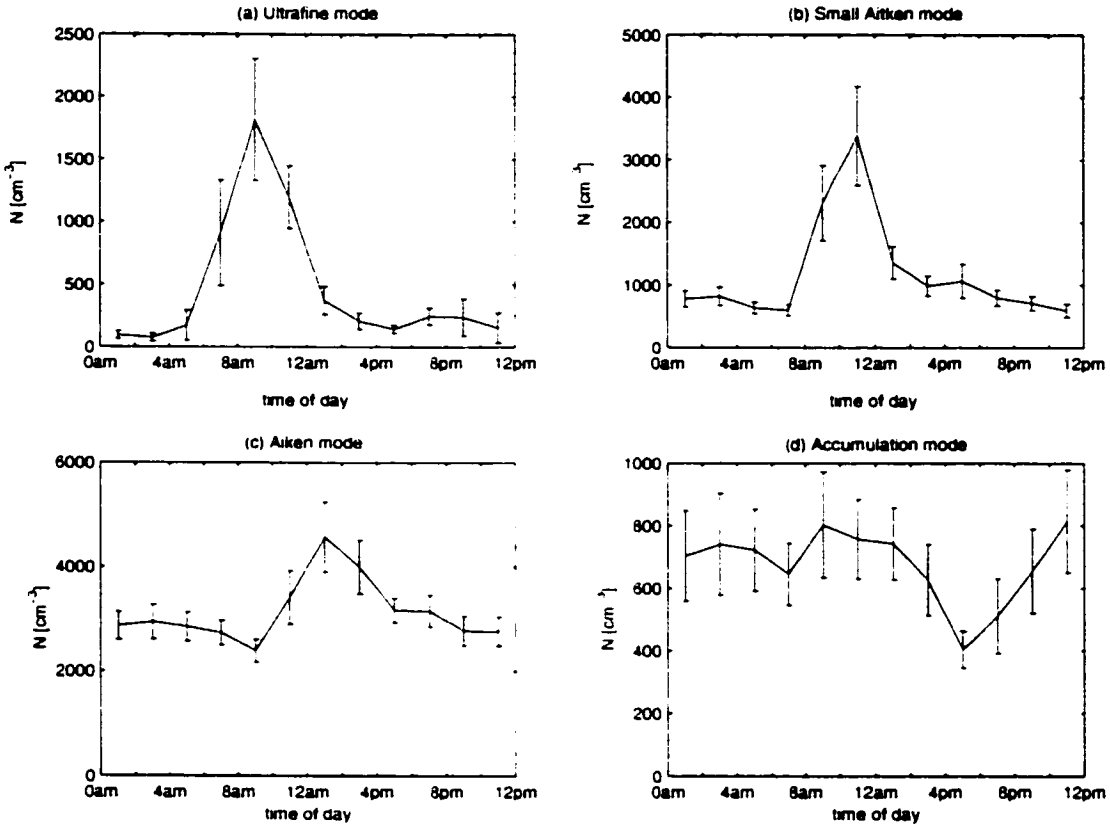

Figure 3.17: Daily variation in particle number concentration averaged over the entire ACE-2 measurement period: (a) number concentration of particles in the ultrafine mode, (b) number concentration of particles in the small Aitken mode, (c) number concentration of particles in the Aitken mode, (d) number concentration of particles in the Accumulation mode

trations are stable around 1000 cm^{-3} for most of the day, but become three times as high between 10am and noon. The first small Aitken mode particles appear later than the first ultrafine particles and the number concentration of the small Aitken mode peaks one to two hours later than the number concentration of the ultrafine mode. It can be concluded that a significant part of small Aitken mode particles is

probably formed by nucleation further upwind of Sagres than the ultrafine particles and grows the mean diameters larger than 10nm during the transport to Sagres. The diurnal composite of Aitken mode particle number concentrations shows that a baseline of about 3000 cm^{-3}, indicating that a significant fraction of particles is present independently of diurnal processes. However superimposed on that baseline is a peak between 10am and 4am. During this time period average particle concentrations increase to up to 4500 cm^{-3}. The additional particles appearing during this time period can be attributed to nucleation and subsequent particle growth. The accumulation mode particles show no comparable diurnal variation. There is a decrease in particle number concentration between 4 and 6 pm that is statistically significant, but hard to explain with any aerosol or meteorological processes, that could be investigated with our ACE-2 data base.

Figure 3.17 indicates that the daily variations in ultrafine, small Aitken and Aitken mode particles are largely due to particle nucleation and subsequent particle growth. In contrast particle nucleation does not seem to have a strong influence on Accumulation mode number concentrations. To test this hypothesis lagged cross correlation coefficients are calculated for time series of Aitken, small Aitken, and ultrafine particle number concentrations. The time series are constructed by linearly interpolating the measured data points to equally spaced times separated by intervals of 15 minutes. Missing data are replaced by linear interpolation of adjacent data points. The lagged cross correlation coefficients are calculated by correlating the number concentration of smaller particles with the number concentrations of larger particles at either earlier or later time periods. Figure 3.18 shows the results of these calculations. The time lag between the time series of particle number concentrations is shown on the x-axis. Positive lag values correspond to cases where the concentration of smaller particles is correlated with the concentration of larger particles measured at later times. Nega-

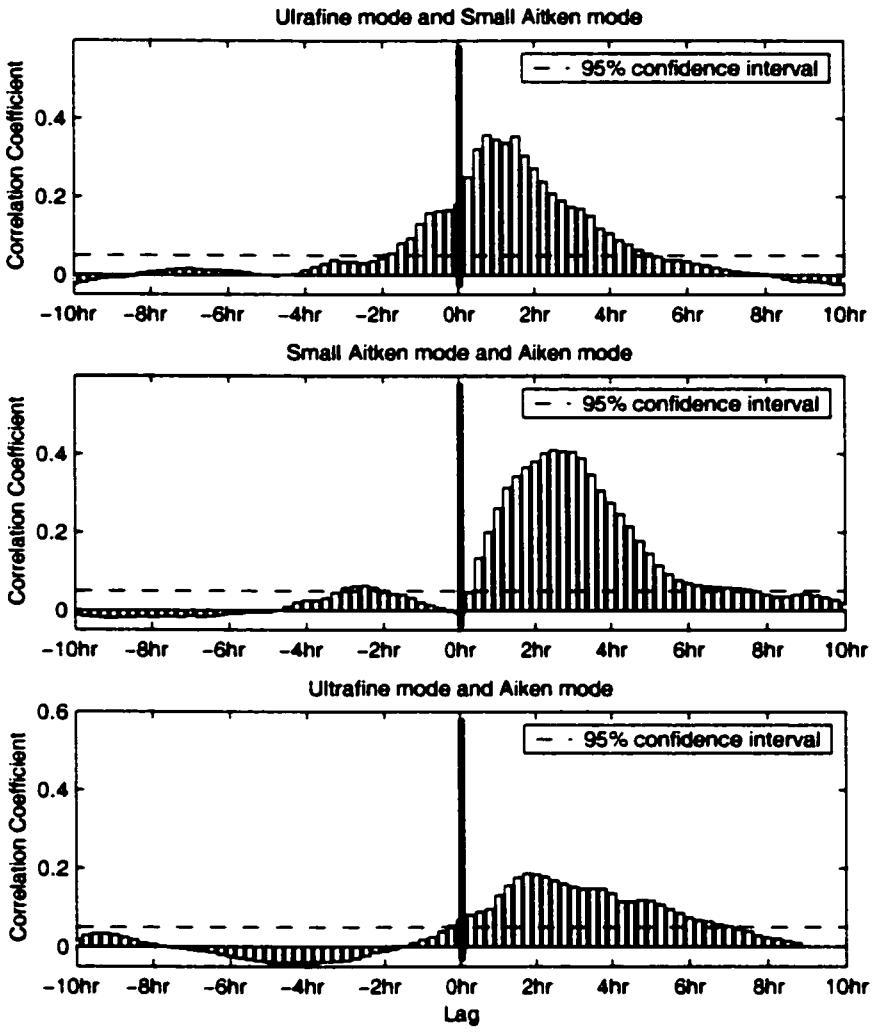

Figure 3.18: Lagged cross correlation coefficients for time series of particle number concentration: (a) correlation of ultrafine mode with small Aitken mode number concentration, (b) correlation of small Aitken mode with Aitken mode number concentration, (c) correlation of ultrafine mode with Aitken mode particles.

tive values correspond cases where the concentration of smaller particles is correlated with the concentration of larger particles measured at earlier times. The vertical

solid line delineates a lag of 0 hours, or the instantaneous cross correlation coefficient of the two time series. The horizontal dashed line indicates the level at which the correlation coefficient is significantly different from 0 at the 95% confidence level.

Figure 3.18 shows that the correlation coefficients increase when concentrations of smaller particles are correlated to concentrations of larger particles measured several hours later. Number concentrations of the ultrafine and the small Aitken mode (Figure 3.18 (a)), show some significant correlation around a lag time of 0 hours, but the correlation coefficient almost doubles at a lag time of approximately 1-2 hours. High number concentrations of ultrafine particles are followed by high number concentrations of small Aitken particles approximately 1-2 hours later. The small Aitken and Aitken mode number concentrations are uncorrelated when measured at the same time. The correlation coefficient is highest at a lag time of approximately 2-3 hours and decreases gradually till it becomes statistically insignificant at a lag time of 6 hours. Even the ultrafine and the Aitken mode are correlated at lag times greater than 0, albeit quite weakly as shown in Figure 3.18 (c).

The correlation coefficients shown in Figure 3.18 are not very high, explaining less than 25% of the variance of the data sets. However high correlations cannot be expected in this situation since diurnal fluctuations only explain some fraction of the variance in the number concentration of each mode. The part of the those short term variations of one mode that is correlated with the short term variations of another more is even smaller. Moreover the fact that the ultrafine mode is present only sporadically, whereas the small Aitken mode and Aitken mode are present more continuously will deteriorate the correlation. The small but statistically significant correlations are consistent with the fact that particle nucleation in the morning hours and subsequent particle growth impose a diurnal signature on the aerosol transported to the Sagres site, raising first the ultrafine particle number concentration, then the

small Aitken and finally the Aitken mode number concentration. The diurnal variations are more important for smaller particles than for larger particles.

3.2.2 Diurnal variations in hygroscopic growth factors

In section 3.1 it was shown that the more hygroscopic growth factors (Gf_{mh}) do not vary strongly between different air mass conditions. The only exception is a decrease in Gf_{mh} when the aerosol is transported from inland during recent pollution episodes. However a time series of more hygroscopic growth factors shows considerable variance at shorter time scales. This is shown in Figure 3.19. The time series for different

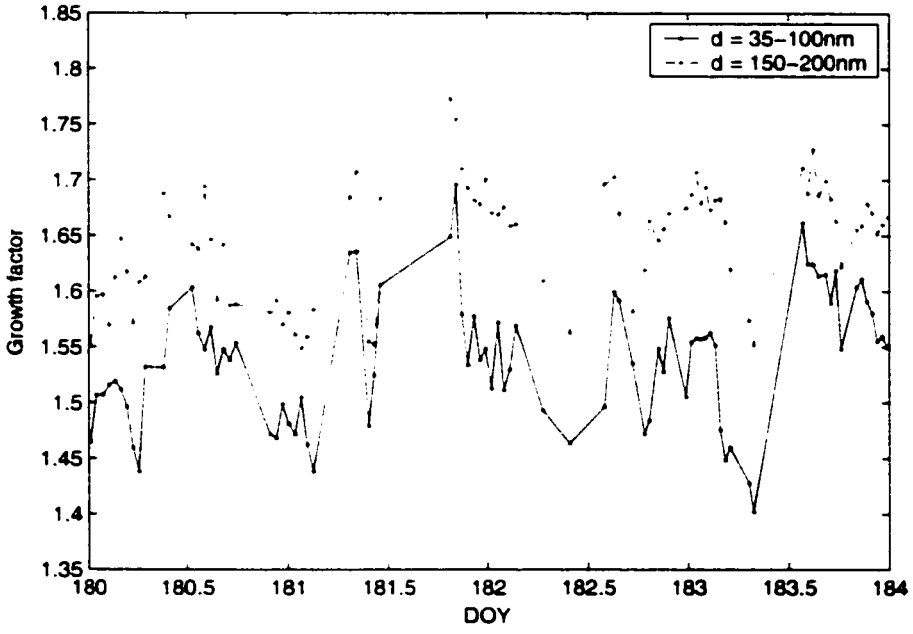

Figure 3.19: Time series of more hygroscopic growth factors showing three consecutive days. The average growth factors of 35 and 50 nm particles are connected by a solid line and the average growth factors of 100, 150 and 250 nm particles are connected by a dashed line

particle size are very similar and highly correlated. For example variations average growth factors for small (35 and 50 nm) and the average growth factors for larger particles (100 - 250 nm) as shown in Figure 3.19 track each other quite well.

There is a characteristic diurnal cycle to the variation in more hygroscopic growth factors. This is shown in Figure 3.20(a), which shows a daily composite of more hygroscopic growth factors for the whole ACE-2 measurement period. Since the pattern is very similar for all particle sizes the more hygroscopic growth factors have been averaged for all particle sizes (35-250nm).

The vertical lines show the average time of sunset and sunrise during the ACE-2 measurement period in Sagres. It can be seen that during daytime the more hygroscopic growth factors increase and decrease in a sinusoidal fashion similar to the amount of solar radiation, approximated in Figure 3.20(e) by the solar elevation angle for Sagres at this time of the year. This could be explained by the fact that photochemical processes add soluble material to the particles during daytime. If this is the case the intensity of solar radiation seems a controlling factor for that process. The uptake of soluble material into the aerosol particles increases during the morning hours and peaks around one pm, even though temperature increases as well, which makes condensation more difficult. SO_2 concentrations are more variable during the day, but do not show a statistically significant diurnal variation. However increased mixing could also influence the aerosol properties during daytime hours.

After the more hygroscopic growth factors reach a minimum near sunset around 7pm, they rise quickly again and then slowly decrease during the night. This pattern is repeated on almost every day, but it is difficult to explain in terms of known aerosol processes. It might reflect a pattern in local or regional emissions. Less particles of medium hygroscopicity be emitted during evening hours. If those particles are normally included among the more hygroscopic ones, this would raise the more

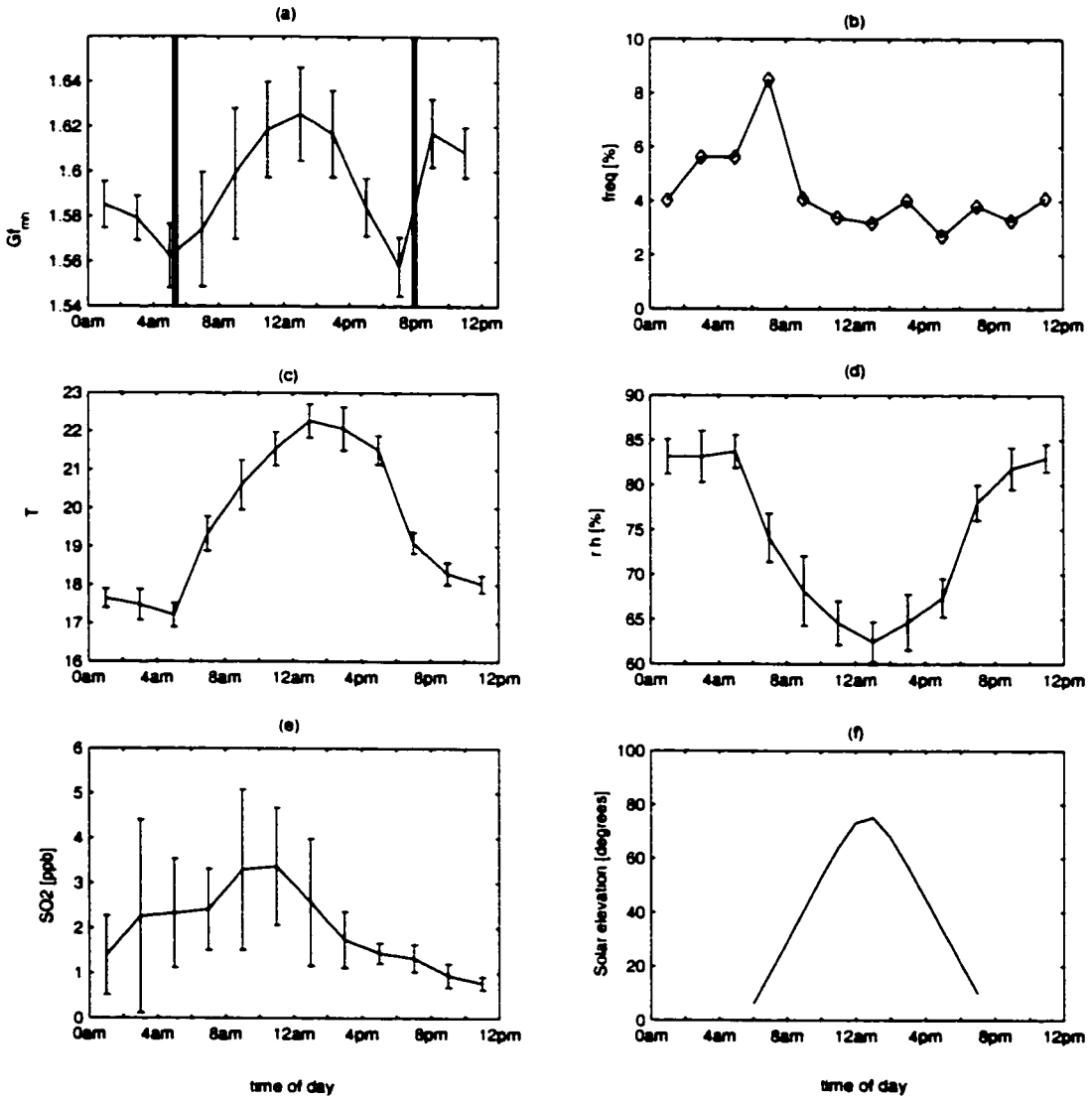

Figure 3.20: Daily composites of (a) more hygroscopic growth factors, (b) abundance of less hygroscopic particles (defined in section 3.1.3), (c) Temperature, (d) relative humidity, (f) SO_2 concentration, and (e) solar elevation angle

hygroscopic growth factor on average. However no conclusive explanation for the increase in more hygroscopic growth factors in the early evening can be given so far.

3.3 Summary

The aerosol number concentration in Sagres during ACE-2 is determined by different processes at different particle sizes. The number concentration of small particles with sizes less than 40nm in seems to be dominated by regional processes with strong diurnal influence and not by large scale air mass characteristics. On the contrary, number concentrations of particles in the Accumulation mode size range (larger than 100nm) show no characteristic diurnal variations and are mostly determined by long range transport. The number concentration of particles at intermediate size ranges are controlled by both long range transport and diurnal variations. The shape of the size distribution changes during pollution outbreaks from the European continent. In marine conditions a clearly separated Aitken and accumulation mode can be observed. Pollution outbreaks that reach Sagres from Northern Europe after approximately two days of aging show a size distribution in which the mean diameters of both Aitken and accumulation mode are larger than in marine conditions and the modes are not as clearly separated. In recent pollution originating on the Iberian Peninsula the size distribution is dominated by a large Aitken mode with a mean diameter of approximately 80nm. The accumulation mode in recent pollution is probably not due to cloud processing, but more likely to direct emission into the atmosphere.

There is evidence of particle nucleation on almost every day during the ACE-2 experiment. Particle nucleation happens mostly during daytime hours, when solar radiation is available. Nucleation events characterized by high ultrafine particle number concentrations are only observed in the morning hours, shortly after sunrise, but ultrafine particles can appear in small quantities throughout the day. This seems further evidence for the hypothesis of Kulmala et al. (2000), that nucleation of clusters, below detectable size occurs continually during daytime hours and that those clusters can grow to detectable sizes if conditions are favorable. The fact that no

nucleation events with high particle number concentrations occur later in the day, although SO_2 concentrations can be quite high occasionally, seems to indicate that solar radiation and the availability of condensible gases is not sufficient for particle growth to detectable sizes. Another meteorological parameter, such as high relative humidity or low temperatures might be required for the production of ultrafine particles. However this issue must remain somewhat inconclusive due to the lack of gas phase measurements of other chemical species such as H_2SO_4 or NH_3.

Particle hygroscopic growth factors show some diurnal variation as well. This variation seems to be connected to the intensity of the solar radiation reaching Sagres. Aerosol particles below 250 nm are not completely soluble, even in Arctic and Atlantic marine air mass conditions. In recent pollution the soluble volume fraction is slightly lower than in the other air mass conditions. Less hygroscopic particles at small particle sizes below 50nm seem to be caused by ship traffic along the coast. This agrees well with measurements of particle size distribution and chemical composition in exhaust plumes of several ships by Hobbs et al. (2000). Less hygroscopic particles at sizes larger than 100nm are probably mostly caused by pollution sources on land.

Chapter 4

AEROSOL NUMBER TO VOLUME RATIOS

Chapter 3 summarizes fundamental aerosol properties in Sagres in terms of both long term variability governed by air mass history and short term variability governed by regional emissions and daily variations in aerosol processes. The number-size distribution and hygroscopic growth are aerosol properties that can be more directly linked to aerosol sources and transportation processes but those properties are not directly related to the direct and the indirect forcing of aerosols on climate. In this chapter as well as in the following chapters aerosol properties are derived that are more useful in the context of the influence of aerosols on climate. One of those aerosol properties is the number to volume ratio of the aerosol (R). The relationship between number and volume concentration of the aerosol in the submicron size range is important for modeling the aerosol radiative forcing of climate. Large scale or global chemical models are usually formulated in terms of aerosol mass. However estimating the direct and especially the indirect effect of aerosols on climate requires information about the submicron particle number concentration. Empirically determined number to volume ratios of the submicron aerosol are the key parameter to link aerosol mass to aerosol number concentration.

To address the indirect effect of aerosols on climate it is not the total number concentration that is important, but only the number concentration of aerosol particles that are likely to become cloud droplets. Marine stratus clouds are considered of special importance to the indirect effect of aerosols on climate. They cover large fractions

of the worlds ocean and usually form in areas where the background aerosol concentrations are low, which makes the cloud albedo sensitive to an increase in particle number concentration. At supersaturations typical for marine stratus cloud droplets usually nucleate on particles greater than 70-120nm. In this context it is necessary to estimate the number concentration of particles larger than a certain diameter (d_c) from the submicron aerosol volume. In this study the value assigned to d_c is 90nm, so that R is calculated as the number of particles with diameters greater than 90nm divided by the total submicron aerosol volume. This cut-off diameter is consistent with the location of the minimum between Aitken and accumulation mode in marine air mass conditions in Sagres during ACE-2. As explained in the previous section, this minimum is usually attributed to cloud processing of aerosol and is a measure of the minimum size of the particles particle that are activated to cloud droplets.

Number to volume ratios of the aerosol over the Atlantic ocean have been studied in the past (e.g. Hegg and Kaufman, 1998; Hegg and Jonsson, 2000; Hegg and Russel, 2000; VanDingenen et al., 2000, and references therein). However the definition of R in all these studies is not strictly the same. In the first three studies the aerosol size distribution is measured using a passive cavity spectrometer manufactured by PMS Inc. This instrument measures particles in the diameter range from 120nm to 3μm. Thus R is calculated as the number of particles greater than 120 nm divided by the volume of particles between 120nm and 3μm. On the other hand VanDingenen et al. (2000) calculate R as the number concentration of particles between 80 and 700nm divided by the volume of particles smaller than 700nm due to the upper cutoff of their instrument. The numerical values of R derived in those studies and this work are thus not strictly comparable. Since Hegg et al. use larger cut-off diameters their values of R can on average be expect to be lower than than the values derived here. The the lower cut-off diameters of VanDingenen et al. (2000) should result in somewhat

higher number to volume ratios.

In past studies long term averages of R have been found to be surprisingly constant (e.g. Hegg and Jonsson, 2000; Hegg and Russel, 2000, and references therein). But over shorter time periods Hegg and Russel (2000) found that R can be quite variable, especially in clean conditions. Some studies indicate that the relationship between submicron aerosol number and volume is approximately linear (Hegg and Kaufman, 1998). The studies by Hegg and Kaufman (1998); Hegg and Jonsson (2000); Hegg and Russel (2000) also suggest that R is, if not constant, at least surprisingly confined. This confinement has been used to draw conclusions about possible processes that determine the aerosol size distribution over the Atlantic. Assuming that the size distribution of the aerosol is lognormal Hegg and Russel (2000) inferred that a constant R of 200 μm^{-3} implies a relationship between mean diameter and standard deviation that is consistent with condensational growth as the main process acting on the size distribution. VanDingenen et al. (2000) find that a simple analytical model for the relationship between submicron aerosol number and volume can explain observed number to volume ratios and especially the dependence of R on aerosol volume. The calculated number to volume ratio is mostly governed by entrainment and coagulation, which suggests in contrast to the results of Hegg and Russel (2000) that these two processes mostly determine the aerosol evolution over the Atlantic.

This chapter offers some theoretical considerations to explain in general terms why the R would be loosely constrained between lower and upper limits. However although the longterm averages of the number to volume ratios measured in Sagres are consistent with values found in previous studies, there is considerable variability in the number to volume ratios. This variability can in some cases be explained in terms of possible sources and processes that act on the aerosol and it can be parameterized for each air mass type.

4.1 *Number to Volume ratios of lognormal size distributions*

The number of aerosol particles larger than a cutoff size of around 100nm and aerosol submicron volume are often found to be linearly related as would be expected if the size distribution were invariant. This linear relationship is most noticeable when the aerosol is sampled on time scales of several hours within a particular air mass, since a change in air mass history tends to destroy such correlations. The linear relationship between number and volume of the aerosol seems surprising at the first glance since the aerosol number concentration is usually dominated by small particles that contribute little to the aerosol volume, whereas the volume size distribution peaks at larger sizes, where particles contribute little to the total number concentration. It is not immediately obvious, why particles at sizes that determine the aerosol number concentration should be linearly related to larger particles that account for most of the aerosol volume. However there are several factors that make a linear relationship more plausible. First, most of the studies that investigate number to volume ratios take into account only particles that are larger than 80-120nm. The highest and most variable particle concentrations occur around 30-70nm (as has been shown in chapter 3) and are thus not influencing the number to volume ratios as defined above. For the limited size range considered here it is more plausible that aerosol number and volume concentration are correlated. Second, in Chapter 2 and Chapter 3 it has been demonstrated on various examples that aerosol size distributions measured in Sagres during ACE-2 have often lognormal shape.

For a lognormal size distribution the number of particles greater than d_c is related to the total particle volume as follows:

$$N(d > d_c) = \frac{6 \cdot V_{tot}}{\pi \cdot d_g^3 \exp\left(9/2 \cdot \ln {\sigma_g}^2\right)} \left(\frac{1}{2} - \frac{1}{2} \cdot erf\left(\frac{\ln\left(d_c/d_g\right)}{\sqrt{2} \cdot \ln \sigma_g} \right) \right), \qquad (4.1)$$

where V_{tot} is the total particle volume concentration, d_g the mean diameter, and

σ_g the standard deviation of the distribution. erf is the so called Error function, obtained by integrating a lognormal size distribution. If the parameters d_g and σ_g do not change considerably over the time period during which measurements are made a linear relationship between particle number and volume can be expected. However over longer time periods d_g and σ_g are expected to vary. A constant number to volume ratio can only be realized if the mean diameter and standard deviation of the size distribution depend on each other in such a way that would make Equation 4.1 constant. Since there is no physical reason for this functional dependence, the number to volume ratio should at least be somewhat variable depending on the mean particle diameter and the standard deviation of the size distribution. The dependence of R on the parameters of a lognormal size distribution is shown in Figure 4.1.

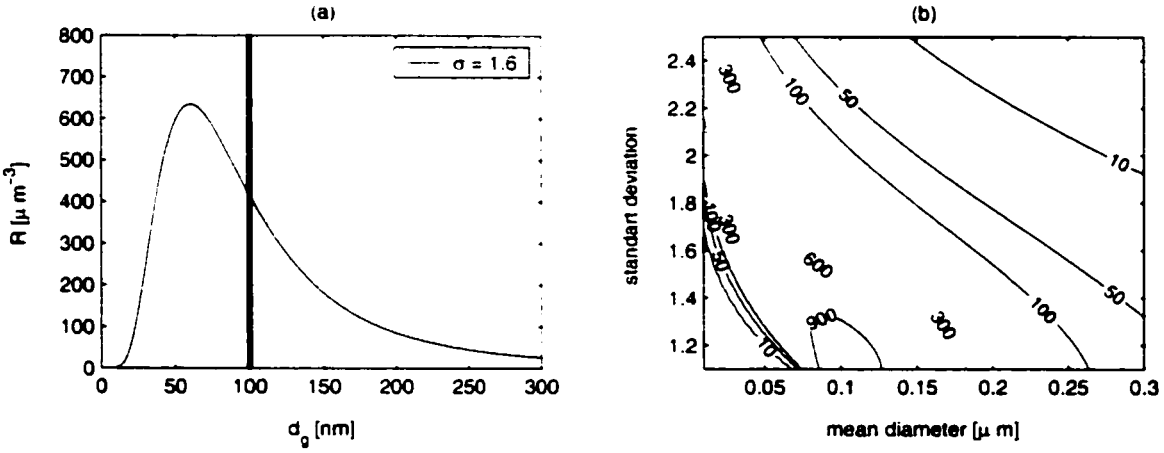

Figure 4.1: Number to Volume ratio (R) of a lognormal distribution: (a) Dependence of R on the geometric mean diameter d_g. The cutoff diameter d_c is shown as a dotted line. (b) Contour plot showing the range of R for lognormal size distributions with mean diameters d_g between 10 and 300nm and geometric standard deviations σ between 1.2 and 2.5. The cutoff diameter d_c is 90 nm.

Figure 4.1(a) shows the dependence of R on the mean diameter of the lognormal

distribution. R is low if the mean diameter is considerably smaller than d_c. In this case only the tail of the lognormal distribution lies in the size range greater than d_c. R increases with mean diameter because the number concentration of particles exceeding 90nm increases more strongly than the total volume concentration as the mean diameter approaches d_c. R reaches a maximum in the vicinity of d_c and then starts to decline. In this regime the increase in d_g increases the total volume concentration more strongly than the number of particles whose diameters exceed 90nm. In Figure 4.1(b) this analysis is generalized for a whole range of size distribution parameters. This figure shows a contour plot of the range of R for possible combinations of d_g and of σ_g. The number to volume ratio of lognormal size distributions with d_g between 10 and 300 nm and σ_g ranging from 1.2 and 2.5 can vary between 10 and 1000 μm^{-3}. The increase in R with increasing diameter for small particle sizes and the decrease at larger particles size is evident regardless of standard deviation of the size distribution. However the location of the maximum shifts to smaller particle diameters with increasing standard deviation. For mean diameters larger than d_c, R decreases with increasing standard deviation since an increase in σ_g shifts more particles to larger sizes where they contribute more strongly to the volume concentration. For mean diameters smaller than d_c the dependence of R on σ is more complex.

The assumption that the particle size distribution has lognormal shape implies the existence of an upper limit to possible values of R. This maximum (R_{max} is shown in Figure 4.2 as a function of σ_g for several possible cutoff diameters d_c. The maximum possible R decreases with increasing standard deviation as well as with increasing cut off diameter. The values of the standard deviation encountered during the ACE-2 experiment in Sagres are mostly between 1.3 and 2. The curve corresponding to the cut off diameter d_c of 90nm used in this study is shown as a bold line indicating that values of R smaller than approximately 1000 μm^{-3} should be expected. The

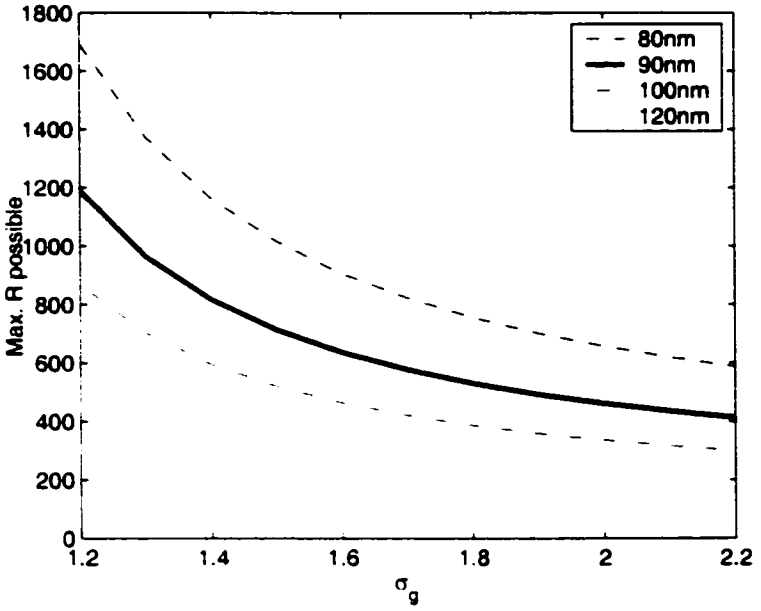

Figure 4.2: Upper limit of R for a lognormal size distribution as a function of geometric standard deviation σ_g. The line styles correspond to different cutoff diameters d_c

dependence of the maximum value of R on d_c is quite pronounced. A cut-off diameter of 120nm limits the number to volume ratio to values below 500 μm^{-3},as long as the size distribution is close to lognormal.

If in reality R is found to be more constrained than can be explained by the upper limit based on the assumption of a particular size-distribution, then some compensating factors have to be taken into account. One possibility is an inverse dependence of σ on d_p as suggested by Hegg and Russel (2000). From Figure 4.1(b) it can be seen that if the standard deviation of the size distribution decreases as the mean diameter increases R can be confined or even held constant over large ranges of mean diameters.

4.2 Observed number to volume ratios in Sagres during ACE-2

In this section actual observations of R in Sagres during the ACE-2 measurement period are discussed. The average number to volume ratio during the ACE2 field experiment in Sagres is $220 \pm 80 \mu m^{-3}$. This is somewhat higher than the number to volume ratios found by (Hegg and Jonsson, 2000; Hegg and Russel, 2000; Hegg and Kaufman, 1998). However due to different methods for calculating R the numerical values of R are not strictly comparable. The larger cut-off diameters for N and V used in those studies lowers the particle number concentration and at the same time increases the particle volume concentration, thereby reducing R. One other reason for the relatively high mean number to volume ratio measured in Sagres is the proximity of pollution sources. For several days during the ACE-2 field the air masses crossed the Iberian Peninsula before reaching Sagres from inland. These air masses brought relatively recent pollution from inland to the measurement site. During these polluted time periods R is significantly higher ($\bar{R} = 340 \pm 50 \mu m^{-3}$) than during time periods not influenced by recent pollution ($\bar{R} = 190 \pm 70 \mu m^{-3}$). R is particularly low in air masses containing aged pollution ($\bar{R} = 170 \pm 30 \mu m^{-3}$). This dependence of R on the air mass history suggests that generally number to volume ratios are quite high (around 350 μm^{-3}) near pollution sources . After the aerosol ages for a few days over the Atlantic, R decreases quickly to background values while both the total number and the total volume are still significantly higher than in background conditions. R seems to relax much more quickly to background conditions than either number or volume concentration of the aerosol.

Figure 4.3 shows a summary of number, volume and R for the entire measurement period. Data points during recent pollution episodes are shown in red and all other data are shown in blue. If time periods of recent pollution are neglected the aerosol number and volume concentration seem to be linearly related as can be seen in Figure

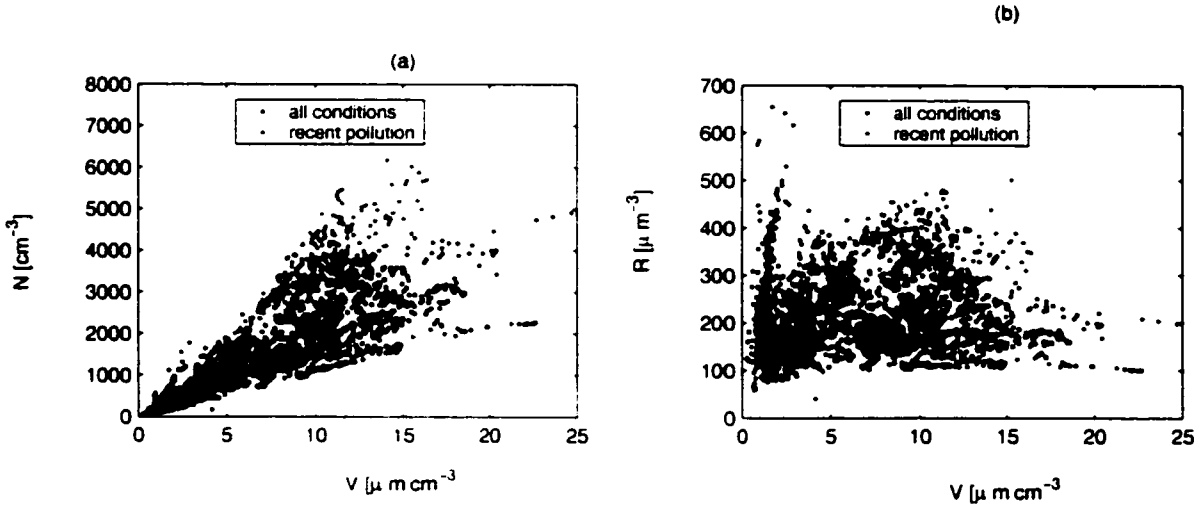

Figure 4.3: Number to volume ratios in Sagres, with data sampled during recent pollution time periods marked in red. (a) Number concentration of particles greater than 90nm vs. submicron aerosol volume concentration. (b) R as a function of submicron particle volume concentration.

4.3(a). The coefficient of determination is relatively high (R^2=0.8). The stronger increase of number concentration in recent pollution (red points) seems to suggest a nonlinear relationship, since a nonzero intercept is not physically meaningful. In recent pollution the dependence of aerosol number on aerosol volume seems to have a steeper slope.

Figure 4.3(b) shows the dependence of R on the submicron aerosol volume concentration. This figure gives a good estimate of the variability of R. In clean conditions characterized by volume concentrations smaller than 5 μm^3 cm^{-3} R is highly variable. This is due occasional influence of coastal pollution that is mixed into the background air mass, as discussed in section 3. These episodes of coastal pollution occurred occasionally throughout the whole ACE-2 campaign when air mass back trajectories were close to the coast. But they affected R mostly during clean conditions, when the

number concentration of the marine background aerosol transported to Sagres was low. These episodes of regional pollution were excluded from further analysis within the marine data sets.

In more polluted conditions characterized by volume concentrations larger than 5 $\mu m^3\ cm^{-3}$ most of the number to volume ratios higher than $300 \mu m^{-3}$ can be explained by air mass back trajectories from inland. If those cases of recent pollution are neglected R is confined between 100 and 300nm. This is a much narrower range than suggested by Figure 4.1(b). This suggests that either particle the size distribution is almost invariant throughout the ACE-2 experiment or that there is a compensating relationship between mean diameter and standard deviation of the size distribution, as suggested by Hegg and Russel (2000). The first hypothesis is rejected by the analysis on chapter 3. The second hypothesis will be investigated in the following sections. Since correlations between aerosol parameters tend to be destroyed by air mass shifts, the data will be analyzed according to the four main air mass types introduced in chapter 3. This will also help to explain and parameterize the remaining variability in R.

4.2.1 Number to Volume ratios in Marine air mass types

Marine air mass types are characterized by air mass back trajectories from the Arctic or Atlantic ocean. In those marine conditions the number to volume ratios are around 200 μm^{-3} which is comparable to the average number to volume ratio in Sagres. However as could be seen in Figure 4.3 (b) R is quite variable. The reasons for this higher variability are investigated in this section.

Typical size distributions of the aerosol in Arctic and Atlantic air mass conditions are shown in Figure 4.4. The dotted line indicates the 90nm cut-off size used for calculating the number to volume ratios (R). Both size distributions have a typical

Figure 4.4: Size distributions typical for marine air mass types: (a) number size distribution in air masses originating over the Atlantic, (b) corresponding Atlantic volume size distribution, (c) number size distribution in air masses originating over the Arctic, (d) corresponding Arctic volume size distribution

'marine' appearance: a bimodal distribution with a minimum around 100nm. Figure 4.4(a) shows that in Arctic air mass conditions the Aitken mode particles do not contribute very much to the particle number above 90nm. However in Atlantic air mass conditions the Aitken mode has larger mean diameters and a tail of Aitken mode particles extends to particle sizes above 90nm. In both cases the Aitken mode particles do not account for a significant fraction of the total aerosol volume as can be seen in Figure 4.4(b) and (d). The tail of the sea salt mode that is apparent in the volume size distribution contributes to the total submicron volume. However this part of the total volume is not very variable during Arctic and Atlantic air mass conditions. It can thus be expected that R is mostly determined by the number to volume ratio of accumulation mode particles, with occasional increases in the number concentration of particles larger than 90nm (N90) due to an increase in the diameter or the number concentration of the Aitken mode.

Figure 4.5 explores the relationship N90 and submicron particle volume. It further shows that in marine conditions R itself is dependent on the particle number concentration. The time periods when the air mass is influenced by regional pollution have been excluded from the data set, which makes the number to volume ratio less variable than in Figure 4.3. Figure 4.5(a) shows that in Arctic air mass types there is not a clear linear relationship between the number concentration of particles larger than 90nm (N90) and submicron particle volume. Most of the correlation between the data points results from the outliers with number concentrations greater than

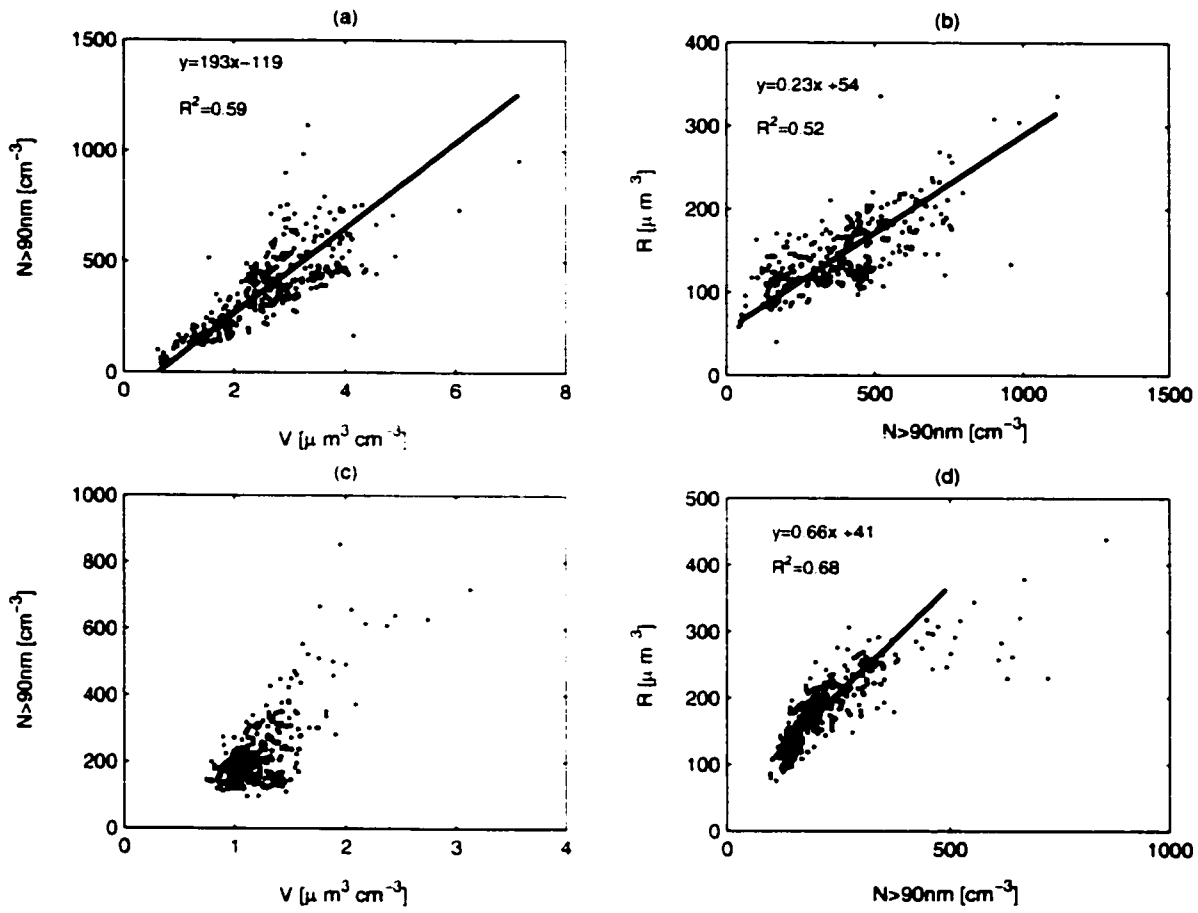

Figure 4.5: Number to volume ratios in marine air mass types: (a) the number concentration of particles larger than 90nm vs. submicron particle volume in air masses originating over the Arctic (b) R as a function of the number concentration of particles larger than 90nm. (c) the number concentration of particles larger than 90nm vs. submicron particle volume in air masses originating over the Atlantic (d) R as a function of the number concentration of particles larger than 90nm

500 cm^{-3}, which are mostly due to a strong increase in Aitken mode number concentration. The variability of N90 increases with increasing particle volume. At volume concentrations of 1 μm^3 cm^{-3} N90 varies between 100 and 300 cm^{-3}, whereas at vol-

ume concentrations of 1.5 μm^3 cm^{-3} N90 varies between 100 and 500 cm^{-3}. The data points with volume concentrations greater than 2 μm^3 cm^{-3} might be slightly influenced by pollution sources such as ships or power plants along the coast. These are conditions characterized by an increase of both particle number and volume concentration. In Atlantic air mass conditions the correlation between N90 and submicron aerosol volume concentration is better, but there is still considerable scatter as can be seen in Figure 4.5(c). The linear relationship fitted to the data points does not intersect at 0. An intercept below 0 can be expected since particles with diameters smaller than 90nm make a contribution to the submicron volume, albeit small. The relatively large intercept however suggests a slightly nonlinear relationship between N90 and the submicron volume concentration.

Figures 4.5(b) and (d) show that in marine conditions R varies from 50 to 350 μm^{-3}, with only a few cases in which the number concentration is higher than 350 μm^{-3}. It is also obvious that R itself increases with increasing N90. 70% of the variability in R can be explained by a linear dependence of R on the total number concentration in Arctic air mass types and 50% in Atlantic air mass types. The regression equations are given in Figure 4.5. There are no statistically significant relationships between R and the total volume concentration. Unfortunately this dependence of R on N90 cannot be used to improve the parameterization already given in Figures 4.5(a) and (c).

The dependence of R on N90 is partly caused by Aitken mode particle penetrating in to the region above 90nm due to fluctuations in Aitken mode mean diameter and number concentration. This addition of small particles can increase N90 without changing the volume significantly. This mechanism is especially important in Atlantic air mass types. In these air mass types more than 40% of the variance of R can be explained by a linear dependence on the number of Aitken mode particles above

90nm. However even when the influence of Aitken mode particles is disregarded, the number to volume ratio of the accumulation mode alone is not constant but increases linearly with the accumulation mode number concentration.This effect is especially pronounced in Arctic air mass conditions.

Figure 4.6 shows the observed dependence of the accumulation mode volume and number concentration on the mean diameter. The particle number concentration

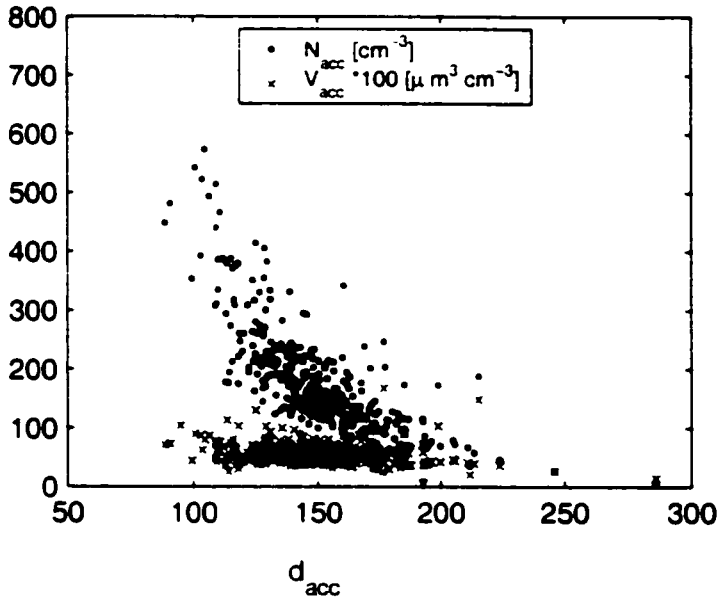

Figure 4.6: Observed accumulation mode number and volume concentration as a function of mean diameter in arctic air mass types .

decreases with increasing mean diameter whereas the volume concentration stays constant. This can be explained by the production of accumulation mode particles by cloud processing in an environment limited in SO_2. During transport from the Arctic roughly a certain limited amount of SO_2 is converted to particulate matter in cloud droplets. If the same amount of sulfate is distributed among fewer particles

(low N90), each individual particle can accumulate more material and the mean diameter of the accumulation mode increases. If more particles are present (high N90), each individual particle accumulates less material and the mean diameter of the accumulation mode stays smaller. This leads to the inverse relationship between the mean diameter and number concentration of the accumulation mode.

4.2.2 Number to Volume ratios in polluted conditions

The size distribution in air mass types associated with either aged or recent pollution is not as clearly bimodal as the size distribution in marine background conditions. The accumulation mode and the Aitken mode overlap to some extent and in some cases it it necessary to consider both the number and the volume concentration to show that two separate lognormal modes are present. A typical example of the size distribution in recent pollution and aged pollution is shown in Figure 4.7. In polluted conditions the mean diameter of the Aitken mode is larger than in marine conditions (Figure 4.7(a),(c)). Aitken mode particles contribute the majority of particles larger than 90nm. Aitken mode particles also account for a significant fraction of the of the submicron volume concentration (Figure 4.7(b),(d)).

In aged pollution the accumulation mode often appears only as a shoulder on the Aitken mode in the number size distribution. From the number size distribution alone it is not completely clear if it is justified to fit this shoulder as a separate mode. But in the volume size distribution it is obvious that the accumulation mode has lognormal shape and distinguished from the Aitken mode. Both modes contribute to the total number as well as to the total volume concentration.

In recent pollution Aitken mode particles account for the majority of N90 is made up of Aitken mode particles. The Aitken mode particles are so abundant that the particle volume contained in the Aitken mode is comparable to the to the particle

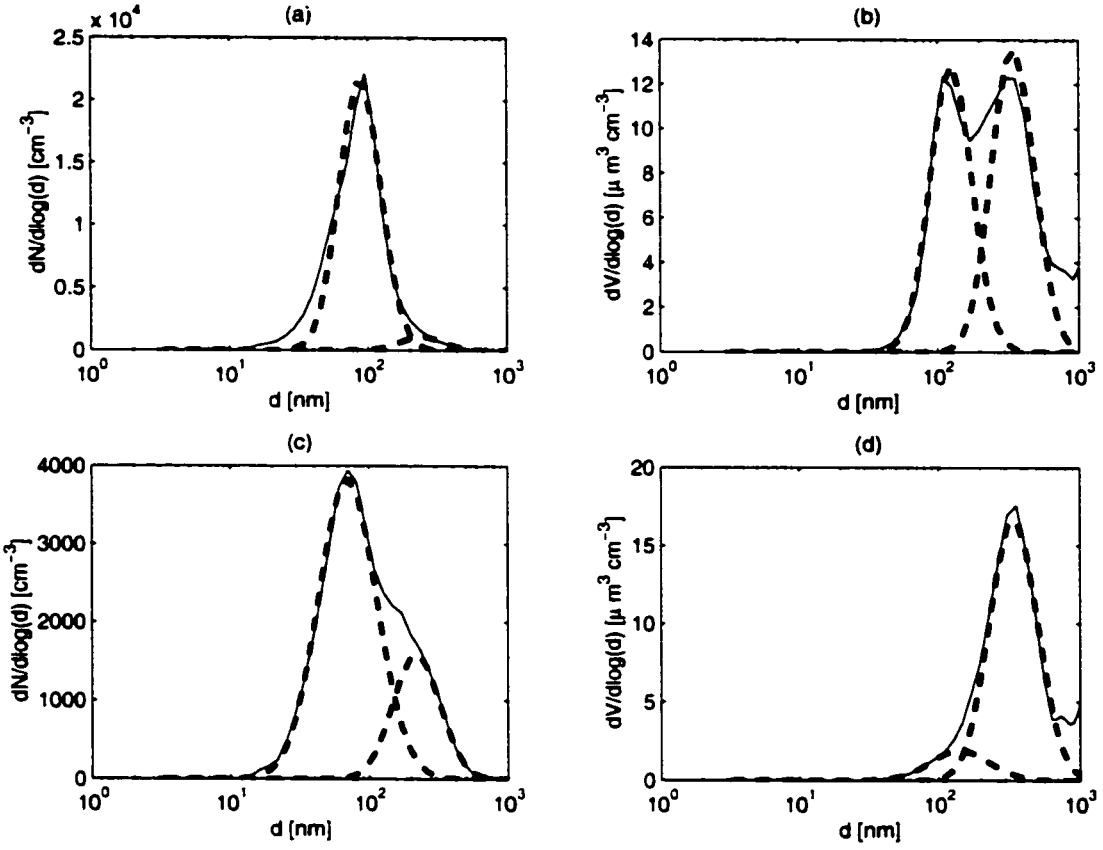

Figure 4.7: Typical size distribution in polluted conditions conditions: (a) number size distribution in air masses influenced by aged pollution, (b) corresponding volume size distribution, (c) number size distribution in air masses influenced by recent pollution, (b) corresponding volume size distribution

volume of the accumulation mode. Since most of the N90 are smaller than 120 nm the aerosol number to volume ratios in recent pollution are significantly higher than in the other air mass types. The volume provided by the few particles in the accumulation mode is not large enough to lower the number size distribution to background conditions.

Figure 4.8 shows the relationship between N90 and submicron particle volume in

polluted conditions. The number to volume ratios in air masses characterized by aged

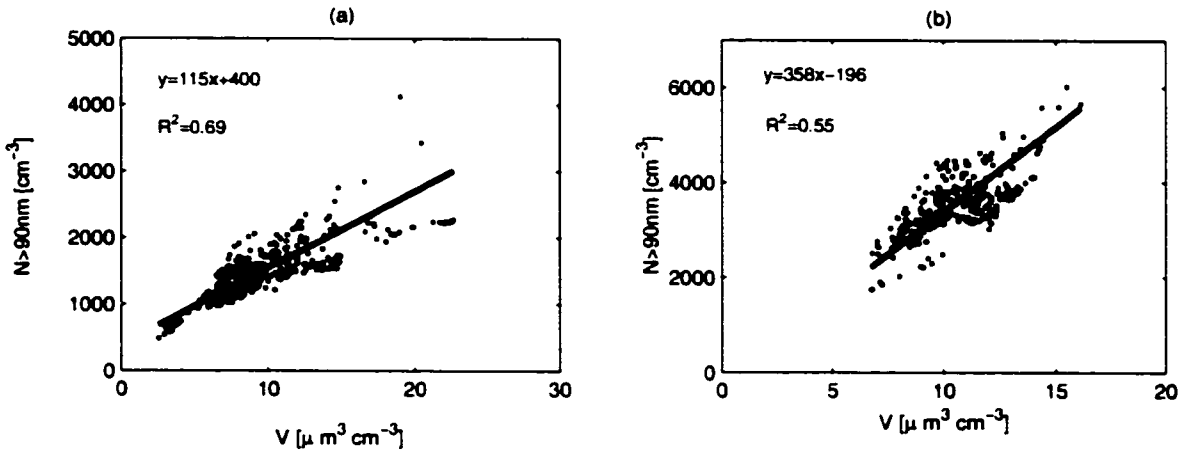

Figure 4.8: Number to volume ratios in polluted conditions: (a) the number concentration of particles larger than 90nm vs. submicron particle volume in aged pollution, (b) the number concentration of particles larger than 90nm vs. submicron particle volume in aged pollution

pollution are generally low and very stable. This is demonstrated in Figure 4.8(a) where the data are clustered much more tightly than in marine conditions. The relationship between N90 and submicron volume is slightly sub-linear and that the aerosol is modified by condensational processes that increase the do not increase the number concentration above 90nm as strongly as the total volume. The relationship between N90 and submicron volume concentration in recent pollution is approximately linear and shows more scatter than in aged pollution. In polluted air mass types R does not increase with N90 as in marine air mass types.

4.3 Stabilization of the number to volume ratio

As demonstrated in section 4.2 the number to volume ratios measured in Sagres during ACE-2 show considerable variability between $100\mu m^{-3}$ and $500\mu m^{-3}$. However the variability is smaller than the variability that is theoretically possible for a lognormal size distribution. According to Figure 4.1 the number to volume ratio could theoretically vary between approximately 10 and 1000 μm^{-3}. It can be concluded that the aerosol size distribution is shaped by processes that somehow work to constrain R. Some possible processes are discussed in this section.

4.3.1 Marine conditions

In marine conditions the size distribution in the size range above 90nm is dominated by accumulation mode particles. If there are any compensating effects that stabilize the number to volume ratio they will be found in the accumulation mode, since it has been already shown that Aitken mode particles larger than 90nm, only increase the variability of R. The volume concentration of the sea salt mode will mostly provide additional volume to lower R.

The accumulation mode has been shown to have approximately lognormal shape during the ACE-2 measurement campaign in Sagres (compare Figure 4.4).For a lognormal size distribution R is only dependent on the mean diameter and the standard deviation of distribution. Figure 4.9 shows the dependence of the accumulation mode standard deviation (σ_{acc}) on the accumulation mode diameter in marine conditions. As postulated by Hegg and Russel (2000), the standard deviation of the accumulation mode decreases with increasing mean diameter. This narrowing of the size distribution as the particles grow stabilizes the number to volume ratio.

The inverse dependence of σ_{acc} on the accumulation mode mean diameter can be seen more clearly in the Arctic data set. In Arctic air mass types, the mean diameter

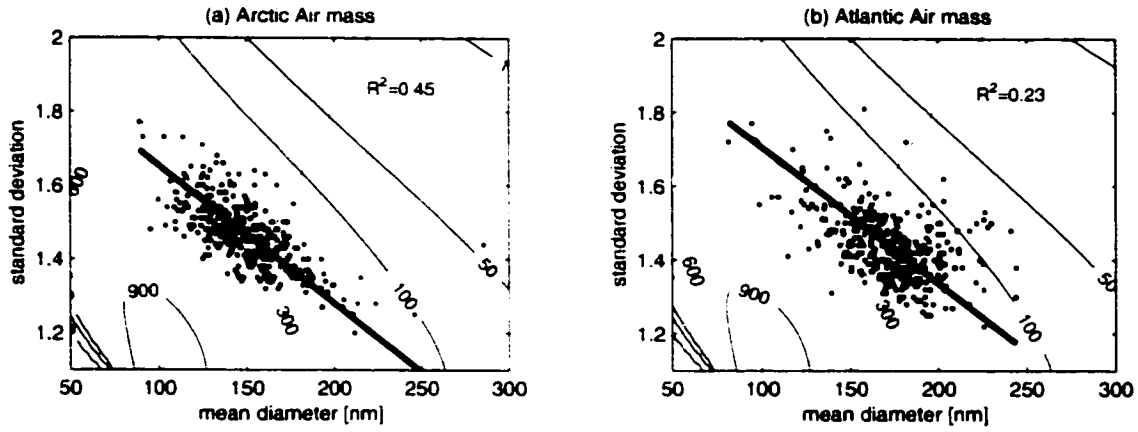

Figure 4.9: The dependence of the accumulation mode standard deviation (σ_{acc}) on the mean diameter in (a) Arctic and (b) Atlantic air mass types. Isolines of constant R are shown as colored lines.

varies over a larger size range and the data have a little less scatter than in the Atlantic data set. A linear regression line has been fitted to the date to show the impact of an inverse relationship between mean diameter and standard deviation on R more clearly. The regression line is tilted in the direction of the isolines of of R. As a result R is approximately 400 μm^{-3} at a mean diameter of 100nm and and a little more than 100 μm^{-3} at a mean diameter of 250nm. This can be compared to a situation where σ_{acc} is independent of the mean diameter and held constant at its mean value of 1.45. In this case R varies from approximately 800 μm^{-3} to below 100 μm^{-3}, for an increase in the mean diameter from 100nm to 250nm. The inverse dependence of σ_{acc} results in a reduction in variation of R by 50%. The decrease of σ_{acc} with mean diameter is not strong enough to achieve constant R, but only sufficient to confine R to a narrower range than could be expected if the mean diameter and the standard deviation of the accumulation mode were not correlated.

In Atlantic air mass conditions most of the data points are confined between mean

diameters of 150 and 200nm. In this size range R is not as strongly dependent on the mean diameter (compare Figure 4.1) and thus more stable than in Arctic air mass types. Therefore the decrease of σ_{acc} with the mean diameter does not play such a big role in stabilizing the number to volume ratio.

4.3.2 Polluted conditions

In polluted air mass conditions both Aitken and accumulation mode particles have have an important influence on the number to volume ratio. The total number to volume ratio can be written as:

$$R = \frac{N90_{acc} + N90_{ait}}{V_{acc} + V_{ait}} = \frac{\frac{N90_{acc}}{N90_{ait}} + 1}{\frac{N90_{acc}}{N90_{ait}} \cdot \frac{1}{R_{acc}} + \frac{1}{R_{ait}}}, \tag{4.2}$$

where $N90_{acc}$ is the number concentration of accumulation mode particles larger than 90nm, $N90_{ait}$ is the number concentration of Aitken mode particle larger than 90nm, R_{ait} the number to volume ratio of the Aitken mode and R_{acc} the number to volume ratio of the accumulation mode. From this equation we can draw two conclusions. First the total number to volume ratio R lies between the number to volume ratio of the Aitken mode and the number to volume ratio of the accumulation mode:

$$min(R_{acc}, R_{ait}) < R < max(R_{acc}, R_{ait}). \tag{4.3}$$

Second if $N90_{acc}$ and $N90_{ait}$ are of the same order of magnitude the total number to volume ratio cannot increase very strongly even if R_{ait} gets arbitrarily large. These conclusions are independent of the actual shape of the size distribution as long as it is bimodal.

Figure 4.10 illustrates the range of R_{acc} and R_{ait} in polluted conditions. The relationship between the standard deviation and the mean diameter of both the Aitken and Accumulation mode are overlaid on lines of constant R. In most cases the R_{ait}

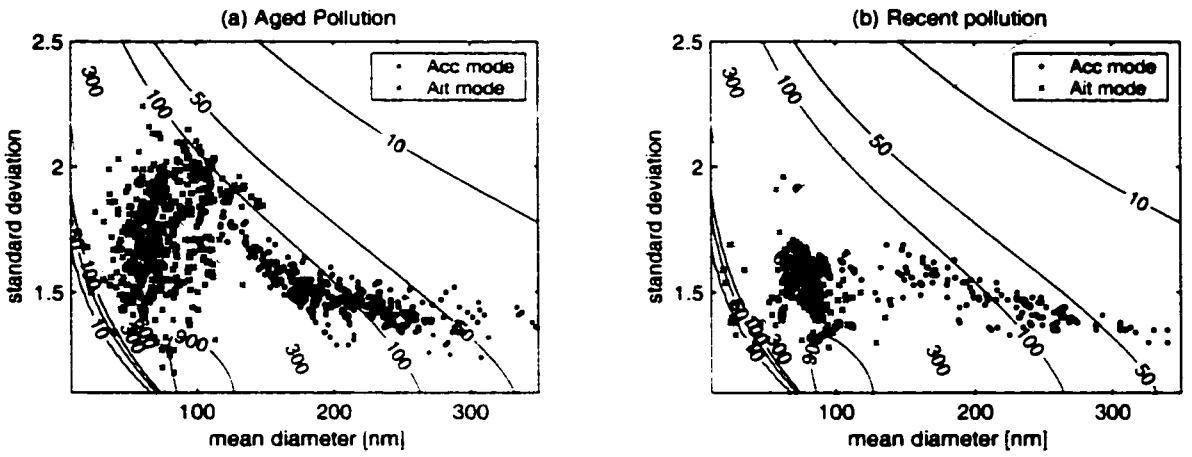

Figure 4.10: Dependence of the standard deviation on the mean diameter of the Aitken mode (x) and the accumulation mode (·): (a) Aged pollution, (b) recent pollution. Lines of constant R are shown in color

is larger than R_{acc}, the only exception is when the Aitken mode mean diameter is unusually small, below 30-40nm.

There are important differences in conditions of aged pollution and recent pollution. In air mass conditions influenced by aged pollution 4.10(a) the number to volume ratio of the Aitken mode is very variable. However since in those conditions $N90_{acc}$ is comparable to $N90_{ait}$ even a strong increase in the number to volume ratio of the Aitken mode increases R only moderately. The number to volume ratio of the accumulation mode itself is very stable for accumulation mode mean diameters between 100 and 200nm. For this range of diameters σ_{acc} decreases with increasing accumulation mode diameter at a ratio that holds R_{acc} constant. Once the mean diameter is larger than 200nm the standard deviation levels off and does not fall below 1.2. This results in low values of R_{acc} for very large mean diameters of the accumulation mode.

In recent pollution the number to volume ratios of the Aitken mode are large and relatively stable. The mean diameters of the Aitken mode are in the size range where the number to volume ratio of a lognormal distribution reaches its maximum. R_{acc} is more variable than in aged pollution, because there no strong inverse relationship between accumulation mode diameter and standard deviation. This is consistent with the conclusion drawn in chapter 3, that the accumulation mode particles in recent pollution are not produced by cloud processing (condensational processes), but are mainly produced by primary emission. Despite the fact that R_{acc} is generally low, the high number concentration of Aitken mode particles larger than 90nm combined with a high R_{ait} makes the total R larger than in other air mass types.

The stability of R in air mass types influenced by aged pollution is quite remarkable and the general principles contained in Equation 4.2 are not sufficient to explain why R is so confined. The reason for the constancy of R seems to be that in aged pollution the parameters of Aitken and accumulation mode are not completely independent. This is demonstrated in Figure 4.11 (a)-(c). The data presented in Figure 4.11 are taken from a selected time period during the aged pollution episodes that spans a little over two days. Sampling over longer time periods tends to obscure correlations between aerosol parameters due synoptic variations and possible changes in the aerosol origin. In Figure 4.11(a) it can be seen that during the time period of interest the standard deviation of the accumulation mode is strongly depended mean diameter as. A second order polynomial was fitted to the data yielding an R^2 of 0.86. Figure 4.11(b) shows that the accumulation mode mean diameter and the Aitken mode mean diameter are somewhat correlated.

Of special importance is that the ratio of $N90_{ait}$ to $N90_{acc}$ depends on the mean diameter of the accumulation mode as shown in Figure 4.11(c). Both axes are logarithmic, so the dependence is exponential. The ratio of $N90_{ait}$ to $N90_{acc}$ determines

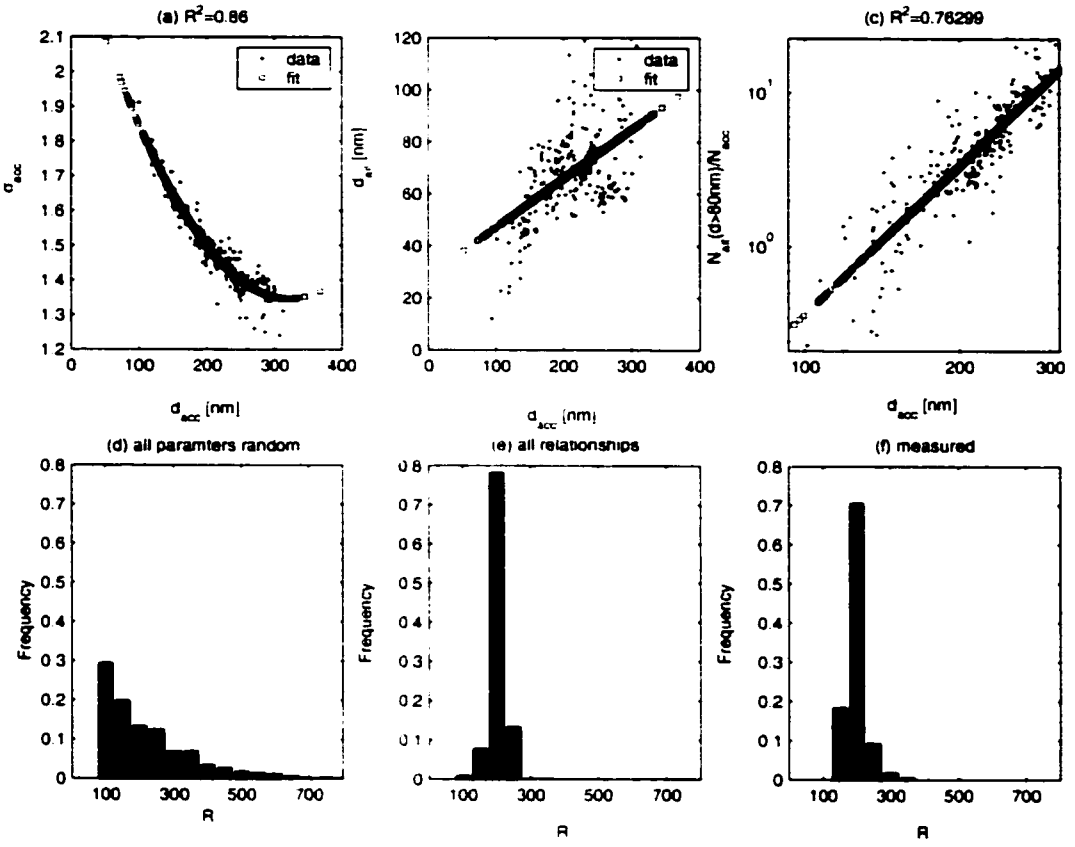

Figure 4.11: Correlations between parameters of the size distribution in aged pollution and their influence on the number to volume ratio: (a) dependence of the accumulation mode standard deviation on the mean diameter, (b) relationship between accumulation mode mean diameter and Aitken mode mean diameter, (c) dependence of $N90_{ait}/N90_{acc}$ on the mean accumulation mode diameter, (d) simulated frequency distribution of R using no correlations between size distribution parameters, (e) simulated frequency of R distributions using the measured relationships shown in (a)-(c), (f) measured frequency distribution.

how sensitive the total number to volume ratio R is to an increase in the number to volume ratio of the Aitken mode. If $N90_{ait}/N90_{acc}$ is close to 1 R can at most

achieve a maximum of $R = 2 \cdot R_{acc}$ if the number to volume ratio of the Aitken mode goes to infinity. However if $N90_{ait}/N90_{acc} = 10$, R can be up to 10 times larger than R_{acc}. Figure 4.11(c) offers a simple explanation why the number to volume ratios of ambient aerosol usually do not get arbitrarily small. As the diameter of the accumulation mode increases, the number concentration of Aitken mode particles larger than 90 increases in relationship to the number concentration of the accumulation mode particles. The decrease in R_{acc} is balanced by an increase in Aitken mode particles that grow larger than the 90nm cut-off diameter. This behavior has a simple physical explanation. The mean diameter of the accumulation mode can only increase above 200nm if a large amount of precursor gases are converted to aerosol. But if the size of accumulation mode particles is increased, the Aitken mode particles are likely to grow as well. The relationship shown in Figure 4.11(c) is typical of polluted conditions during ACE-2, but is not as strong in marine air mass types.

That the number to volume ratio of the ambient aerosol is actually limited by these correlations can be demonstrated by simulating R in the following manner. 1000 bimodal number size distributions are randomly generated. Each distribution has an accumulation and an Aitken mode with a certain mean diameter, standard deviation and number concentration. In the first set of simulations the mean diameter, the standard deviation and the number concentration of the Aitken and of the Accumulation mode are all randomly generated. Each parameter is assumed to be normally distributed around the actually measured mean value with the measured standard deviation. Then number to volume ratios of the 1000 distributions are calculated. In the second set of simulations the mean diameter and the number concentration of the accumulation mode are randomly chosen as described above, but the standard deviation is calculated for each mean diameter according to the relationship shown in Figure 4.11(a). Then the Aitken mode mean diameter and number concentration

are calculated using the relationships shown in Figure 4.11(b) and (c), whereas the Aitken mode standard deviation is randomly chosen.

The results of the two simulations are shown in Figure 4.11(d) and (e), which display the frequency distribution of the resulting number to volume ratios. If all size distribution parameters are randomly chosen (Figure 4.11(d)), the frequency distribution of R is relatively broad and high values of R (up to 800 μm^{-3}) are occasionally found. The frequency distribution of R calculated in the second set of simulations is much narrower. Taking into account the relationships between size distribution parameters constrains R closely to values around 200 μm^{-3}. The frequency distribution of R resulting from the second set of simulations is very close to the frequency distribution of R derived from the actual measurements of the size distributions.

4.4 Summary

The number to volume ratios (R) in the different air mass conditions are summarized in the frequency distributions in Figure 4.12. In Arctic and Atlantic conditions the frequency distributions are similar. The values of R lie most frequently between 100 and 300μm^{-3} although outliers of higher R occur occasionally. In aged pollution R has approximately the same mean value, but is significantly less variable. In recent pollution R is higher than in the other air mass conditions.

The variability of R is in all cases relatively constrained compared to the variability theoretically possible for a lognormal size distribution (see Figure 4.2. In the Arctic and Atlantic marine air masses this is due to the fact that the number to volume ratio seems to be dominated by accumulation mode aerosol, whose geometric standard deviation depends inversely on the mean diameter of the mode. This inverse dependence has been hypothesized by Hegg and Jonsson (2000) and has now been verified in this work. It indicates that condensational processes determine the size

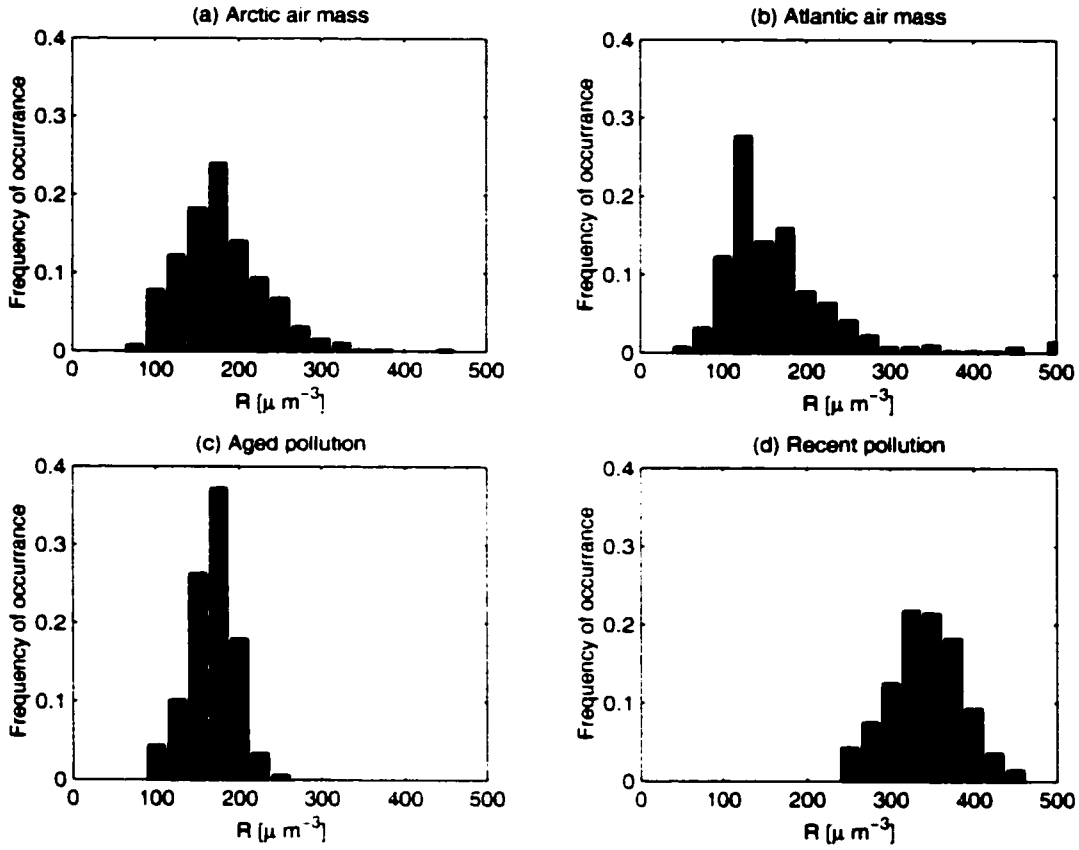

Figure 4.12: Frequency distribution of R in different air mass conditions

distribution of the accumulation mode aerosol or that cloud processing of the aerosol results in an inverse dependence of the standard deviation of the processed aerosol on the mean diameter. In aged pollution the variability of R is further reduced due to correlations between Aitken and Accumulation mode parameters, as demonstrated in Figure 4.11. A simple reason consistent with aerosol processes can be given to explain why the variability of the number to volume ratio decreases in cases where it is determined by a bimodal number size distribution.

Chapter 5

CCN SPECTRA DERIVED FROM SIZE DISTRIBUTIONS AND HYGROSCOPIC PROPERTIES OF THE AEROSOL

5.1 Introduction

Stratus clouds, which cover large parts of the oceans are important for the radiative balance of the global atmosphere. At visible wavelengths stratus clouds have a much higher albedo than the underlying ocean surface and reflect more solar radiation back to space while the long wave radiation emitted by those low cloud systems is comparable to that of the ocean surface. Stratus clouds have thus a net cooling effect on the climate. It has been proposed (e.g. Twomey et al., 1987; Twomey, 1991) that the albedo of stratus clouds is to some extent controlled by the number concentration of the aerosol particles that serve as nucleation sites for the cloud droplets. An increase in aerosol number concentrations may result in clouds with more, but smaller droplets and a higher albedo, which enhances their cooling effect on the climate system. The increase of cloud albedo caused by an increase in aerosol concentrations is commonly referred to as the indirect effect of aerosols on climate. This effect has been confirmed by experimental evidence. This includes measurements of aerosol and cloud properties in ship tracks (e.g. Ferek et al., 1998), changes in the relationship of long- and short wave cloud reflectance due to pollution outbreaks from the European continent during ACE-2 (Brenguier et al., 2000), and seasonal differences in stratus clouds off the coast of Australia, that can be explained by

fluctuations in the natural background aerosol (Boers et al., 1998).

The quantification of the indirect effect has as yet large uncertainties but its existence is quite well established locally. Thus it can be expected that globally an increase in aerosol number concentrations by anthropogenic emissions could result in a negative radiative forcing of the climate system (e.g. Charlson et al., 1992) by increasing the particle concentrations in areas where the background concentrations are low. These are the areas where the cloud albedo is expected to be most sensitive to anthropogenic influence. However it is difficult to quantify this anthropogenic indirect forcing and to relate a change in global cloud albedo to the anthropogenic increase in aerosol mass or number concentrations. One of the complications is that cloud droplets nucleate only on a subset of all aerosol particles. The identification of this subset of the aerosol population can thus be considered a first step in linking the indirect radiative forcing to total aerosol number or mass concentration.

The concept of cloud condensation nuclei (CCN) has been useful in this context. CCN are usually defined as the aerosol particles that 'activate' (i.e. grow by water uptake that is kinetically rather than thermodynamically limited) at a certain supersaturation (S). This concept inherently involves the assumption that prior to activation the droplets are in equilibrium with the surrounding water vapor. If this assumption is justified the number concentration of activated particles is only dependent on the maximum supersaturation and not on the history of S. Whether this equilibrium assumption is valid in ambient clouds is still a subject under study (e.g. Chuang et al., 1997; Nenes et al., 2001). CCN are usually measured using CCN counters (e.g. Hudson, 1989). In these instruments the aerosol is subjected to a defined S and particles that grow to the sizes of cloud droplets are counted as CCN. CCN can also be calculated using Koehler theory, if the number-size distribution and chemical composition of the aerosol particles is known.

In this investigation we propose and test a method to calculate CCN spectra (i.e. the CCN as a function of S) based on measured particle size distributions and hygroscopic properties. Subsequently, we present calculated CCN spectra for the ACE-2 measurement period from 16 June to 24 July 1997 in Sagres, Portugal (Raes et al., 2000; Verver et al., 2000). In the past and also during the ACE-2 experiment calculated and measured CCN concentrations have often been found to disagree strongly by factors of up to 5 (Chuang et al., 2000; Wood et al., 2000; Snider and Brenguier, 2000). During ACE-2 some of the measured CCN spectra could be explained with very low soluble fractions in the aerosol particles (Raes et al., 2000), but this is in contradiction to hygroscopic growth factor measurements (Swietlicki et al., 2000). To shed more light on this problem we will test the consistency of measured hygroscopic growth factors and chemical composition of the particles. We will also compare the calculated CCN spectra to CCN spectra measured by a new type of instrument called a Cloud Condensation Nucleus Remover (Ji et al., 1998). Moreover we will include extensive sensitivity studies to investigate a possible influence of organic compounds on the CCN spectra.

The data from the measurement site in Sagres offer the opportunity to study the aerosol characteristics in various air mass types ranging from marine background to continentally polluted conditions. One further objective of this work is to complement the limited number of measured CCN spectra with a data set of calculated CCN spectra, that covers the whole ACE-2 measurement period. This allows us to compare CCN spectra in different air mass types and to estimate how much the marine background CCN concentrations are increased by anthropogenic pollution.

5.2 *Calculation of CCN spectra using number size distributions and hygroscopic growth factors*

The equilibrium droplet size and cloud nucleating properties of an aerosol particle at cloud humidities are most commonly described by the Koehler theory (e.g. Pruppbacher and Klett, 1997). According to Koehler theory each particle is characterized by a critical water vapor supersaturation (S_c). If the ambient supersaturation (S_a) in a cloud exceeds S_c the particle will become 'activated', i.e. it will grow to the size of a cloud droplet by water uptake that is kinetically rather than thermodynamically limited.

The classical Koehler theory is valid for aerosol particles consisting of water soluble inorganic salts and an insoluble core. For particles containing significant soluble material (more than 20%) S_c is to a first approximation only dependent on the number of soluble ions and molecules (N_i) in the particle and the influence of the insoluble core can be neglected. In this case S_c can be written as

$$S_c = \left(\frac{4 \cdot A^3}{27 \cdot B \cdot N_i} \right)^{0.5} . \tag{5.1}$$

where $A := 3.3 \cdot 10^{-7}/T$, $B := 4.3 \cdot 10^{-6}$ and T the ambient temperature (compare Seinfeld and Pandis (1998, pg. 787)). The classical Koehler theory neglects the influence of soluble and slightly soluble organic substances on the particle water uptake. However there is empirical evidence that organic aerosols contribute to the CCN concentrations (e.g. Novakov and Penner, 1993; Novakov and Corrigan, 1996). Significant modifications to the Koehler theory to incorporate the effect of slightly soluble and surfactant organic substances and the uptake of soluble gases have been developed recently (Laaksonen et al., 1998; Shulman et al., 1996; Kulmala et al., 1997). Currently it is not possible to consider this influence of organics in the calculation of CCN spectra directly. Only a small fraction of the organic species in the ambient aerosol

has been analyzed and classified so far (e.g. Rogge et al., 1993) and the solubility and effects on surface tension of organic species are largely unknown (Saxena and Hildemann, 1996). The CCN spectra presented in this study are therefore calculated using classical Koehler theory. Possible errors which may result from the neglect of organic species in the calculations are estimated in a sensitivity study in section 2.2.

This section shows how the number of soluble species (ions and molecules) in a particle and consequently S_c can be estimated from its hygroscopic growth factor at high relative humidities (r.h.) near 90%. The number of ions and molecules per particle can in principle also be estimated more directly by analyzing inorganic and organic compounds collected on filter or impactor samples of the aerosol. However, those measurement methods have generally poor size resolution, incomplete chemical analysis and require measurement times of the order of hours. On the other hand, hygroscopic growth factors can be measured directly by a Tandem Differential Mobility Analyzer (TDMA) (Rader and McMurry, 1986), which has a very fine size resolution and the time to complete one growth factor measurement is approximately 10 minutes.

5.2.1 Estimation of droplet size and S_c from hygroscopic growth factors

A common measure for the hygroscopic growth of an aerosol particle is the diameter growth factor (Gf), defined as the ratio of the hydrated particle diameter at some specified relative humidity (r.h.) to the dry particle diameter. The growth factors used in this study have been measured by the Tandem Differential Mobility Analyzer (TDMA). In this study growth factors measured at 90% r.h. are used to estimate the number of soluble ions and molecules in an atmospheric particle by calculating the mass of a known model salt that is required to give the same growth factor. This determines the number of soluble ions in the model particle which is 'equivalent' to

the number of soluble molecules and ions in the atmospheric aerosol. We term this equivalent ions.

If the model salt is fully dissolved at 90% r.h., the number of equivalent ions can be calculated as the product of the mass of water (m_w) contained in the droplet and the molality of the solution (η):

$$N_i^{eq} = i \cdot \eta \cdot m_w, \tag{5.2}$$

where i is the number of ions in which the salt can dissociate. m_w and η can be estimated using the hygroscopic growth factor and empirical assumptions about the water activity of concentrated electrolytic solutions.

Assuming spherical particle shape, the mass of water contained in an aerosol particle at 90% r.h. can be calculated from the measured hygroscopic growth factor (Gf) at 90% r.h.:

$$m_w = \frac{\pi \cdot d_{dry}^3 \cdot (Gf^3 - 1) \cdot \rho_w}{6}. \tag{5.3}$$

where d_{dry} is the dry particle diameter and ρ_w the density of water.

The calculation of the molality η is not so straight forward. The aerosol droplets at 90% r.h. are fairly concentrated so that non-ideal solution effects have to be considered. The vapor pressure over the droplet surface is not only a function of the number concentration of ions in the solution, but also of the specific salt present. This information however cannot be obtained through growth factor measurements alone. This is the reason we choose a model salt (e.g. ammonium sulfate, $(NH_4)_2SO_4$) to estimate equivalent ions. For such a model salt it is possible to calculate the molality η of the solution droplet at 90% r.h. with the help of an empirical relationship between η and the water activity (a_w).

In this work we follow an approach by Swietlicki et al. (1999) and use an empirical formula for the molality of a $(NH_4)_2SO_4$ solution determined by Potukuchi and

Wexler (1995):

$$\eta = 135.9 - 464.03 \cdot a_w + 492.36 \cdot a_w^2 + 94.33 \cdot a_w^3 - 459.29 \cdot a_w^4 + 200.7 \cdot a_w^5. \quad (5.4)$$

For small solution droplets the water activity (a_w) is related to the ambient r.h. as follows:

$$a_w = r.h. \cdot exp\left(-\frac{4 \cdot \sigma \cdot M_w}{\rho \cdot R \cdot T \cdot Gf \cdot d_{dry}}\right), \quad (5.5)$$

where σ is the surface tension of the solution, M_w and ρ_w the molecular weight and density of water, R the universal gas constant, T the temperature, and Gf and d_{dry} the growth factor and dry diameter of the aerosol particle.

Combining (2)-(5) it is possible to calculate the equivalent number of ions (N_i^{eq}) in a particle, i. e. the number of ions of ammonium sulfate that would produce the observed hygroscopic growth at 90% r.h.. Using N_i^{eq} in (1) the critical supersaturation S_c for any particle can be estimated from the knowledge of its dry diameter and the hygroscopic growth factor at high humidities. If hygroscopic salts other than ammonium sulfate or slightly soluble materials contribute to the hygroscopic growth at 90% r.h. N_i^{eq} is not necessarily equal to the actual number of soluble molecules or ions in the particle. However, estimating the actual number of ions in the particle is not the goal of this study. The equivalent ion number concentration is used as a tool to extrapolate the hygroscopic behavior of the particle as measured at 90% r.h. to higher humidity and supersaturations. This approach uses one main assumption: The ratio between water uptake of the actual soluble material in the particle at 90% r.h. and at S_c is similar to that of ammonium sulfate. If this is not the case errors can be introduced in the calculation of the critical supersaturation. The potential magnitudes of these errors are estimated in the next section.

5.2.2 Sensitivity studies

There are several reasons that the ratio between water uptake at 90% r.h. and water uptake at S_c of an actual particle might differ from that of ammonium sulfate, which is used to calculate equivalent ions, S_c and finally CCN spectra in this study. The hygroscopic material in the particle might be an inorganic salt other than ammonium sulfate. The particle may contain some slightly soluble material that is only partially dissolved at 90% r.h. but dissolves fully at higher supersaturations. The surface tension of the particle could be different at 90% r.h. and at S_c. Soluble gases dissolve in the diluted particle near S_c but not at 90% r.h..

The sensitivity studies presented in this section have two major objectives: The first is to explore a wide variety of aerosol compositions to see in which cases the method of calculating CCN concentrations described in this work can be used. The second is more specifically to investigate if this method is applicable to the conditions in Sagres during ACE-2. A quantitative treatment can only be attempted regarding the effects of inorganic and soluble organic species. The uncertainties associated the uptake of soluble gases are too large to attempt a meaningful quantification and are thus only discussed qualitatively.

Inorganic compounds

If the water activity of the solution at 90% r.h. can be approximated by Raoult's law (ideal solution), S_c is independent of the salt used to calculate N_i^{eq}. Errors in S_c are thus only due to differences in the nonideal solution effects among different inorganic salts at 90% r.h.. For sulfate compounds (such as NH_4HSO_4, $(NH_4)_2SO_4$ or Na_2SO_4) these differences are generally small and it can be shown that S_c is fairly insensitive to the specific hygroscopic salt used in the calculation of N_i^{eq}. For example if Equation 4 is replaced by a similar empirical expression for ammonium bisulfate

(Tang and Munkelwitz, 1994) the resulting number of ions differs less than 10% from N_i^{eq} obtained by using ammonium sulfate. This corresponds to a relative difference in S_c of less than 3% (i.e. an absolute difference of 0.0003 at S_c=0.01) for an assumed particle composition of ammonium sulfate vs. ammonium bisulfate and does not result in any significant difference in the calculated CCN concentrations. For sea salt (or pure NaCl) particles the errors in CCN concentrations can be larger (approximately 25%), if the equivalent ions are calculated using the empirical expression for ammonium sulfate. These possible errors however are of little practical concern for several reasons. Significant amount of sea salt is usually present only at sizes larger than the accumulation number mode and sea salt particles generally constitute only a minor fraction of the total particle number greater than 80nm. When present, sea salt particles usually appear as a separate mode in the hygroscopic growth factor measurements, even if they are associated with small amounts of sulfate through atmospheric processing (Berg et al., 1998b). These particles can be thus be identified and their critical supersaturation can be estimated separately with an appropriate empirical expression for NaCl (e.g. as measured by Tang (1997)). If there are smaller amounts of NaCl internally mixed with the sulfate particles, the errors introduced into the CCN spectra will be much smaller than 25% depending on the amount of sea salt present. Impactor measurements in Sagres show that sea salt contributed less than 5% of the mass in particles smaller than 250 nm, which provide the majority of the CCN.

Soluble organics

In the approach described in section 2.1 S_c is calculated using equivalent ions that represent all the compounds contributing to the hygroscopic growth at 90% r.h.. Therefore all organic material that is in solution at this r.h. will be represented as an

equivalent amount of ions, while the rest is classified as insoluble. For the accurate estimation of S_c however it is not the material dissolved at 90% r.h., but the material dissolved at slight supersaturations that is of crucial importance. Thus, the method presented here will be most inaccurate if organic species are present that do not dissolve in the fairly concentrated droplets around 90% r.h. but are able to dissolve when the r.h. nears the critical supersaturation and the droplet is more diluted.

If these soluble compounds were analyzed chemically and their solubilities in sulfate solutions and effects on the surface tension were known their effect could be modeled using a modified Koehler equation (Laaksonen et al., 1998; Shulman et al., 1996; Kulmala et al., 1997). However only a fraction of the organic compounds in the ambient aerosol have been analyzed so far. Dicarboxylic acids are the only compounds whose solubilities in sulfate solutions of various concentrations and whose effect on the surface tension has been measured (Shulman et al., 1996). Those acids are therefore used as model compounds for other soluble organics in the following sensitivity analysis. To estimate errors that could arise in our calculations due to the presence of dicarboxylic acids in the inorganic aerosol particles we compare S_c derived from (2)-(5) to the critical supersaturation obtained by the more exact treatment using the modified Koehler equation.

Figure 5.1 demonstrates this comparison for the extreme example of a 60nm particle that consists of a mixture of 10% ammonium sulfate and 90% organic acid (molar fraction). The dicarboxylic acids considered are: glutaric acid, which is highly soluble, succinic acid, which is moderately soluble, and adipic acid, which is only slightly soluble. Since it is not clear if or how strongly dicarboxylic acids dissociate in solution the modified Koehler curves have been calculated for a Van't Hoff factor i ranging from 1 to 3 and are shown as a shaded area. Also shown are the classical Koehler curves for a 60nm particle consisting of pure ammonium sulfate (solid line) and a

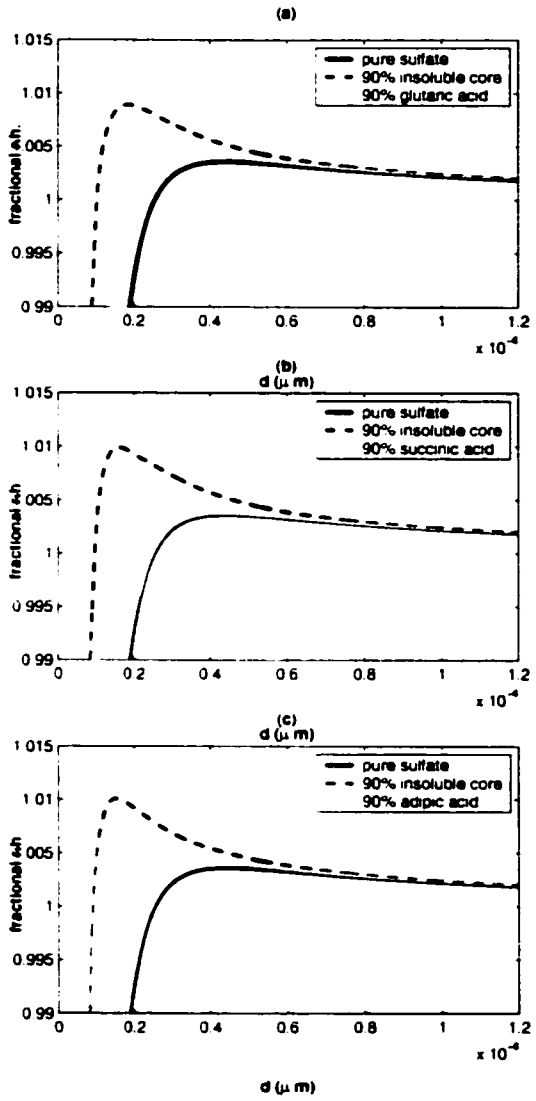

Figure 5.1: Modified Koehler curves for 60nm particles consisting of 10% ammonium sulfate and 90% dicarboxylic acids are shown as shaded areas, taking into account that the Van't Hoff factor might vary between 1 and 3. The classical Koehler curves for a particle of pure ammonium sulfate and a particle that contains 10% ammonium sulfate and 90% insoluble core are shown for comparison

60nm particle that contains an equal volume of insoluble material instead of the organics (dashed line). The first curve represents the Koehler curve that would result from our calculations based on equivalent ions, if the organic acid was fully dissolved and fully dissociated at 90% r.h.. The second curve represents the Koehler curve we would result from our calculations if the organic acid was completely insoluble at 90% r.h..

Figure 5.1(a) shows that the modified Koehler curves for particles containing large amounts of strongly soluble organic material such as glutaric acid. The Koehler curve for the fully dissociated acid (lower boundary of the shaded area) is very close to the solid line representing ammonium sulfate. If an organic acid is mostly dissolved at 90% r.h., it seems justified to approximate its hygroscopic behavior by an equivalent amount of totally soluble, dissociated ions and treat it with the classical Koehler curve.

The hygroscopic behavior of a particle containing a large fraction of a moderately soluble substance cannot be adequately described using hygroscopic growth factors and the classical Koehler theory. Figure 5.1(b) shows that at an r.h. below 99% the modified Koehler curve approaches the Koehler curve of a particle with an insoluble core. That means that only a very small fraction of the moderately soluble substance dissolves below 99% r.h and it will not influence the hygroscopic growth at 90% r.h.. The organic acid is therefore interpreted as totally insoluble material when N_i^{eq} are calculated from hygroscopic growth factors at 90% r.h. using (2)-(5). The calculated critical supersaturation is thus close to the maximum of the dashed line in Figure 5.1(b) representing the Koehler curve of a particle containing an insoluble core. However, this curve deviates strongly from the modified Koehler curve at supersaturations close to S_c and CCN concentrations can be considerably underestimated.

Figure 5.1(c) shows the case of a particle containing a slightly soluble substance

such as adipic acid. This compound does not dissolve very much at either lower r.h. or at supersaturations close to S_c. It will be interpreted as insoluble material in the calculation of N_i^{eq} from hygroscopic growth factors at 90% r.h. and acts as such at supersaturations close to S_c. The equivalent ions thus provide a good estimate of S_c.

A sensitivity study is conducted for particle sizes from 0.02 to 0.4μm and for ammonium sulfate particles containing 0 to 90% dicarboxylic acid by mass. It is assumed that calculations using the modified Koehler equation give the correct S_c. Errors in S_c estimated by (2)-(5) are calculated as follows:

- The highly soluble glutaric acid is assumed to be fully dissolved and, for simplicity, fully dissociated (i=3) at 90% r.h.. Since for a fully dissolved substance errors in S_c are independent of the degree of dissociation, this assumption does not influence the results of this analysis. For i=3 S_c estimated based on hygroscopic growth factors is close to the critical supersaturation of a particle consisting of ammonium sulfate S_c^{sulf}, whereas the actual critical supersaturation of the mixed particle is given by the modified Koehler equation (S_c^{mod}). The percentage error in S_c can thus be estimated as $(S_c^{sulf} - S_c^{mod})/S_c^{mod} \cdot 100$.

- Succinic and adipic acid are presumably not dissolved at 90% r.h.. S_c calculated based on hygroscopic growth factors is close to the critical supersaturation of a particle containing insoluble material instead of an organic acid S_c^{ins}. A Van't Hoff factors (i=2) is assumed for these calculations. The percentage error in S_c can thus be calculated as $(S_c^{ins} - S_c^{mod})/S_c^{mod} \cdot 100$.

The percentage errors are shown in Figure 5.2 for particles consisting of ammonium sulfate and glutaric acid (a), succinic acid (b) and adipic acid (c). Errors for particles consisting of glutaric acid and ammonium sulfate are generally negative, i.e. the critical supersaturation of such particles is underestimated by the calculations.

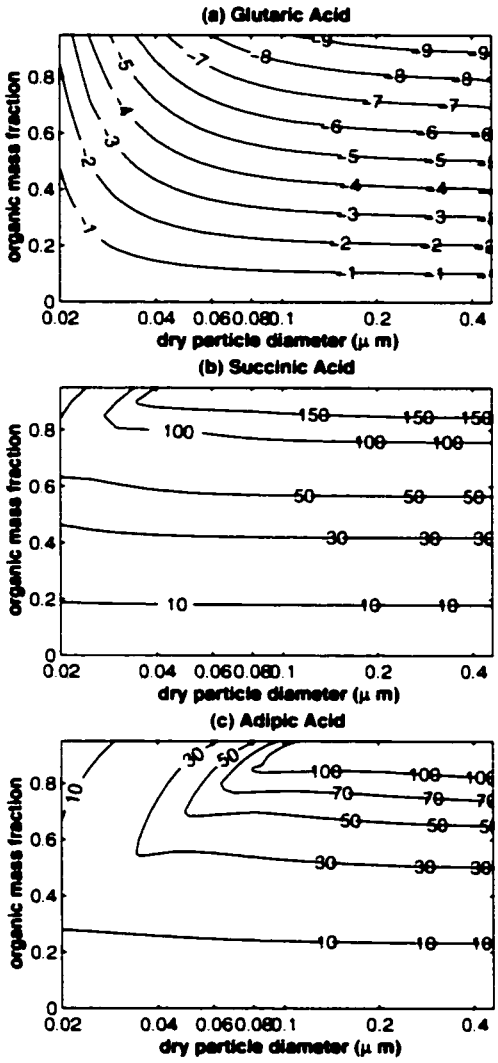

Figure 5.2: Deviation of the critical supersaturation calculated using Koehler theory and hygroscopic growth factors from the values of S_c obtained by the full calculations based on the modified Koehler theory. The deviations are shown in % for a range of particle sizes and organic mass fractions. Negative values indicate an underestimate of S_c by the classical Koehler theory, positive values indicate an overestimate.

These errors are mostly due to effects of glutaric acid on the surface tension of the droplet near critical supersaturations. The magnitude of these errors is <10% for organic mass fractions <0.9 and is not expected to affect the calculated CCN concentrations strongly. The critical supersaturations for ammonium sulfate particles containing succinic and adipic acid are overestimated and the errors are much larger than for particles containing glutaric acid. The errors are mostly caused by the fact that only a negligible part of these dicarboxylic acids is in solution at 90%, but they dissolve to a larger extent near the critical supersaturation. In this case changes in surface tension are only second order effects. For adipic acid the errors in S_c are smaller than 30%, at organic mass fractions less than 60%. For succinic acid the errors are smaller than 30% at organic mass fractions less than 50%.

Assuming that dicarboxylic acids are appropriate as model compounds for other soluble organic species the sensitivity studies indicate the errors in the calculations will not be too large unless large quantities (larger than 50% by mass) of slightly or moderately soluble material such as succinic or adipic acid are present in the aerosol. Considering that about 30 to 70% of the organic material in the atmospheric aerosol is insoluble (e.g. Saxena and Hildemann, 1996) this corresponds to an organic mass fraction of at least 80%. Such high concentrations of organics are not very common in the atmosphere, but can be found in aerosols from forest fires in South America or Africa (Yamasoe et al., 2000; Andreae et al., 1998).

During the ACE-2 field experiment submicron mass fractions of total carbon were on average about 15% at the Sagres site. Even if all this carbon was slightly soluble, which is highly unrealistic, the resulting errors in S_c still would be below 10%. The sensitivity study indicates that during ACE-2 not enough organic material is present at Sagres to introduce significant errors into our calculation by the 'dissolution effect' of slightly soluble organics.

Other effects

Some of the effects that might cause the calculated CCN concentration to be inaccurate are not known well enough to be included in a systematic sensitivity study. It has sometimes been proposed that certain organic species might inhibit or slow down the particle water uptake. If such compounds were present in atmospheric aerosol the CCN concentrations would be overestimated by the calculations in section 2.1. However, little is known about the occurrence of such substances in the ambient atmosphere. Some laboratory studies indicate that even thick coatings of water insoluble materials (DOP) cannot inhibit CCN formation (Cruz and Pandis, 1998).

Some surfactant organic species might have a stronger effect on the surface tension and lower the critical supersaturations much more strongly than dicarboxylic acids. The calculated number of equivalent ions is not very sensitive to the surface tension at 90% r.h. but the the activation behavior of the particle is much more strongly dependent on the surface tension. If the surface tension of the droplet decreases by 10% due to surfactant species, CCN concentrations could be underestimated by the calculations by up to 30%. However the surface tension of cloud water sampled in Tenerife during ACE-2 did not differ from that of pure water Faccini et al. (2000). This is an indication that the effects of surfactant species are probably not very important for this general aerosol type.

Moreover the uptake of soluble gases into the growing droplets could decrease S_c significantly. The uptake of soluble gases into concentrated solution droplets is difficult to estimate since it depends on the composition, concentration and pH of the solution. The uptake of soluble gases would lead to an underestimate of CCN concentrations by the calculations. For this study, it is impossible to estimate the magnitude of this effect because of lack of air chemistry and thermodynamic data.

Despite these possible shortcomings it can be useful to the calculate CCN spec-

tra in situations where the organic mass fractions are low. Both the hygroscopic growth factor and the aerosol size distributions can be measured using established, calibrated techniques at high size and temporal resolution. Using simple and tried measurement methods combined with calculations even if some assumptions have to be made can be an advantage to more complicated instruments that are susceptible to larger measurement uncertainties. In the following section one crucial assumption is tested against measurements to assure that it does not introduce significant errors into the CCN calculations.

5.3 Hygroscopic consistency study

The calculation of CCN based on hygroscopic growth factors involves the crucial step of estimating the number of equivalent ions in the aerosol particles which are representative of all hygroscopic and soluble species that contribute to the hygroscopic growth at 90% r.h.. If the aerosol does not contain much soluble organic material the number of equivalent ions based on hygroscopic growth factors should be comparable to the number of chemically analyzed inorganic ions in the particle. At Sagres, where the aerosol was mainly composed of ammonium and sulfate (on average more than 80% of the submicron mass) such a comparison is possible. Thus, a comparison of the number concentrations of equivalent ions calculated using hygroscopic growth factors and particle number size distribution to the number concentrations of inorganic ions found by the chemical analysis of impactor samples can be made. Similar studies have been done previously by Swietlicki et al. (1999); Berg et al. (1998a). If this internal consistency study is successful it gives confidence in the impactor and growth factor measurements and also in our ability to derive inorganic ions from growth factor measurements.

5.3.1 Data base

The data necessary for the hygroscopic consistency study are: the number concentration of inorganic ions chemically analyzed in impactor samples, the particle number size distributions from 50 to 800 nm, and hygroscopic growth factors to calculate the numbers of equivalent ions in a single aerosol particle. The latter two measurements can be combined to estimate the number concentration of equivalent ions in certain particle size ranges. During the ACE-2 measurement campaign in Sagres aerosol particles were sampled using a Berner type, low pressure impactor (Berner and Lürzer, 1980). The impactor collected aerosol in 5 stages with d_{50} cut-offs at 0.05, 0.14, 0.42, 1.2, 3.5, and 10 μm aerodynamic diameter (d_{ae}) at a controlled humidity of 60% r.h.. The deposits were extracted in deionized water and analyzed by capillary zone electrophoresis. Organic and elemental carbon were determined by a thermal desorption method. The experimental methods and the chemical data are described in more detail in Neusüß et al. (2000). The hygroscopic growth factors of particles with dry diameters of 35, 50, 100, 150 and 250 nm were measured using a TDMA (Swietlicki et al., 2000). Number size distributions were measured by a high resolution Twin Differential Mobility Analyzer(TDMPS) (Birmili et al., 1999) in the size range from 3 to 800nm.

This consistency test is done for the second impactor stage that collects particles with d_{ae} between 0.14 and 0.42 μm. The aerodynamic cut-off sizes of impactor stage 2 refer to particle sizes at the impactor sampling r.h. of 60% ($d_{ae}^{60\%}$), where the particles are probably still hydrated due to hysteresis effects and the occurrence of hygroscopic salts with low deliquescence humidities such as ammonium bisulfate. In the TDMPS and TDMA system the aerosol particles are dried to an r.h. of <10% before the measurements are made. Therefore the impactor cut-offs have to be converted to dry Stokes diameters (d^{dry}) to be comparable to the TDMA and TDMPS measurements:

$$d^{dry} = \frac{d_{ae}^{60\%}}{\sqrt{\rho(60\%) \cdot Gf(60\%)}} = d_{ae}^{60\%} \sqrt{\frac{Gf(60\%)}{\rho_{dry} + (Gf(60\%)^3 - 1) \cdot \rho_w}} \qquad (5.6)$$

where ρ_{dry} is the density of the dry aerosol particles, $\rho(60\%)$ the density of the aerosol particles at 60% r.h., ρ_w the density of water, and $Gf(60\%)$ the hygroscopic growth factor of the particles at 60% r.h.. Using (6) the lower and upper cut-off diameters of impactor stage 2 are converted to dry Stokes diameters of 0.1 μm and 0.29μm respectively. Campaign averages of the growth factors at 60% (1.21 at 0.1 μm and 1.25 at 0.25 μm) and a dry density of 1.6 g/cm^3 were used.

5.3.2 Calculation procedure

The concentration of equivalent ions for particles in the size interval between 0.1 and 0.29 μm is estimated from hygroscopic growth factors and the number size distribution. The hygroscopic growth factors at 100, 150 and 250nm are interpolated to the diameters of size distribution measurements. At those diameters the equivalent number of ions per particle N_i is calculated as described in section 2.1 using (2)-(5). Aerosol collected on impactor stage 2 consists almost exclusively (numbers) of ammonium and sulfate. The measured ammonium to sulfate ratio R of each impactor sample is used to decide if ammonium sulfate ($(NH_4)_2SO_4$, $R > 1.75$), letovicite ($(NH_4)_3H(SO_4)_2$, $1.25 < R < 1.75$) or ammonium bisulfate (NH_4HSO_4, $R < 1.25$) is the dominant sulfate compound. For ammonium sulfate and letovicite an appropriate empirical expression similar to (4) is used in the calculation. The empirical expressions are based on measured data by Tang and Munkelwitz (1994).

The growth factor measurements indicate that sometimes the aerosol at Sagres consists of an external mixture of more hygroscopic and less hygroscopic particles. For those external mixtures N_i values were calculated separately for the more hygroscopic

particles (N_i^{mh}) and the less hygroscopic particles (N_i^{lh}). The number concentration of equivalent ions $dN_i/d\log(d)$ at each diameter d_k of the size distribution measurements are calculated as follows:

$$\frac{dN_i}{d\log(d_k)} = N_i^{mh}(d_k) \cdot \frac{dN}{d\log(d_k)} \cdot n_{mh}(d_k) + N_i^{lh}(d_k) \cdot \frac{dN}{d\log(d_k)} \cdot n_{lh}(d_k) \qquad (5.7)$$

where $dN/d\log(d_k)$ is the number size distribution at diameter d_k and $n_{mh}(d_k)$ and $n_{lh}(d_k)$ are the relative number fraction of more and less hygroscopic particles at diameter d_k.

The number concentration of ions at the 7 diameters d_k that lie within the size interval between the cut-off diameters of impactor stage 2 are averaged. Since the impactor sampling time is much longer than the time for a TDMPS measurement, equivalent ions are calculated for each TDMPS measurement during one impactor run and subsequently averaged. Samples, for which less than 50% of the impactor run time is covered by DMPS and TDMA measurement are excluded from the analysis.

5.3.3 Results

The number concentration of inorganic ions as measured by chemical analysis of the deposits on impactor stage 2 vs. the number concentration of equivalent ions calculated from hygroscopic growth factors is shown in Figure 5.3 along with uncertainty estimates described below. Most of the data points lie close to the 1:1 line. Since the data points have uncertainties both in the x and y direction the reduced major axis regression (RMA) was used to fit a straight line to the data (Ayers, 2001). Unlike the conventional linear regression the RMA method yields a fit line that is invariant to exchanging the x and y axes. The resulting linear fit ($dN_i^{est}/d\log(d) = k \cdot dN_i^{meas}/d\log(d) + d$) yields k=0.91 and d=11 with R^2=0.9.

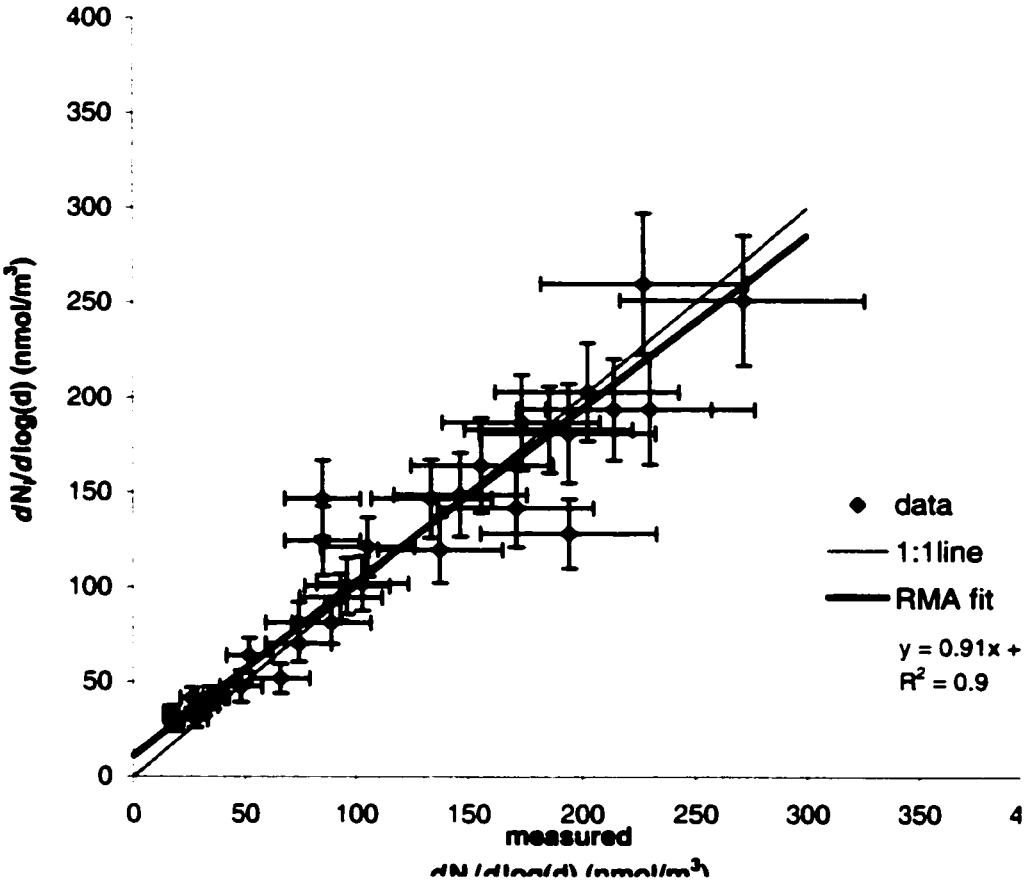

Figure 5.3: Comparison of the measured and the calculated ion number concentrations for impactor stage 2.

On average the ratio of calculated ion number concentrations to the measured ones is 1.11±0.28. This overestimate by 11% is mostly due to a difference in measured and calculated ion number concentrations in clean conditions. It can be seen that the measured values are significantly lower than the calculated values at very low aerosol

concentrations. If the 7 data points with ion number concentrations lower than 40 nmol m^{-3} are excluded, the average ratio of calculated to measured ions decreases to 1.03±0.21.

The consistency test can be considered successful if the differences in measured and calculated ion number concentrations can be explained by the measurement uncertainties. The consideration of the uncertainties in both measurements and calculations is thus an important part of a consistency test (see e.g. Quinn et al. (1996)). The uncertainties in the chemical analysis, particle number concentrations, and growth factors are estimated based on the 1σ standard deviation of repeated measurements, calibrations and counting statistics.

The 1σ uncertainty in number concentration of ions determined by the chemical analysis is roughly ±20% Neusüß et al. (2000). The experimental uncertainty of the hygroscopic growth factors at 90% r.h. is estimated to be ±5% due to sizing, flow and counting statistics in the TDMA system. Also the uncertainty in the fraction of more hygroscopic and less hygroscopic particles is approximately ±5% arising mostly from inaccuracies in the fitting routine. The particle number concentration is known to approximately ±10% and sizing errors of the TDMPS and TDMA system lead to an uncertainty in dry particle size of about ±1%.

The uncertainties in particle number concentrations and growth factor have to be propagated through the ion concentration calculation. A Monte Carlo approach is used for the error propagation. The input parameters (the more and less hygroscopic growth factors Gf^{mh} and Gf^{lh}, the fraction of more hygroscopic particles n_{mh}, the particle diameter d, and the particle number concentration $dN/d\log(d)$) are each randomly generated assuming that they are normally distributed around the measured value with a standard deviation of the measurement uncertainty. Then the number concentration of equivalent ions is calculated. This procedure is repeated

10,000 times and the mean and the standard deviation of the resulting 10,000 ion number concentrations are calculated. The standard deviation of the Monte Carlo results represents the uncertainty in the ion number concentrations arising from the measurement uncertainties. These uncertainties are averaged over the impactor size interval and measurement times.

The uncertainties in calculations and measurements are shown as uncertainty bars about the data points in Figure 5.3. These uncertainty bars represent 1 standard deviation, i.e. a probability of 68% that the 'true' ion concentration lies between those uncertainty bars. It follows that including uncertainty bars 68% or more of the data points must lie on the 1:1 line if the difference in calculated and measured ions is due to measurement uncertainties alone. In this experiment approximately 75% of the data include the 1:1 line within their uncertainty bars. This shows that the calculated and measured ion number concentrations agree within the measurement uncertainties and that the calculations and measurements are consistent within our experimental uncertainty.

5.3.4 Discussion

The results of the hygroscopic consistency study show that in the presence of low concentrations of organic material as observed in Sagres and generally during ACE-2 (Neusüß et al., 2000; Putaud et al., 2000) the calculated equivalent ion concentrations reproduce the measured number concentrations of inorganic ions successfully. This suggests that the hygroscopic growth factor measurements are valid and that it is possible to use those measurements for predicting the number of ions in a particle.

On average the calculated ion number concentrations are 11% greater than the chemically measured ion number concentration. At low number concentrations (clean conditions) this difference is significant. This is an indication that the particle water

uptake at 90% r.h. is higher than that attributed to the measured inorganic ions alone implying that other species such as soluble organics could have contributed to the hygroscopic growth. However, there is no indication that the particle water uptake not explained by inorganic ions increases when the mass fraction of organic compounds in Sagres is high. In fact these two quantities are completely uncorrelated. Thus there is no indication that organics contribute to the hygroscopic growth even in clean conditions when the organic mass fractions are higher. It is more likely that in clean conditions the detection level of the impactor measurements is approached. Systematic errors in the chemical analysis at those low sample amounts are most likely the explanation for the differences between measurements and calculations at low ion number concentrations.

5.4 CCN spectra in Sagres during ACE-2

Direct measurements of CCN spectra during ACE-2 in Sagres are limited to a few days. One objective of this work is to compare calculated and measured CCN spectra. Another more general objective is to calculate a larger data set of CCN spectra based on hygroscopic growth factors and number size distributions to be able to compare CCN spectra representative of different air masses and air mass histories that occurred during ACE-2. The number size distribution measured by the TDMPS system and growth factors measured by the TDMA are used in the calculations. For all particles in the size distributions the critical supersaturation S_c is estimated as described in section 1 using (1)-(5). The ammonium to sulfate ratios of impactor samples were used to identify the dominant sulfate salt and an appropriate empirical expression for each salt was used as equation 4. The number concentration of particles activated at supersaturation S is calculated as the sum over all particles with $S_c < S$. Experimental uncertainties in the measurements of hygroscopic growth factors,

particle diameters and number concentrations are propagated to CCN concentrations using a Monte Carlo method analogous to the one described in section 3. CCN spectra are calculated for all time periods in the ACE-2 field campaign in Sagres during which size distribution and growth factor measurements are available.

5.4.1 Comparison of calculated and measured CCN spectra

CCN spectra were measured using a CCN remover (CCNR) (Ji et al., 1998). In this instrument number size distributions are measured downstream of a supersaturation chamber, where S is varied from 0% to approximately 1% and nucleated particles are removed by gravitational settling. After passing the supersaturation chamber the particles are dried and their size distributions are measured by a electrical mobility analyzer. The difference between the number concentration of particles measured at S=0%, the reference size distribution, and the number concentration at a higher S yields the number concentration of CCN.

Each of the CCNR measurements was compared to calculated CCN spectra averaged over the CCNR run time. Figure 5.4(a) and (b) shows a comparison of calculated and measured CCN spectra on two different days. In both examples calculated and measured spectra are similar in shape but appear shifted by a constant concentration factor. This shift is most likely caused by a sample flow or dilution error in the CCNR as can be argued by comparing the dry reference size distributions measured by the CCNR and by the TDMPS system. As examples the reference size distributions of both instruments corresponding to the above CCN spectra are shown in Figure 5.4(c) and (d). Over all sample days the size distributions of both instruments are in most cases very similar in shape but like the CCN spectra they are shifted by a constant concentration factor. Since the DMPS size distributions have been validated in various comparisons (e.g. the hygroscopic consistency study in the previous chapter, a

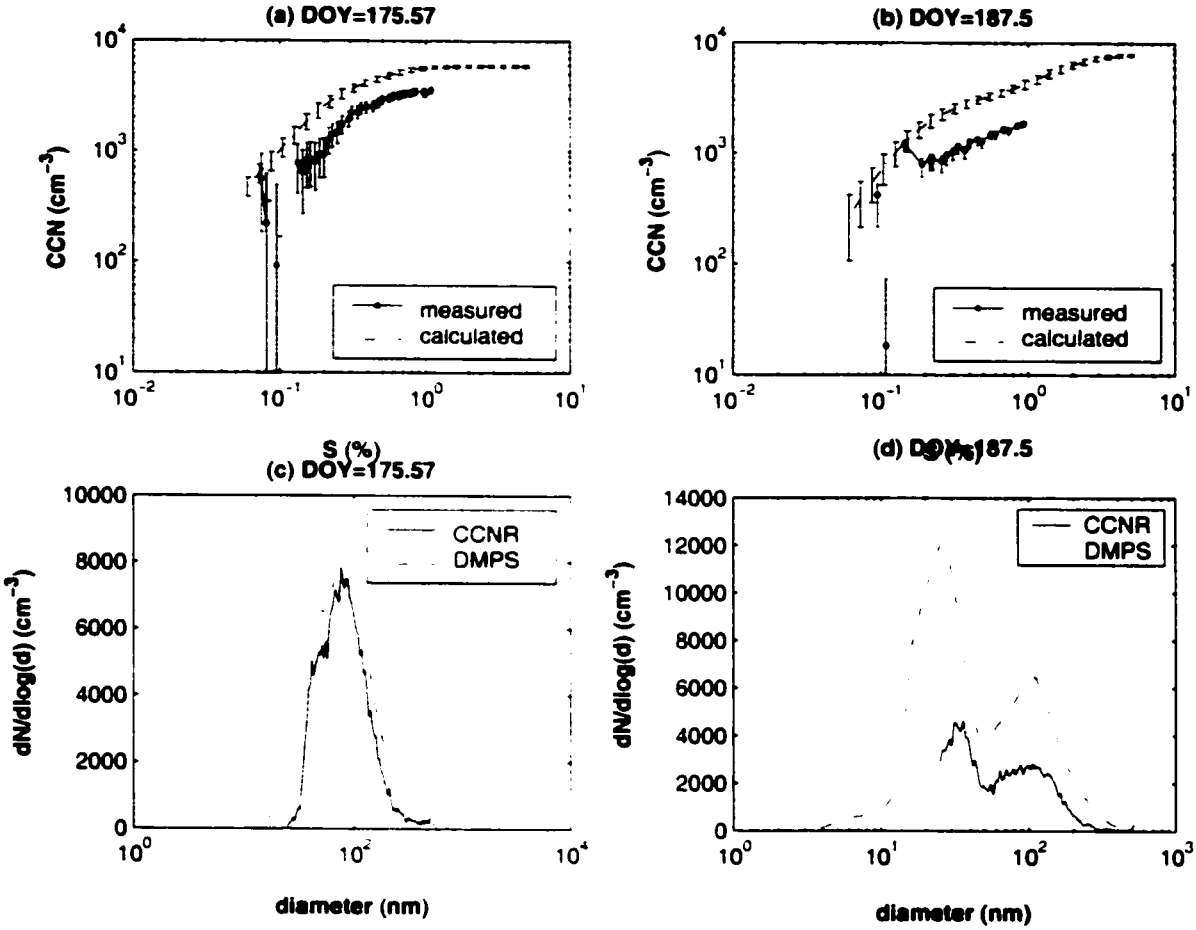

Figure 5.4: The upper panels show measured and calculated CCN spectra an two different days. The lower panels show the corresponding base size distributions as measured by the CCNR and the TDMPS system

closure study involving impactor mass. Neusüß et al. (2000), and a comparison of total number with a condensational particle counter) it seems likely that the size distributions in the CCNR are affected by a dilution and flow error.

Thus a further comparison of the differences in calculated and measured CCN spectra requires a correction of the CCNR concentration. Therefore, each CCN spec-

trum measured by the CCNR is multiplied by a correction factor to make the CCNR reference size distribution agree best with the TDMPS size distribution. After this first order correction, it seems that there is an additional loss of fine particles with diameters less than 40nm in the CCNR and occasionally there is a loss of larger particles. The causes for the fine particle loss are unclear at present since diffusion losses should not be large at 40nm. The loss of larger particles can be explained by the fact that the CCNR reference size distributions are measured after the aerosol passed the supersaturation chamber at S=0%. At these high relative humidities some of these particles can take up enough water due to hygroscopic growth that they fall out of the air stream as if they were cloud droplets and are missing in the base size distributions. These second-order differences in the reference size distributions are not corrected since the loss mechanisms are not completely clear and there is no consistent method for correction.

After the first-order correction the measured CCN spectra show a much better agreement with the calculated CCN spectra. The final results of this comparison are shown in Figure 5.5. The calculated and measured CCN number concentrations at S= 0.3%, 0.5%, 0.7% and 0.9% are plotted in Figure 5.5(a)-(d) along with the least square best fit (solid line) and the 1:1 line (dotted line). The results for the slope and residual of the linear regression lines ($CCN_{calc} = k \cdot CCN_{meas} + d$) are given in Table 5.1.

The R^2 values are generally high, between 0.89 and 0.93. The calculated CCN concentrations still seem to be larger than the measured CCN concentrations. The measurements and calculations differ on average by 35±20% at S=0.3%, 34±14% at S=0.5%, 27±10% at S=0.7% and 28±10% at S=0.9%. The difference is significant at the 95% confidence level in all cases. However it should be noted that at S=0.3% the mean difference between measurements and calculations is of the same order of

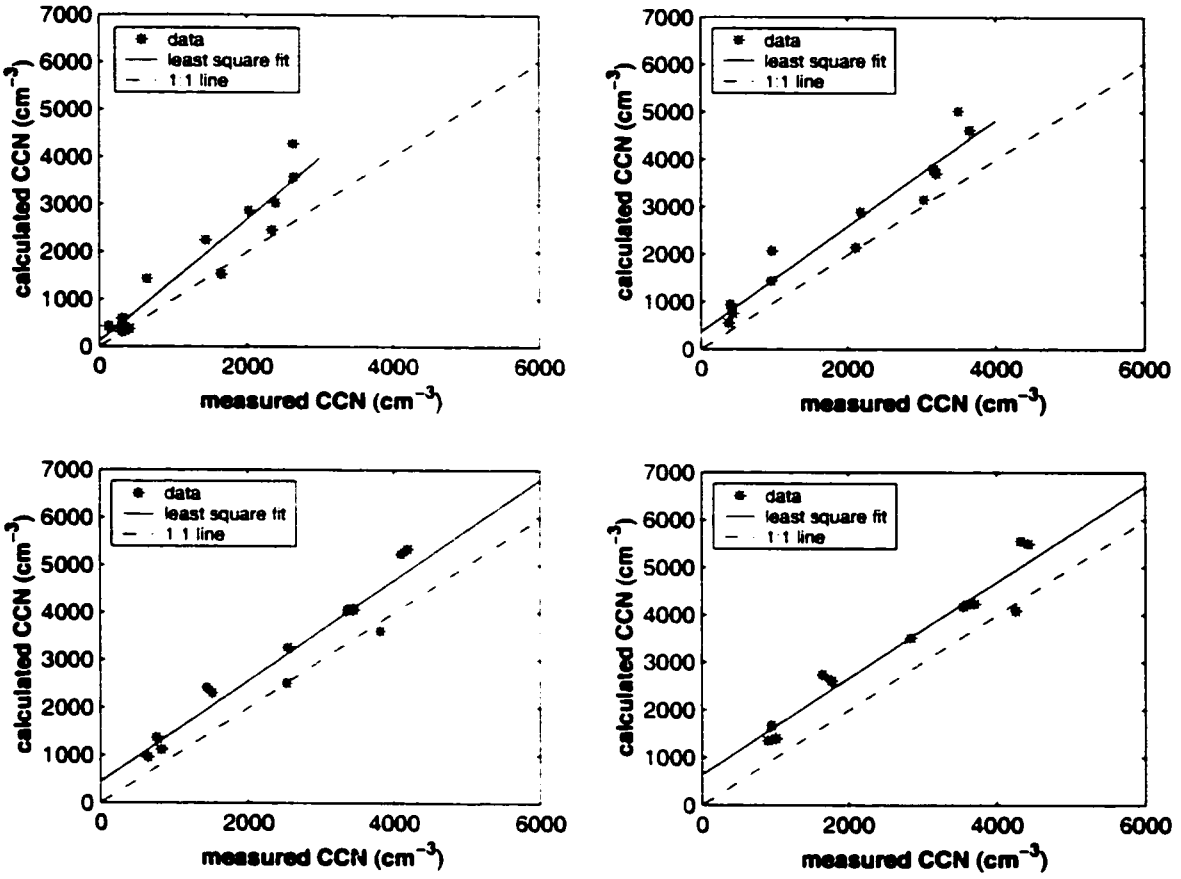

Figure 5.5: Calculated vs. measured CCN concentrations at different supersaturations. Also shown are the 1:1 line and the linear least square fit for each case

magnitude as the measurement uncertainties.

The overestimate could have different reasons. After the dilution correction there are still some differences in the base size distributions. for example due to the selective loss of large particles in the CCNR as explained above. These second-order differences in the base size distributions could explain some of the discrepancy between measured and calculated CCN spectra. but surely not all of it. Another possible reason is

Table 5.1: Slopes (k) and residuals for the linear least squares fits shown in Figure 5.5, with the corresponding 95% confidence intervals (CI)

S (%)	k	95% CI	d (cm^{-3})	95% CI	R^2
0.3	1.29	0.98-1.59	116	-403-635	0.89
0.5	1.12	0.89-1.33	367	-150-885	0.93
0.7	1.06	0.84-1.28	447	-150-1045	0.92
0.9	1.01	0.81-1.21	643	24-1261	0.93

that some of the aerosol particles might contain organic species that inhibit or slow down the water uptake. In this case particles that are technically activated at the supersaturation in the CCNR might grow too slowly to fall out of the air stream in the instrument. There have been indications that the Van't Hoff factor of ammonium sulfate might be lower than 3 in droplets of sizes near the critical radius. If the Van't Hoff factor was decreased by 30% in the growing droplets the assumption that the inorganic species are fully dissociated could introduce an error that varies from 20% to 10% for supersaturations from 0.3% to 1%.

Finally kinetic limitations could prevent the activation of some particles in the instrument. It has been proposed that this process might influence the CCN concentrations in stratus clouds (Chuang et al., 1997; Nenes et al., 2001). However due to the long residence time of the particles in the CCNR (greater than one minute) this effect is very unlikely. Thus the difference between measurements and calculations cannot be explained with certainty, especially since the hygroscopic consistency study showed agreement between measured ion number concentrations and equivalent ions derived from growth factor measurements. However it is also important to keep in mind that there are few data points in this comparison and the 95% confidence levels

on both the slopes and the residuals are quite large. The results should thus not be over interpreted.

The fact that the calculated CCN concentrations are larger than the measured ones suggests that in Sagres neither soluble gases, nor moderately soluble or surfactant organic compounds have a strong influence on the instrumental CCN activation. Surfactant organic species, slightly soluble organics, and soluble gases, all decrease the critical supersaturation (S_c). If any of those effects were significant in Sagres the calculated CCN concentrations would be lower than the measured concentrations. It might also be possible that these effects are present but their influence on the critical supersaturation is accounted for by the estimation of equivalent ions from hygroscopic growth factors.

In other recent studies (Chuang et al., 2000; Wood et al., 2000; Snider and Brenguier, 2000) the differences between measured and calculated CCN concentrations are larger than in this work and are in extreme cases as large as a factor of 5. In this context the comparison presented here seems to be reasonably successful after the dilution correction has been applied. There is a strong similarity in the shape of the calculated and measured CCN spectra and calculated and measured CCN concentrations are strongly correlated. It seems thus useful to complement the limited number of measured CCN spectra with a larger, calculated data set, that covers most of the ACE-2 period in Sagres, bearing in mind that CCN concentrations might be somewhat overestimated.

5.4.2 Calculated CCN spectra in different air mass conditions

During the ACE-2 field experiment the measurement site at Sagres was influenced by several different air mass types. For the first half of the experiment clean air coming from the Atlantic prevailed, whereas during the second half polluted air masses

originating over the European reached Sagres more frequently. The whole data set of CCN spectra is subdivided into clean and polluted time periods according to air mass back trajectories. Trajectories for the clean time periods originate over the Atlantic or the Arctic ocean as defined in Chapter 3. Trajectories for the polluted time periods are subdivided according to the distance, time and pathway from the source region as explained in Chapter 3. Air masses containing aged pollution originate over France or Great Britain and flow out over the Atlantic, where they spend several days before reaching Sagres. Air masses containing more recent pollution originate over central Europe or the Mediterranean region and cross the Iberian Peninsula before they reach Sagres from inland.

Figure 5.6(a) shows a comparison of average CCN spectra in clean conditions, aged and fresh pollution. The spectra in polluted air are similar at low supersaturations (S), but at S>0.1% the CCN concentrations in the recently polluted air mass exceed the CCN concentration in aged pollution by a factor of up to 3. This result agrees with observations that recently polluted air masses contain more newly formed particles and the aerosol size distribution is shifted towards smaller particles. These small particles are activated at higher supersaturations resulting in CCN spectra that increase strongly at higher S. In the aged pollution those fine particles have mostly vanished due to coagulation and growth processes. At the same time the number of larger particles in the air mass contaminated by aged pollution increases so that at low S the CCN spectra in aged pollution are comparable to the ones in fresh pollution. The clean air masses are comparatively devoid of large particles that activate at low supersaturations but the CCN spectra in clean conditions and aged pollution are similar at S>1%.

The CCN that are activated at supersaturations typical for stratus clouds are most important in the indirect effect of aerosols on climate. Those supersaturations

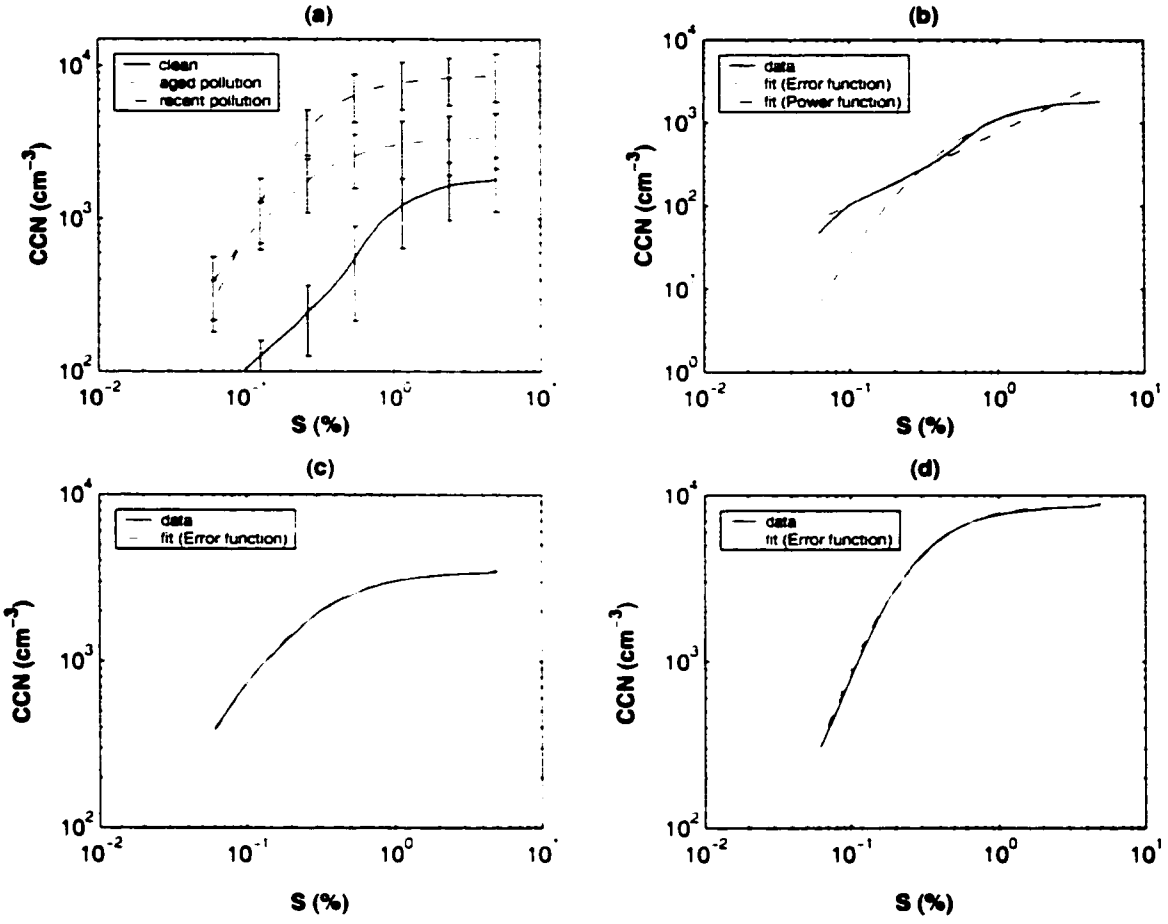

Figure 5.6: (a) Calculated CCN spectra averaged over all clean time periods (solid line) and over the time periods when Sagres received aged pollution (dashed line) and recent pollution (dash-dotted line). (b) Mean CCN spectrum for clean conditions is shown along with a fitted Error function (dashed line) and a fitted power function. (c) The average CCN spectrum in aged pollution (solid line) together with the best fit Error function (dotted line, mostly invisible because it coincides with the measured spectrum). (d) same as in (c) but for recent pollution

are generally estimated to lie below 0.5% (e.g. Cantrell et al., 1999; Vong and Covert, 1998). CCN activated at those low supersaturations are increased strongly by pollution. The CCN concentrations at S=0.2% are on the average 400-500 cm^{-3} in clean conditions and increase to approximately 1500 cm^{-3} in aged pollution and to 2500 cm^{-3} in recent pollution. Even aged pollution in air masses that spent several days over the ocean has a large effect on the CCN concentrations at supersaturations typical for stratus clouds. Similarly high cloud droplet number concentrations have been measured in a cap cloud in Tenerife during the ACE-2 measurement period when polluted air masses reached the island after days of transport over the ocean (Martinsson et al., 2000).

5.4.3 Parameterization of CCN spectra based on lognormal size distributions

The CCN spectra in different air mass conditions can be parameterized for modeling purposes. Traditionally a power function of the form $S = C \cdot S^k$ has been used for that purpose (e.g. Twomey, 1959; Hudson et al., 1998). However there is no physical reason why the CCN spectra should follow a power law. This has also been noted by Ji and Shaw (1998) who propose an exponential function for the description of CCN spectra. It is well established that the size distribution of the atmospheric aerosol within the Aitken and accumulation mode range can be described by one or a combination of two or more lognormal distributions. Since a CCN spectrum is to a first approximation an integration of the size distribution, the CCN spectra should have the form of an Error function (erf). In this work we thus chose the following function for the parameterization of the CCN spectra:

$$N_{ccn} = A\left(1 + erf\left[\frac{-log\,(S) + B}{C}\right]\right), \tag{5.8}$$

Table 5.2: Error function fit parameters for different air mass conditions

air mass	A (cm^{-3})	B	C
clean	940	0.2	1.4
aged pollution	1700	1.4	1.6
recent pollution	4240	1.2	1.2
clean (two error	86	2.4	-
functions)	805	0.1	-

with A, B and C as adjustable parameters.

The error function proposed in (8) was fitted to the three average CCN spectra in Figure 5.6(a). The parameters A, B, and C for each spectrum are summarized in Table 5.2.

The fitted curves are shown as the dashed lines along with the CCN spectra (solid lines) in Figure 5.6(b)-(d) for the three different air mass conditions. A single error function proposed in (8) provides an almost perfect fit for the CCN spectra in polluted conditions. These spectra clearly do not follow the traditional power function which would appear as a straight line on a log-log plot. Instead the spectra become sub linear near supersaturations of about 0.3% consistent with a lognormal particle size distribution. However the error function proposed in (8) does not provide a good fit for the average CCN spectrum in clean conditions. The CCN at low S are seriously underestimated as can be seen in Figure 5.6(b). This discrepancy arises because the particle size distributions in clean marine conditions are generally bimodal and cannot be approximated by a single lognormal distribution. Indeed the CCN spectra

of aerosol with a bimodal size distribution appear roughly linear in the log-log plot. The power function is therefore a better approximation for the clean CCN spectra than a single Error function although it is not theoretically linked to the particle size distribution. The power function is useful to approximate marine CCN spectra, but our results show that it cannot be simply extrapolated to polluted conditions. A better approximation for the clean CCN spectra is however achieved by using a linear combination of two error functions:

$$N_{ccn} = A1\,(1 + erf\,[-log\,(S) + B1]) + A2\,(1 + erf\,[-log\,(S) + B2])\,, \qquad (5.9)$$

where the parameter C has been set to 1. to avoid too many free parameters. The values of the parameters can be found in the lower part of Table 2. The fit (not shown in Figure 5.6(b)) is not visually distinguishable from the measured spectrum.

5.5 *Summary*

In this paper we proposed a method of calculating CCN spectra from measured number size distributions and particle hygroscopic growth factors. The hygroscopic growth factors are used to derive equivalent ions and equilibrium droplet growth and subsequently the critical supersaturation (S_c). Errors can be introduced into the calculations if the aerosol contains very high fractions of moderately soluble organic species, by the uptake of soluble gases into the growing droplet and by the presence of surface active organic compounds. In those cases the CCN concentrations would be underestimated. However, in Sagres the calculated CCN concentrations are larger than the measured ones. Therefore it can be concluded that organic species and dissolution of soluble gases did not have a strong influence on the CCN activation at

this location.

The method of estimating equivalent ions from hygroscopic growth factors was independently tested by an internal hygroscopic consistency study. The number concentration of calculated equivalent ions was compared to the number concentration of ions obtained from chemical analysis of impactor samples. Measured and calculated ions agree within the respective uncertainties except for samples taken on days with low particle number concentrations. In those very clean conditions the calculated ion concentrations are substantially higher than the measured concentrations and it is likely that the detection level of the impactor/chemical analysis method is reached.

CCN spectra were calculated throughout the ACE-2 measurement period whenever size distribution and growth factor measurements were available. The spectra were averaged over time periods when Sagres received clean North Atlantic air masses and air masses influenced by aged or recent pollution from continental Europe. CCN concentrations at supersaturations typical for stratus clouds are strongly enhanced by pollution outbreaks compared to CCN concentrations in marine background conditions. Even in air masses that contain aged continental pollution and spent several days over the Atlantic before reaching Sagres the CCN concentrations at S=0.2% are about 3 times higher than in clean air masses. In recent pollution when air masses reach Sagres from inland or the Mediterranean sea the CCN concentrations are about 5 times higher than in clean air masses.

In polluted air masses the shape of the CCN spectra changes. The clean spectra can be described by the power function often used in the literature, although this function is not physically linked to the particle size distribution. This power function is only a good approximation to the clean CCN spectra if the size distribution is bimodal in marine background air masses. When continentally polluted air masses reach Sagres the number size distribution resembles a unimodal lognormal

distribution. In those polluted cases an error function provides a very good fit to the data.

Chapter 6

HYGROSCOPIC GROWTH AND AEROSOL PROPERTIES

Parameterizations of diameter growth factors and of the humidity dependence of aerosol optical properties are important for assessing the direct effect of aerosols on climate. Climate models face the challenge to link mass concentrations of anthropogenic aerosol to the direct radiative forcing (DF) of these particles. Often a semi-empirical equation is used to relate DF to the aerosol burden. An example for a semi-empirical expression is the equation proposed by Charlson et al. (1992) that expresses the direct radiative forcing of anthropogenic sulfate (DF_{SO_4}) aerosols as a function of sulfate column mass burden $\bar{B}_{SO_4}$ and several empirically determined radiative properties of the sulfate aerosol:

$$DF_{SO_4} = -\frac{1}{2} F_T \cdot T^2 \cdot (1 - A_c) \cdot (1 - \bar{R}_s)^2 \cdot \bar{B}_{SO_2} \cdot \alpha_{SO_4} \cdot f_s(r.h.) \cdot \bar{\beta}. \qquad (6.1)$$

The first four parameters characterize radiative properties of the earth-atmosphere system, that are independent of the aerosol. F_T is the top of the atmosphere radiative flux, T the transmittance of the atmosphere above the sulfate layer, A_c the fractional cloud cover and $\bar{R}_s$ is the mean albedo of the underlying surface. The remaining parameters characterize radiative properties of the aerosol particles. α_{SO_4} is the scattering coefficient per unit mass of the dry aerosol. However ambient aerosol particles are not usually in the dry state, but contain a certain amount of water

dependent on the ambient relative humidity. f_s(r.h.) represents the average increase in the light scattering coefficient due to particle water uptake in the ambient atmosphere. The product of α_{SO_4}, $\bar{B}_{SO_4}$, and f_s(r.h.) is the column averaged light scattering of sulfate aerosols at ambient conditions. The fraction of incoming radiation scattered back to space is obtained by multiplying the total light scattering with the up-scatter fraction $\bar{\beta}$. $\bar{\beta}$ represents the radiation scattered in the upward hemisphere averaged over a whole diurnal cycle. More refined equations have been proposed to include aerosol absorption (e.g Haywood and Shine, 1995; Chylek and Wong, 1995). All the expressions found in the literature have in common that the direct aerosol forcing depends on f_s(r.h.).

Calculated values of f_s(r.h.) for the aerosol measured in Sagres during are presented in this chapter. They are derived using the diameter growth factors measured by the HTDMA and the dry number size distributions measured by the HTDMA. First ambient, humidified number size distributions are calculated. The humidified and the dry size distribution are used in Mie calculations to derive scattering properties for the dry and the humidified aerosol. This approach makes it possible to relate f_s(r.h.) to diameter growth factors and properties of the number-size distribution. This ability to derive simple parameterizations of f_s(r.h.) is an advantage of calculating f_s(r.h.) from more basic aerosol properties.

The measurement methods of both the size distribution and hygroscopic growth factors are relatively simple and established and have been evaluated in several consistency studies (e.g. Swietlicki et al., 1999; Berg et al., 1998a; Birmili et al., 2000). This might be an advantage to using more complicated instruments that measure f_s(r.h.) more directly, but are more susceptible to measurement errors and not well characterized. However the calculations rely on some assumptions about the particle refractive index and shape, that could lead to errors in the calculated f_s(r.h.). During

ACE-2 in Sagres measurements of the light scattering of dry and humidified particles are available. This gives an opportunity to compare the calculated f_s to direct measurements.

6.1 Theory

Particles scatter light by re-radiating incident energy at the same wavelength but in a direction different from the direction of the incident light. The intensity of the scattered light varies with scattering angle ϕ. The direction of the scattering angle is defined as ϕ=0 for light scattered in the same direction as the incident beam (forward scattering) and ϕ=π for scattering in the opposite direction as the incident beam (backscattering). This is illustrated in Figure 6.1.

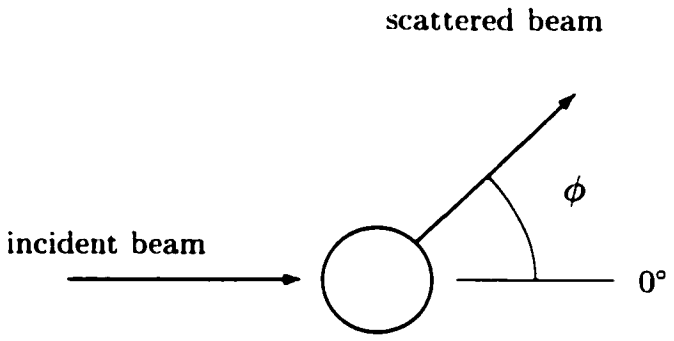

Figure 6.1: Definition of scattering angle ϕ

Due to complicated interaction of a small particle with an electro-magnetic field particles often remove a different amount of light from the original beam, than the 'shadow' they cast by their geometric cross section. The scattering efficiency Q_s is

defined as the ratio of the scattering cross section and the geometrical cross section of an aerosol particle. Q_s depends only on the particle reflective index m and on the ratio of particle diameter to the wavelength of the incident light.

$$Q_s = \frac{1}{\alpha^2} \int_0^{\pi} (i_1(\phi, \alpha, m) + i_1(\phi, \alpha, m)) \cdot sin(\phi) d\phi. \tag{6.2}$$

where the size parameter α is defined as:

$$\alpha = \frac{\pi d}{\lambda}. \tag{6.3}$$

d is the particle diameter, λ is the wavelength of incident light. i_1 and i_2 are the so-called angular intensity functions. These angular intensity functions relate the intensity $I(\phi)$ scattered into the angle ϕ to the incident intensity I_0. For unpolarized incident light the component of $I(\phi)$ polarized normally to the scattering plane is given as:

$$I(\phi)^{\perp} = I_0 \cdot \frac{i_1(\phi, \alpha, m)}{k^2 r^2} \tag{6.4}$$

and the component of $I(\phi)$ polarized normally to the scattering plane is given as:

$$I(\phi)^{\parallel} = I_0 \cdot \frac{i_2(\phi, \alpha, m)}{k^2 r^2}. \tag{6.5}$$

where k is the wave number and r is the distance from the particle to the observer. Mie theory provides a method of calculating i_1 and i_2 by solving the Maxwell equations subject to the particle surface boundary conditions. A Mie routine by Wiscombe (1980) is used for the calculations presented in in this work.

The scattering coefficient σ_s of an aerosol with number size distribution dN/dlog(d) can be calculated as:

$$\sigma_s = \int_0^{d_{max}} Q_s(\alpha, m) \cdot \frac{\pi d^2}{4} \cdot \frac{dN}{dlog(d)} dlog(d). \tag{6.6}$$

Figure 6.2 shows the scattering cross section as a function of particle size compared to the actual cross section of the particle.

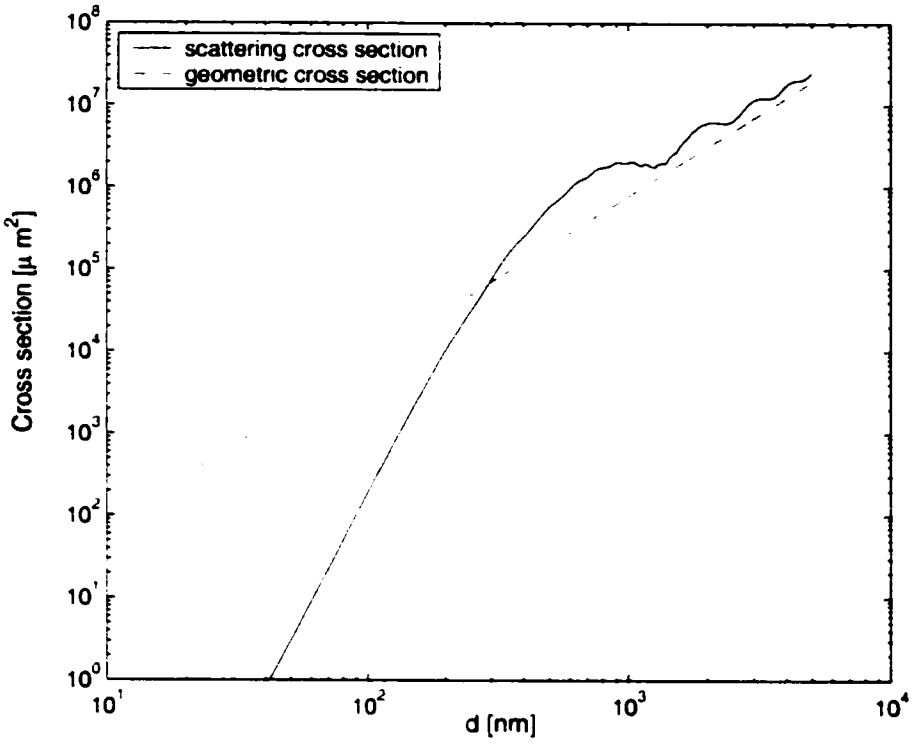

Figure 6.2: Scattering cross section as a function of particle size for an incident wavelength of 500nm

The scattering cross section is calculated for an incident wavelength of 550 nm, a wavelength near the peak of the solar spectrum. At particle diameters below 200nm the scattering cross section is lower than the physical cross section of the particle. Particles in the Aitken mode size range and even small accumulation mode particles do not scatter light very efficiently. Particles with sizes from 300 to 1000nm scatter more light than their physical cross section blocks out of the incident beam and the

scattering cross section for particles in the coarse mode range shows oscillates between the physical cross section and values larger than the physical cross section. Except for small ripples on the main peaks the scattering cross section increases monotonically with size. The main reason why hygroscopic growth increases the scattering of the particles is to a first order the increase in particle surface area.

Figure 6.2 can be used to qualitatively explain the fact that the humidity dependence of the scattering is in general dependent on the dry particle size distribution. For a single particle of a certain dry size the increase in scattering by hygroscopic growth can be estimated by increasing the particle size by a factor of 1.5 to 2, which is typical for hygroscopic growth at 80-90% and compare Q_s at both sizes. For particles smaller than 200nm the scattering cross section increases very strongly with particle size. If the particle size doubles the scattering cross section increases nearly two orders of magnitude. The increase of scattering with particle diameter is approximately linear in the log-log plot, indicating that in this size region the increase in scattering with humidity is independent of dry particle size and only dependent on the diameter growth factor. However at larger sizes where most of the scattering occurs the shape of the curve is more complicated. The increase in scattering with humidity is dependent on the dry particle diameter or, if a whole size distribution is considered, on the dry size distribution.

The calculations presented in this chapter focus on submicron particles. There is evidence that anthropogenic coarse particles, such as road dust or dust from disturbed soils contribute to the direct forcing of climate (Tegen et al., 1996).However these particles generally exhibit little hygroscopic growth, which is supported by some measurements on the hygroscopic growth of coarse mode particles in an urban environment (Hitzenberger et al., 1997) and a study on the light scattering of mineral dust (Li-Jones et al., 1998). In the marine environment most of the coarse particles

are sea salt particles, which are hygroscopic in nature. However since these particles are of natural origin they are generally not important for the anthropogenic aerosol forcing of climate.

6.2 Scattering consistency study

6.2.1 Direct measurements of scattering coefficients at high and low relative humidity

During the ACE-2 field experiment scattering coefficients at high and low r.h. were measured by a controlled humidity nephelometry system (Carrico et al., 1998, 2000) at the Sagres measurement site. The system is a Tandem-Nephelometer consisting of two integrating nephelometers model TSI 3563. The first nephelometer is operated at relative humidities smaller than 30% to assure a relatively dry aerosol. The second nephelometer is operated at relative humidities near 82%. Before the aerosol enters the Tandem-Nephelometer a defined upper cut-off size is imposed by an impactor. This cut-off size alternates between 1μm and 10μm. The consistency study is limited to the measurements with an upper cut-off size of 1μm, since the calculations present later in this section focus on sub micrometer particles.

The directly measured scattering humidification factor f_s^m(r.h.) is defined as the ratio between the scattering coefficients measured in the dry and the humidified nephelometer: $f_s^m(\text{r.h.})=\sigma_s^m(\text{r.h.})/\sigma_s^m(\text{dry})$ at r.h.=82%. Figure 6.3 shows the measured scattering coefficients at 28% and 82% r.h. and f_s^m(82%) for the ACE-2 measurement period.

The first half of the measurement period was dominated by clean air masses originating over the Atlantic interrupted by a few pollution episodes. The second half of the measurement period was dominated by polluted air mass originating over Europe. The scattering coefficients in polluted periods were up to 50 times larger than

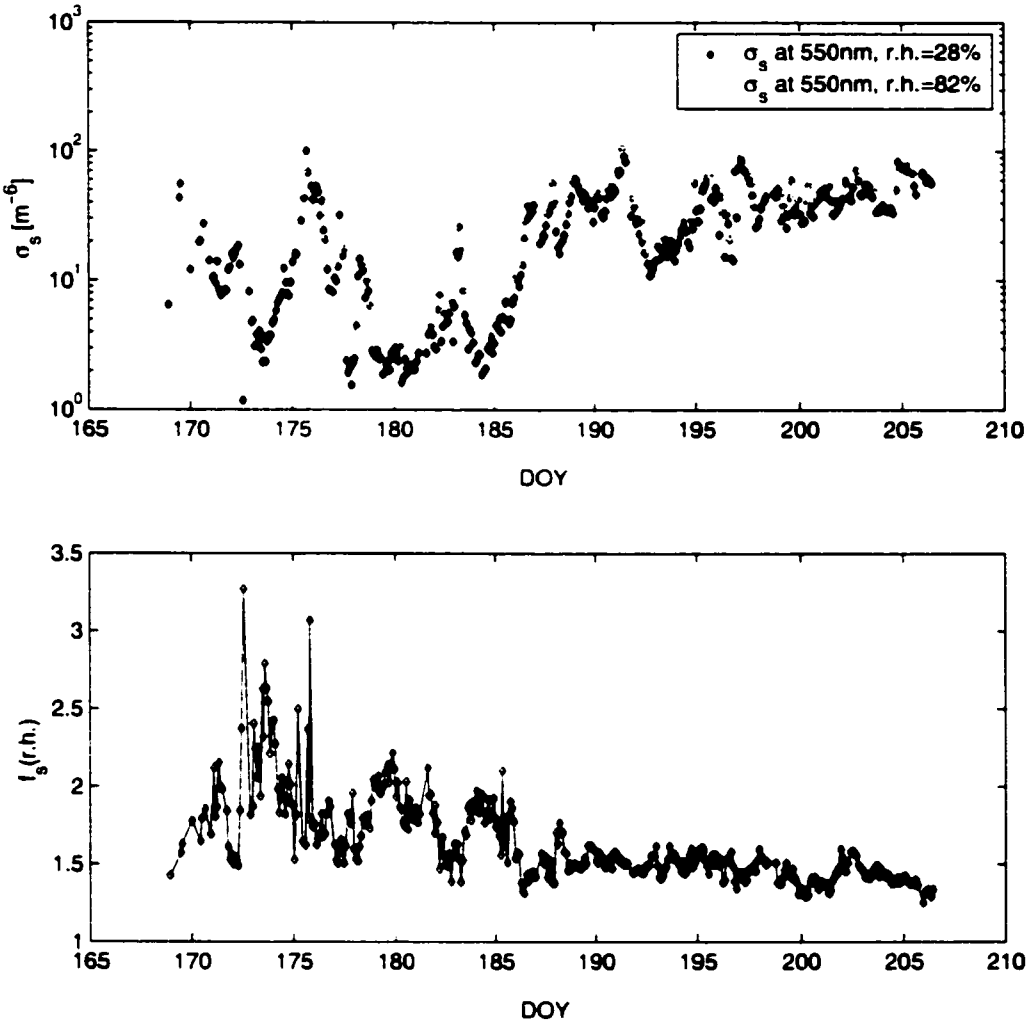

Figure 6.3: Overview of the measured scattering at Sagres during ACE-2:(a) Scattering coefficients at 28% r.h. and at 82% r.h.. (b) $f_s^m(82\%)$

those in clean periods. The increase due to the humidification is a second order effect compared to the increase in scattering caused by increased particle concentration during polluted periods . f_s^m is higher and more variable during the first part of the experiment. It decreases to approximately 1.5 and is surprisingly stable during the

second, more polluted part of the experiment.

6.2.2 *Modeling the nephelometer data based on number size distributions and diameter growth factors*

The scattering coefficient measured by the nephelometer is slightly lower than the actual scattering coefficient because the nephelometer measures light scattered into the angles between approximately 7° and 170° degrees and not 0° and 180° degrees as it ideally should. The effect of this truncation is not very large for sub-micrometer particles (Anderson et al., 1996), but has to be included into the calculations. To estimate the scattering measured by the nephelometer (σ_s^m) the scattering efficiency is calculated similar to Equation 6.2, but with modified integration limits:

$$Q_s^c = \frac{1}{\alpha^2} \int_{7°}^{170°} (i_1(\phi, \alpha, m) + i_1(\phi, \alpha, m)) \cdot sin(\phi) d\phi. \tag{6.7}$$

The size distribution measured by the DMPS system is not a continuous distribution as used in Equation 6.6 , but a discrete series of particle number concentration ΔN_i counted in certain finite diameter intervals Δd_i. To calculate the scattering coefficient a discretized version of 6.6 is used:

$$\sigma_s^c = \sum_{d_{min}}^{d_{max}} Q_s^c(d_i, \lambda, m) \cdot \frac{\pi d_i}{4} \cdot \Delta N_i, \tag{6.8}$$

where ΔN_i is the number concentration of particles in the size bin Δd_i with central diameter d_i.

To calculate σ_s at 82% r.h. the central diameters of the DMPS size bins are shifted to larger sizes d_i^w using diameter growth factors. Those d_i^w were then used in Equation 6.8 instead of d_i. The details of the calculation, such as estimating the diameter growth factors at 82% r.h., the calculation of the wet size distribution and the particle refractive indices are explained in the following sections.

Estimating the hygroscopic diameter growth factors at 82% r.h.

The Tandem Differential Mobility Analyzer (TDMA) measures diameter growth factors at 90% r.h. and at dry particle diameters of 35, 50, 100, 150, and 250 nm. The diameter growth factors measured by the TDMA were corrected to 82% r.h. using the correction method developed by Swietlicki et al. (1999) and summarized in Equations 2.9-2.12 in Chapter 2. The average diameter growth factors at 82% r.h. are summarized in Table 6.1 for the cleaner first half (DOY 171-186) and the more polluted second half (DOY 186-205) of the ACE-2 measurement period. The table includes both more and less hygroscopic growth factors (Gf_{mh} and Gf_{lh}) and the average number fraction of less hygroscopic particles Nf_{lh}. Unlike f_s^m(r.h) the particle

Table 6.1: Hygroscopic properties of the aerosol in Sagres in the cleaner first half of the experiment and in the more polluted second half of the experiment. The growth factors are at 82% r.h.

	35nm	50nm	100nm	150nm	250nm
			DOY 171-186		
Gf_{mh}	1.28	1.28	1.31	1.33	1.34
Gf_{lh}	1.10	1.10	1.12	1.11	1.10
Nf_{lh}[%]	30	23	13	14	10
			DOY 186-205		
Gf_{mh}	1.27	1.28	1.29	1.30	1.33
Gf_{lh}	1.09	1.09	1.09	1.10	1.10
Nf_{lh}[%]	24	15	12	10	15

hygroscopic properties at 82% r.h. do not differ strongly between clean and polluted time periods.

The diameter growth factors do not cover the whole submicron size range. A significant fraction of the scattering is done by particle larger than 250nm and in this size range no direct information on diameter growth factors is available. The growth factors for particles larger than 250 are estimated using the chemical composition of particles collected on the third stage of a low pressure cascade impactor that was operated at the Sagres measurement site. This impactor stage has cut-off sizes of 0.42 and 1.2μm equivalent aerodynamic diameter at 60%. These aerodynamic diameters are corrected to geometric dry diameters assuming a dry particle density of 1.8 g cm^{-3} and hygroscopic growth factors of 1.16 at an r.h. of 60% and using Equation 5.6. This results in a central diameter for the third impactor stage of approximately 510nm.

The average chemical composition of particles collected on the third impactor stage during the ACE-2 field experiment is shown in Figure 6.4. The aerosol particles in this size range consist mostly of ammonium and sulfate, but a significant fraction sodium and black and organic carbon can be found in the submicron particles as well.

The water uptake of particles in the size range of 300 to 850 is estimated by using the program AIM (Clegg et al., 1998), which calculates the water uptake of particles of known composition at a specified r.h.. The input chemical species required by AIM are mass concentrations of H+, Cl^-, Na^+, NH_4^+, SO_2^{2-} and NO_3^-. It is assumed that organic species do not contribute to the water uptake, which is a good approximation for the aerosol in Sagres where volatile carbon concentrations are low.

Once the mass concentration of particulate water (m_w) at 82% r.h. is calculated, mass growth factors (Gf_m) can be calculated as:

$$Gf_m = \frac{m_{dry} + m_w}{m_{dry}}, \tag{6.9}$$

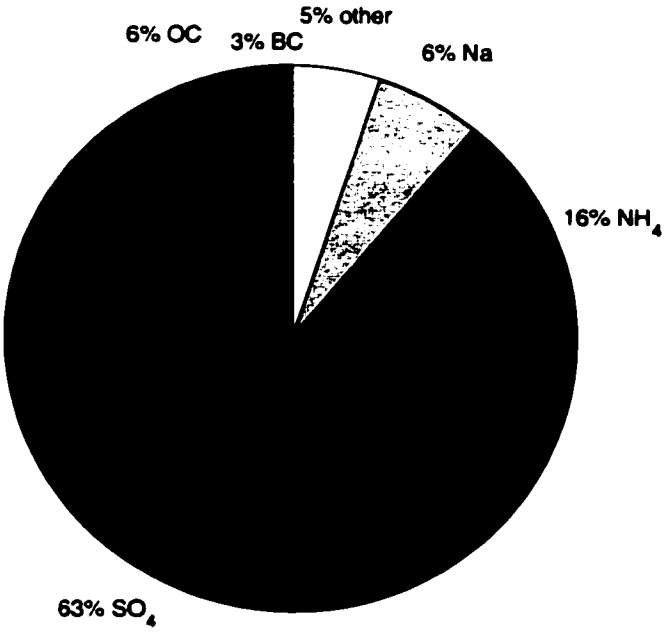

Figure 6.4: Average chemical composition of impactor stage 3 for the ACE-2 measurement period in Sagres

where m_{dry} is the dry particle mass. This dry particle mass is somewhat difficult to estimate, since the impactor samples were stored and weighed at 60% r.h.. Atmospheric particles in the atmosphere are usually somewhat hydrated, since they are on the upper part of hysteresis curve but the water uptake of deposited particle samples is questionable. Neusüß et al. (2000) estimated the dry mass concentration, but for the third impactor stage this dry mass concentration is on average 10% smaller than the mass of all analyzed chemical species, which indicates that the water uptake at 60% r.h. is overestimated. Considering this uncertainty regarding the water uptake of deposited particles at 60% r.h. two extremes cases are assumed for the purpose of this consistency study. First the assumption is made that the particles are dry at 60% r.h. which results in an upper limit of the dry mass and thus in a lower limit of

the estimated hygroscopic growth factors. Second the assumption is made that the dry mass derived by Neusüß et al. (2000) is correct which results in an upper limit of the estimated hygroscopic growth factors.

Having estimated Gf_m, the diameter growth factors Gf at 510nm are calculated as:

$$Gf = \left(1 + \frac{\rho_{dry}}{\rho_w} \cdot (Gf_m - 1)\right)^{1/3}, \tag{6.10}$$

where ρ_{dry} is the density of the dry particles and ρ_w is the density of water. ρ_{dry} is calculated as the mass weighted average density of the chemical species found on the third impactor stage. The resulting diameter growth factors are on average 1.45 for the higher estimate of dry mass and an upper limit of 1.55 for the lower estimate of dry mass. The hygroscopic growth of particles greater than 250 nm has large uncertainties. Moreover the duration of impactor measurements is between half a day and two days, but generally the hygroscopic growth factors show considerable variability on shorter time scales. The average growth factor over the impactor measurement period might not be representative of the hygroscopic growth factor at any given time during that period. Therefore it is not possible to compare the measured f_s(r.h.) on a case by case basis. However a comparison of longer averages of f_s(r.h.) or the humidified scattering coefficient should still be possible.

Calculation of the humidified particle size distributions

To calculate humidified size distributions the diameter growth factors of the more hygroscopic (mh) and, if present, of the less hygroscopic (lh) particles are interpolated linearly to the central diameters d_i of the DMPS size bins. The diameter growth factors derived from particle chemical composition are treated as an additional hygroscopic growth factor at a particle diameter of 510nm. The same is done with the fraction of more hygroscopic particles F_{mh}. The interpolated hygroscopic properties

are referred to as Gf_i^{mh}, Gf_i^{lh} and F_i^{mh} in the following derivations. If less hygroscopic particles are present the hydrated size distributions for more and less hygroscopic particles are calculates separately. Each is described by a set of wet diameters and corresponding ΔN_i that are calculated according to:

$$d_i^{w,mh} = Gf_i^{mh} \cdot d_i \qquad \text{with} \qquad \Delta N_i^{mh} = \Delta N_i \cdot F_i^{mh} \tag{6.11}$$

and

$$d_i^{w,lh} = Gf_i^{lh} \cdot d_i \qquad \text{with} \qquad \Delta N_i^{lh} = \Delta N_i \cdot F_i^{lh} \tag{6.12}$$

An example of the resulting hydrated size distributions of more and less hygroscopic particles are shown in Figure 6.5.

Wet scattering coefficients are separately calculated for the size distribution of more hygroscopic particles and the size distribution of less hygroscopic particles using Equation 6.8. The resulting two scattering coefficients are subsequently added. The lower size limit d_{min} used in Equation 6.8 is 3nm which is the minimum size of the DMPS measurements. The upper size limit d_{max} is defined by the 1 μm aerodynamic cut off size of the impactor prior to the Tandem Nephelometer. Assuming a dry particle density 1.8 g cm^{-3}, this cut-off corresponds to a geometric diameter of approximately 720nm.

Estimation of refractive indices

The calculated scattering coefficients depend on the refractive index of the submicron aerosol particles. However the refractive index of the aerosol was not measured directly, and has to be estimated using the measured chemical composition of submicron particles in Sagres during ACE-2. The average chemical composition of the submicron aerosol is shown in Figure 6.6 for clean and polluted conditions. In both cases the particle composition is dominated by ammonium and sulfate. In clean con-

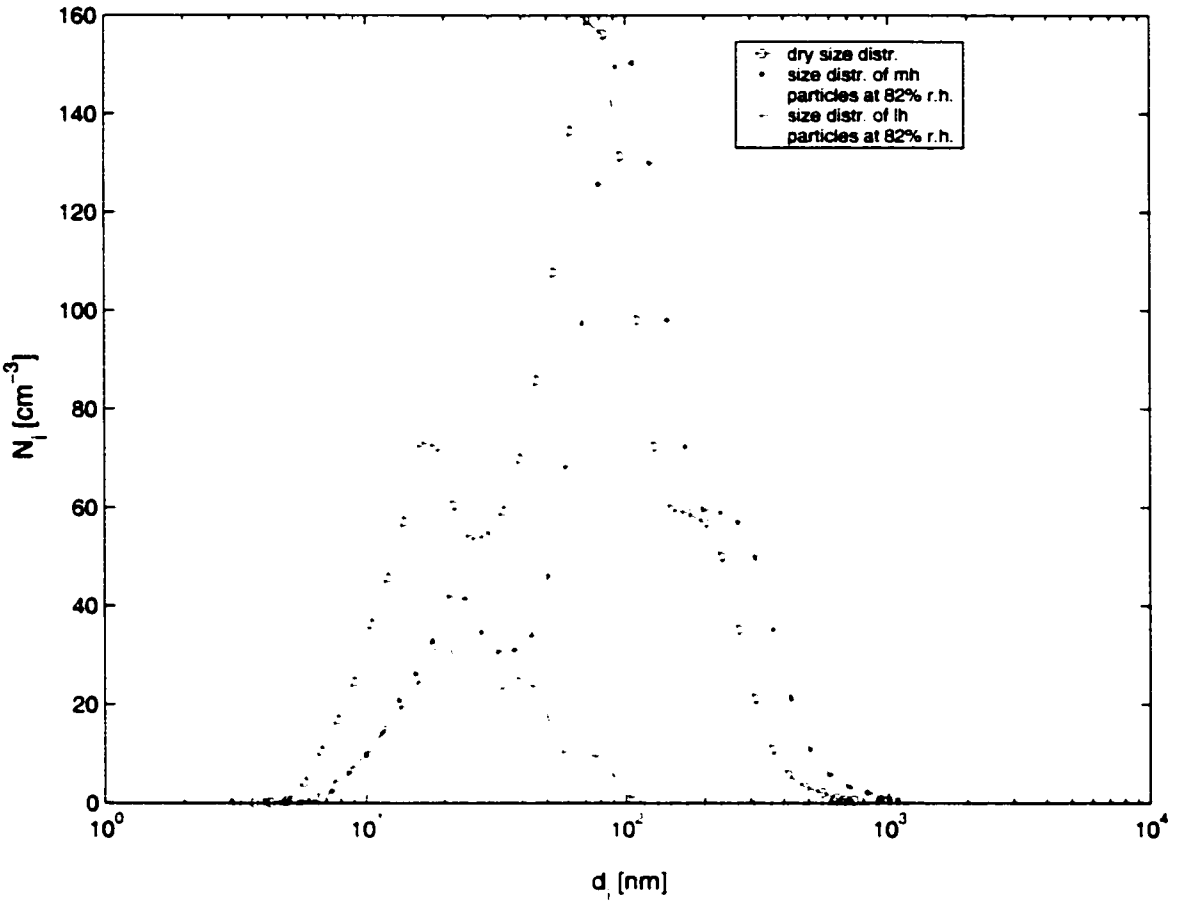

Figure 6.5: An example of dry and hydrated size distributions: (a) number size distribution, (b) volume size distribution

ditions ammonium and sulfate account for almost 60% of the submicron mass, and in polluted conditions these compounds account for more than 80% of the submicron mass. Concentrations of black and organic carbon are generally low. In clean conditions sea salt contributes significantly to the particle mass.

The real and imaginary parts of the refractive index m=n-ik for chemical compounds important in Sagres during ACE-2 is given in Table 6.2. The data are taken

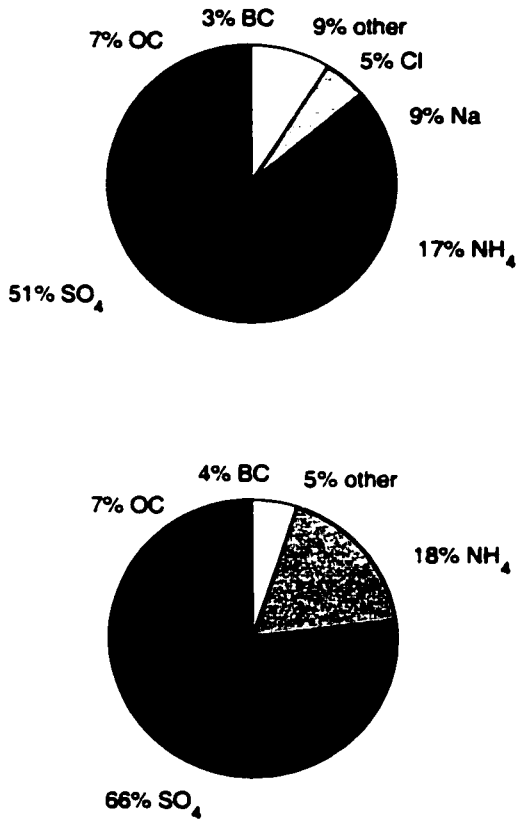

Figure 6.6: Chemical composition of submicron particles: (a) clean conditions (b) polluted conditions

from Seinfeld and Pandis (1998).

Table 6.2 shows that the refractive index of sulfate compounds depends on the neutralization state of sulfate. It increases from 1.43 to 1.52 for ammonium to sulfate ratios from 0 (H_2SO_4) to 2 ($(NH_4)_2SO_4$). The refractive index of sea salt is slightly higher that the refractive index of sulfates. Black carbon is the only absorbing species in this scenario.

The refractive index for the submicron aerosol is estimated as the mass weighted

Table 6.2: Refractive indices of selected chemical compounds important for the atmospheric aerosol in Sagres

Substance	n	k	λ
NaCl	1.544	0	589
H_2SO_4	1.426	0	589
NH_4HSO_4	1.473	0	589
$(NH_4)_2SO_4$	1.521	0	589
black carbon	1.96	0.66	550

average of the refractive index of individual chemical compounds. The ammonium to sulfate ratio is 1.73 in clean and 1.43 in polluted conditions. This is consistent with a mixture of 73% ammonium sulfate and 27% ammonium bisulfate in clean conditions and 43% ammonium sulfate and 57% ammonium bisulfate in polluted conditions. Since the refractive index of organic carbon and the other minor components is not known exactly the refractive indices of those compounds is assumed to have a lower bound of 1.4 and an upper bound of 1.6. This results in a refractive index between 1.51+0.020i and 1.54+0.020i for clean conditions and between 1.50+0.026i and 1.52+0.026i in polluted conditions. Since those refractive indices are not too dissimilar a refractive index of 1.51+0.02i is assumed as a base case for all particles.

The refractive index of humidified particles is calculated as a volume weighted average of the dry refractive index and the refractive index of water, as proposed by Bruggeman (1935).

$$m_{wet} = \frac{m_{dry} + m_w\,(Gf^3 - 1)}{Gf^3} \tag{6.13}$$

6.2.3 Results

Figure 6.7 shows a comparison of the measured and simulated scattering coefficient at dry conditions for the whole ACE-2 experiment in a base case simulation using a constant refractive index m=1.51-0.02i and a dry cut-off diameter d_{cut}=725nm. Figure 6.7 shows that the measured data can be reasonably well approximated using a

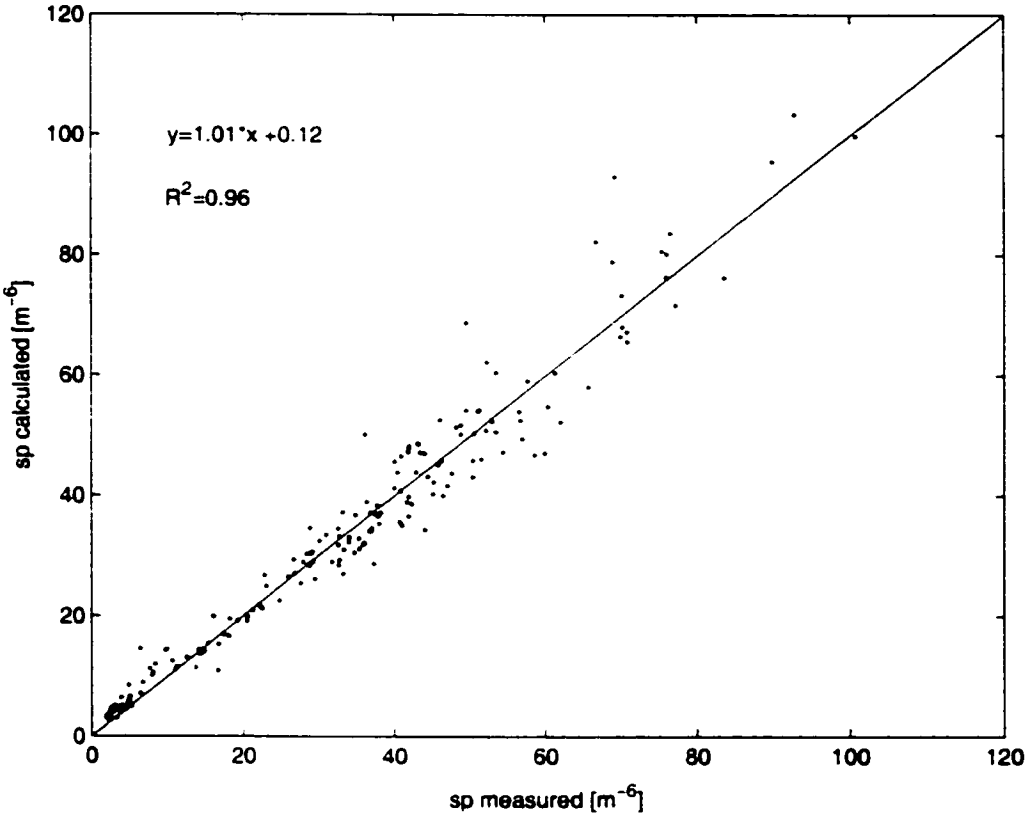

Figure 6.7: Measured and simulated scattering coefficients at dry conditions for the base case: m=1.51-0.02i and d_{cut}=725nm. The 1:1 line is shown as solid line. The parameters of a linear regression fitted to the data points are shown in the upper left hand corner

reasonable refractive index consistent with the chemical composition of the submicron

aerosol. The data lie close to the 1:1 line and the coefficient of determination is high. The scatter in the data is probably due to short term variations in the particle refractive index. The comparison could probably be improved by calculating a time-dependent refractive index based on the chemical composition of individual impactor samples. However the main focus of this chapter is on the change of σ_s with relative humidity. For this purposes the agreement at dry conditions is adequate.

Figure 6.8 compares the measured and calculated scattering coefficient at 82% r.h.. Figure 6.8(a) shows the calculated scattering scattering based on the lower limit of the hygroscopic growth factors of particles larger than 250nm and Figure 6.8(b) shows the calculated scattering based on the upper limit of the hygroscopic growth factors of particles larger than 250nm . The measured scattering coefficient at 82% r.h. is significantly lower than the calculated scattering coefficient in both cases. Using higher growth factors at large particle sizes the slope of the fit indicates that on average the calculations are almost a factor of 2 higher than the measurements. Using the lower growth factors the overestimate is still around a factor of 1.5. The average measured f_s(r.h.) is 1.6. while the average calculated f_s(r.h.) bounded between 2.3 and 2.8.

The reason for this difference at 82% is hard to explain considering that the measured dry scattering coefficient agreed well with calculations using a refractive index consistent with the particle chemical composition. Several assumptions have been made in the calculations that could influence the resulting humidified scattering coefficient. Both wet and dry particles are assumed to be spherical, whereas the dry particles can deviate significantly from spherical shape. The angular sensitivity function of the nephelometer was assumed to be constant. Finally the refractive index of humidified particles was calculated as the volume weighted average of the dry particle refractive index and the refractive index of water, which neglects any non-

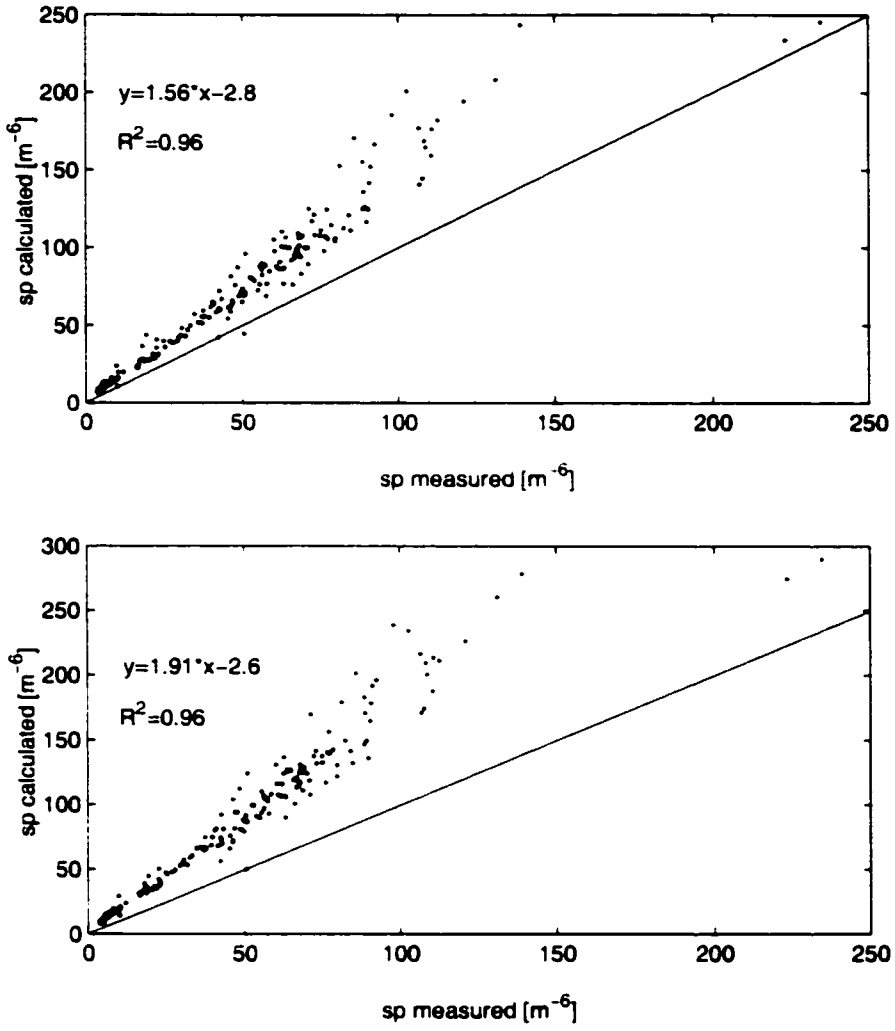

Figure 6.8: Measured and simulated scattering coefficients at a r.h. of 82% for the base case: m=1.51-0.02i and d_{cut}=725nm. The 1:1 line is shown as solid line. The two outlier points with a measured scattering coefficient greater than 200 m^{-6} are excluded from the linear fit (a) Lower limit of the growth factor at 510nm. (b) upper limit of the growth factor at 510nm

linear effects. However all of these approximations should not change the humidified scattering coefficient by more than a few percent.

A possible instrumental error that could lead to an underestimate of f_s(r.h.) are particle losses between the first and the second nephelometer. However both nephelometers were run at low r.h. occasionally during the ACE-2 experiment and the particle losses were negligible. Another possible factor might be uncertainties in the upper cut-off diameter imposed by the impactor. However the influence of the cut-off diameter on f_s(r.h.) is not large enough to explain the difference between measurements and calculations. If d_{cut} varies from 520 to 600 to 900nm the average calculated f_s(r.h.) increases from 2.0 to 2.2 to 2.3 for the lower case of the diameter growth factor at 510nm. However at a cut-off diameter of 520 nm the real part of the particle refractive index would have to be 1.58 to reproduce the dry scattering correctly, which in not consistent with the submicron particle composition.

A possible error in the calculated scattering could be that the diameter growth factors at 82% are overestimated. However a sensitivity study shows that the measured increase in particle diameter due to hygroscopic growth at 82% r.h. has to be reduced by approximately 50% before the calculated and measured f_s(r.h.) are comparable. The difference between measured and calculated scattering at 82% r.h. is thus not likely due to errors in the hygroscopic growth factors. The hygroscopic growth factors at 90% r.h. have been validated in a consistency study presented in chapter 5. The correction to 82% r.h. should not introduce errors larger than a few percent. The growth factors needed to reconcile the calculations and the measurements are more similar to growth factors measured at 60% r.h. than growth factors at 82%. It is also unlikely that the relative humidity in the second nephelometer was as low as 60%.

Remaining explanations for the discrepancy between calculated and measured f_s(r.h.) is a possible particle loss in the humidified nephelometer itself, or that the absorption due to internally mixed black carbon is large enough to heat up the particles

and evaporate some of their water. However these options cannot be investigated in the context of this thesis. Therefore the true cause of the difference between measurements and calculations cannot be established. Considering the discrepancy between measurements and calculations it seems useful to provide an alternative, calculated data set of the humidity dependence of the scattering coefficient.

6.3 Parameterization of the hygroscopic growth factors

The dependence of the diameter growth factors on the relative humidity can be parameterized using a simple two parameter formula:

$$Gf(r.h.) = 10^{C} \cdot (1 - r.h.)^{\gamma}, (6.14)$$

where the r.h. is given as the fractional relative humidity and not in %. The coefficients C and γ are empirical parameters obtained by fitting Equation 6.14 to measured data. Growth factors were measured routinely at 90% but once a day the relative humidity in the second DMA was lowered and growth factors at 60% r.h. were measured. The growth factors at 90% r.h. were averaged over a period of 5 hours before and after that measurement. This results in two data points at different relative humidities per day. The parameters C and γ on each day are determined by a least square fit to those two data points and to the additional data point Gf(0)=1. The parameter C is never significantly different from 0, so that the humidity dependence of the growth factors could be equally well described by $Gf(r.h.)=(1\text{-}r.h.)^{\gamma}$.

Figure 6.9 shows the parameterization for different particle sizes. The data are separately averaged for time periods of recent pollution and all other time periods just as it was done in Chapter 3. Averages of the measured data points are shown as circles and rectangles and the fitted functions are shown as solid and dashed lines. Two separate data points are shown at 60% r.h.. The two data points refer to

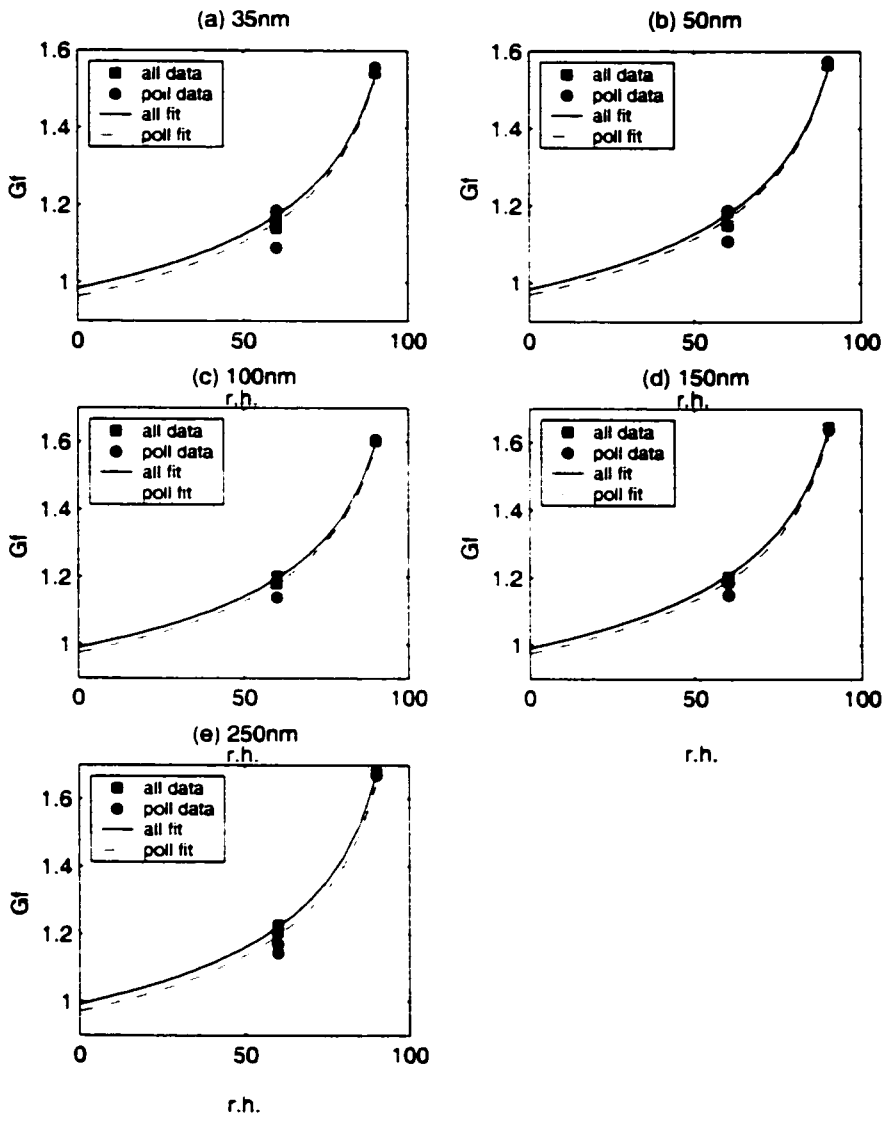

Figure 6.9: Parameterization of the diameter growth factor. Measured growth factors in recent pollution are shown as circles. Measured growth factors at all other times are shown as squares. The fits are shown as dashed lines (recent pollution) and as solid lines (other time periods)

measurements at increasing and at decreasing relative humidity. For the data points at increasing relative humidity the particles are humidified to 60% r.h. directly from the dry state at 10% r.h. For the data points at decreasing relative humidity particles are first subjected to a relative humidity greater than 80% and subsequently dried to 60% r.h.. The growth factors measured at decreasing relative humidity are usually greater than the growth factors measured at increasing humidity due to a hysteresis effect. This hysteresis effect more pronounced in recent pollution than at other times and it decreases with particle size.

The fits are a good approximation to the measurements and the individual R^2 values are usually above 0.98. The fits should only be used in the relative humidity range between 60% and 90% . Below 60% it is possible that a step wise change from humidified to dry conditions can occur, however it is difficult to predict the relative humidity at which that change occurs for ambient particles.

Figure 6.10 summarizes the parameter γ as a function of particle size for recent pollution and all other conditions. The error bars represent $\pm$ 1 standard deviation. It can be seen that the variability in γ is larger than the differences between clean conditions and pollution.

6.4 Parameterization of f_s(r.h.)

This section describes a parameterization of f_s(r.h.) that can be used in global circulation models. These models usually predict the mass concentration of chemical species and often a mean or effective diameter of the aerosol. The particle chemistry can be used to estimate hygroscopic growth factors at various relative humidities. However the increase in light scattering with relative humidity does not only depend on the particle hygroscopic growth factors, but also on the initial dry size distribution, as has been shown by Hegg et al. (1993). In this section we will investigate

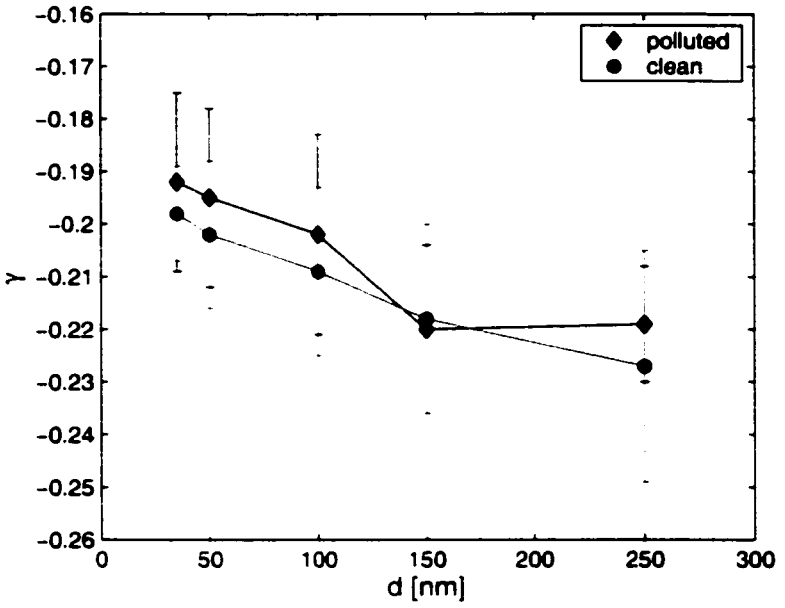

Figure 6.10: Parameter γ as a function of particle size in recent pollution (circles) and other conditions (squares)

which parameters of the dry size distribution are most useful in the parameterization of f_s(r.h.) for our purposes.

6.4.1 Finding the functional form

The first step to parameterizing the increase in light scattering with relative humidity is finding and appropriate functional form for the parameterization. Idealized size distributions are generated for this purpose. They consist of two lognormal modes, an Aitken and an Accumulation mode. The number mean diameter of the Aitken mode is allowed to vary between 20nm and 80nm, and the Accumulation mode number mean diameter between 100 and 600nm. The number concentration of the Aitken mode varies from 0 to 1000 cm^3 and the number concentration of the accumulation

mode between 100 and 1000 cm^3. The standard deviation of each mode is assumed to be 1.6. The resulting size distributions vary from typical 'marine' appearance with two well separated modes. to overlapping modes characteristic of recent and aged pollution (see Chapter 3.2).

A further assumption is that all particles in the size distribution exhibit identical hygroscopic growth with diameter growth factors (Gf) ranging from 1.2 to 1.8. Humidified size distributions are calculated by shifting the mean diameters of the two modes to larger sizes. This is done by multiplying the mean diameters of each mode by the respective growth factor ranging from 1.2 to 1.8. This can either be interpreted as an increase of the fraction of hygroscopic material in the particles at constant humidity or as an increase in relative humidity while particle hygroscopic properties stay the same. The particle refractive index is assumed to be 1.51-0.02i, typical for the sulfate dominated aerosol in Sagres.

Dry scattering coefficients (σ_s(dry). calculated using the original size distribution) and humidified scattering coefficients (σ_s(wet), calculated using the size distributions shifted to larger diameters as explained above) are derived at a wavelength of 550nm for all possible combinations of Aitken and Accumulation mode mean diameters and Aitken and Accumulation mode number concentrations. For each size distribution σ_s(wet) are divided by σ_s to obtain f_s. The results of the calculations are shown in Figure 6.11. f_s is plotted as a function of volume mean diameter of the dry size distribution (d_v). Different diameter growth factors are denoted by different symbols.

The data f_s increases with increasing diameter growth factor, but the magnitude of the increase depends strongly on d_v. At volume mean diameters around 200nm f_s increases by a factor of 6 as Gf increases from 1.2 to 1.8. At the volume mean diameters around 600nm f_s increases only by a factor of 2 for the same increase in Gf. In the first case a larger fraction of particles are in the range where the scattering cross

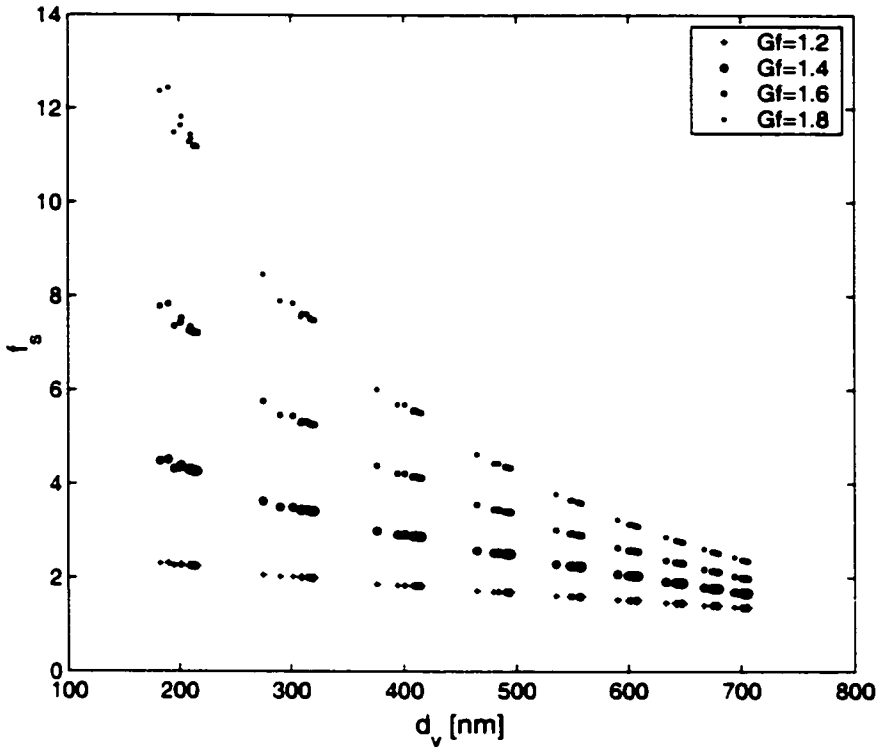

Figure 6.11: f_s as a function to the volume mean diameter of the dry size distribution for various diameter growth factors

section increases strongly with particle diameter, whereas in the latter case most of the scattering occurs at larger particle sizes where the scattering cross section increases only slowly with increasing particle size.

The volume mean growth factor explains the considerable variability of f_s(r.h.) at constant diameter growth factors better than any other size distribution parameter. Neither the mean diameter, or as might be expected the surface mean diameter can be used to represent the shape of the dry size distribution. The volume mean diameter seems to characterize the region where most of the scattering occurs and thus provides a good approximation of the particle diameter that represents the scattering of the

whole size distribution.

To find a parameterization for the dependence of f_s(r.h) Gf and the volume mean diameter d_v, the clusters of data points around volume mean diameters of 200nm, 300nm, 400nm, 550nm and 640nm are averaged. The dependence of f_s(r.h.) on Gf for different volume mean diameters is shown in Figure 6.12.

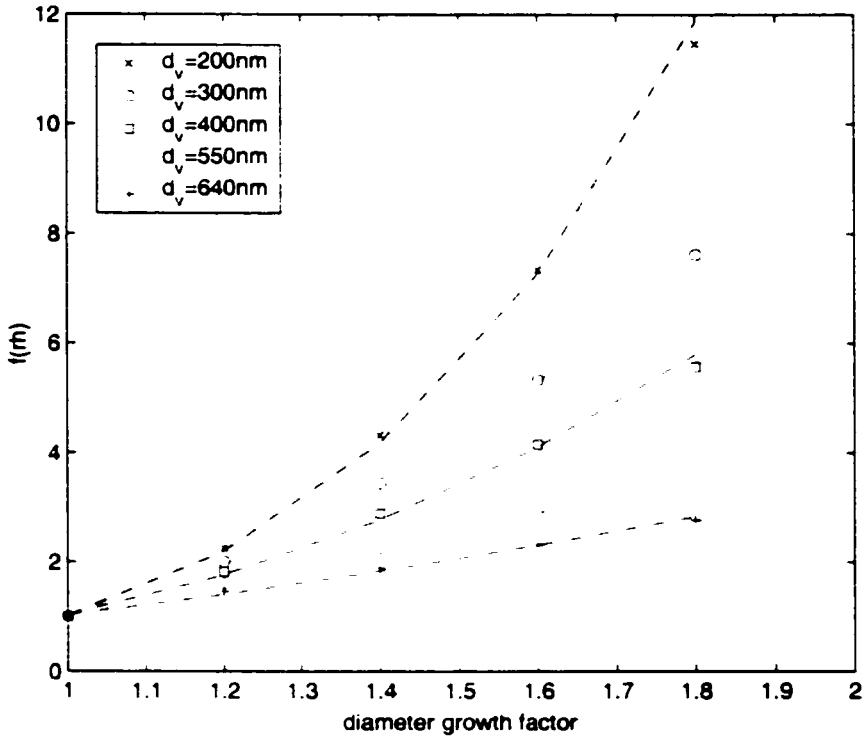

Figure 6.12: f_s(r.h.) as a function of the diameter growth factor (Gf) for volume mean diameters (d_v) between 200nm and 640nm. The dashed lines are exponential fits of the form: $f_s(r.h.)=Gf^k$

The dependence of f_s(r.h.) on the diameter growth factor is exponential ($f_s(r.h.)=Gf^k$) with a different exponential for each volume mean diameter. The dashed lines show the best fit lines, with k determined by a least square fit. The clustering that can

be observed in the data is due the change in the number mean diameter of the accumulation mode from 100 to 500nm in steps of 50nm. Since the accumulation mode accounts for most of the particle volume, the accumulation mode number mean diameter mostly determines the volume mean diameter of the whole size distribution. The variations of the volume mean diameter within each cluster are due to variations in the Aitken mode mean diameter and/or the relative number of particles in each mode.

The remaining step is to parameterize the dependence of the exponential parameter k on the volume mean diameter. Figure 6.13 shows the dependence of the parameter k on the volume mean diameter. It can be seen that k decreases linearly with increasing d_v.

This results in the following final form for the parameterization of f_s on Gf and d_v:

$$f_s(r.h) = Gf(r.h.)^{a+b \cdot d_v}. \tag{6.15}$$

where the parameters a and b have to be empirically determined by fitting Equation 6.15 to ambient data.

6.4.2 Application to the aerosol in Sagres during ACE-2

The application of Equation 6.15 to actual ambient aerosol data has two crucial problems. The equation has been derived using lognormal size distribution, whereas the ambient size distribution can deviate from lognormal shape. Also an idealized assumption has been made regarding hygroscopic growth factors. The diameter growth factors were assumed to be independent of particle size whereas in reality the hygroscopic growth factors generally increase with particle size. If the diameter growth factors are independent of dry particle size hygroscopic growth only shifts the size distribution to larger diameters. If the growth factors are size dependent, hygro-

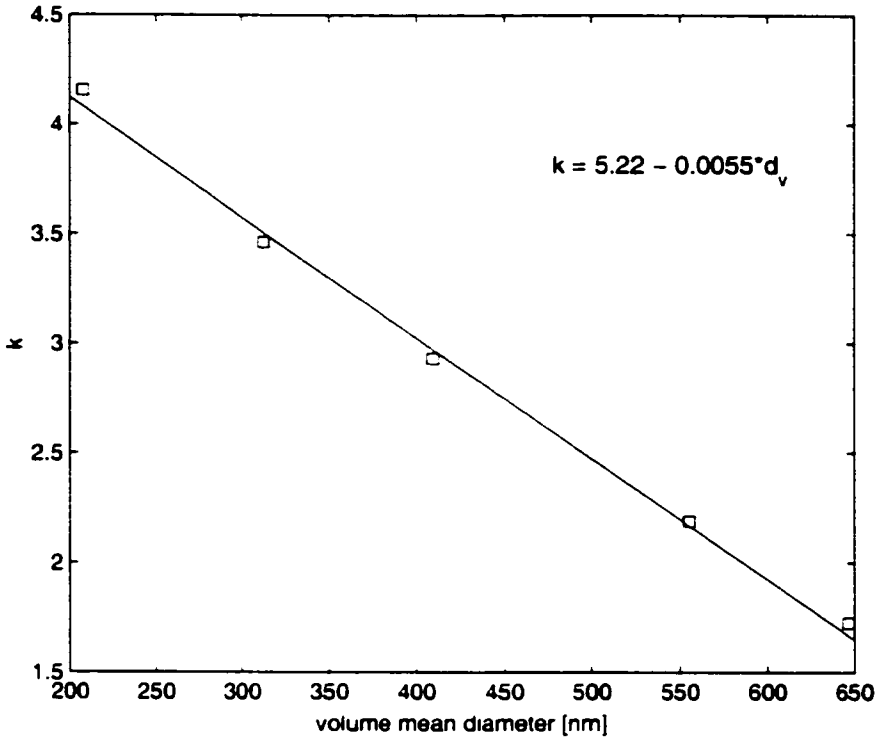

Figure 6.13: Dependence of the parameter k on the volume mean diameter.

scopic growth also distorts the shape of the size distribution, especially when less hygroscopic particles are present. However if those effects, the deviation of the size distribution from lognormal shape and the dependence of the diameter growth factors on particles size, are second order effects the parameterization can still be valid.

If the hygroscopic growth factors are dependent on particle size and less hygroscopic particles are present, it is necessary to define an effective growth factor that is representative of the hygroscopic growth of the whole size distribution. For this purpose a volume weighted mean diameter growth factor (Gf_v) is defined as follows:

$$Gf_v = \frac{\sum_{d_{min}}^{d_{max}} \left(Gf_i^{mh} \cdot F_i^{mh} + Gf_i^{th} \cdot (1 - F_i^{mh}) \right) dN_i \cdot d_i^3}{\sum_{i=d_{min}}^{d_{max}} dN_i \cdot d_i^3}. \qquad (6.16)$$

where Gf_i^{mh} and Gf_i^{lh} are the more and less hygroscopic growth factors at diameter d_i, F_i^{mh} the fraction of more hygroscopic particles, and dN_i the particle number concentration in the DMPS size bin with central diameter d_i.

To test if the parameterization proposed in Equation 6.15 is applicable to atmospheric aerosol, dry and humidified scattering coefficients for the aerosol in Sagres are calculated at 82% r.h. as described in Section 6.2. The upper cut-off diameter is 1 μm in these calculations to include all submicron particles. For each pair of dry and humidified scattering coefficients the volume mean diameter of the corresponding dry size distribution (d_v) and Gf_v are calculated as well.

Figure 6.14 shows the overall results of the calculations. The ratio of the logarithm of f_s(r.h.) and of Gf_v decreases linearly with increasing volume mean diameter for the whole ACE-2 data set. The fact that the data fall on a straight line suggests that f_s(r.h.) can be parameterized in terms of Gf_v and d_v with a single set of empirical parameters for the whole ACE-2 experiment, despite the fact that air mass conditions were very variable, changing from marine background to aged and recent pollution episodes. The empirical fit parameters derived from a linear fit to the data in Figure 6.14 (shown as solid line) are a = 3.74 and b=-0.0027. The parameterization derived in Section 5.4.1 for lognormal size distributions and constant diameter growth factors can be applied to the ambient aerosol. This suggests that the real size distribution can be well approximated as a linear combination of lognormal distributions, as was already demonstrated in Chapter 3. It also indicates that for the purpose of characterizing the direct radiative forcing of aerosol on climate a single volume weighted mean diameter growth factor can be used to represent the complex hygroscopic behavior of atmospheric aerosol. This indicates that growth factors derived from the bulk chemical composition predicted in chemical transport models are a good representation of the aerosol hygroscopic behavior.

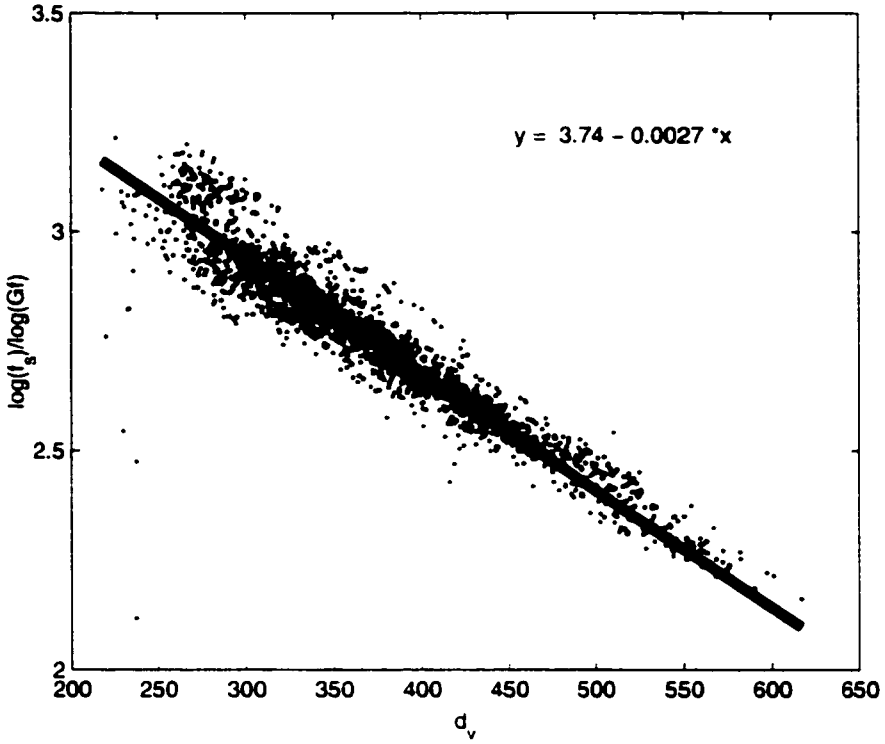

Figure 6.14: Parameterization of the f_s(r.h.) for Sagres data. The solid line is the best linear least square fit. The resulting parameters for the parameterization are a=3.74 and b=0.0027

Figure 6.15 shows a test of the parameterization on subsets of the data. Three subsets of scattering data calculated from dry size distributions with d_v close to 300nm, 400nm and 500nm are shown along with the parameterization $f_s(\text{r.h.})=Gf_v^{3.74-0.0027 \cdot d_v}$. The data with low d_v are more scattered, but overall the parameterization reproduces the dependence of f_s on Gf_v at constant d_v very well.

Figure 6.16 shows a similar test, but a subset of data is chosen within a narrow section of Gf_v. This is a test how well the parameterization reproduces the dependence of f_s(r.h.) on the volume mean diameter at constant Gf_v. The dependence of f_s(r.h.)

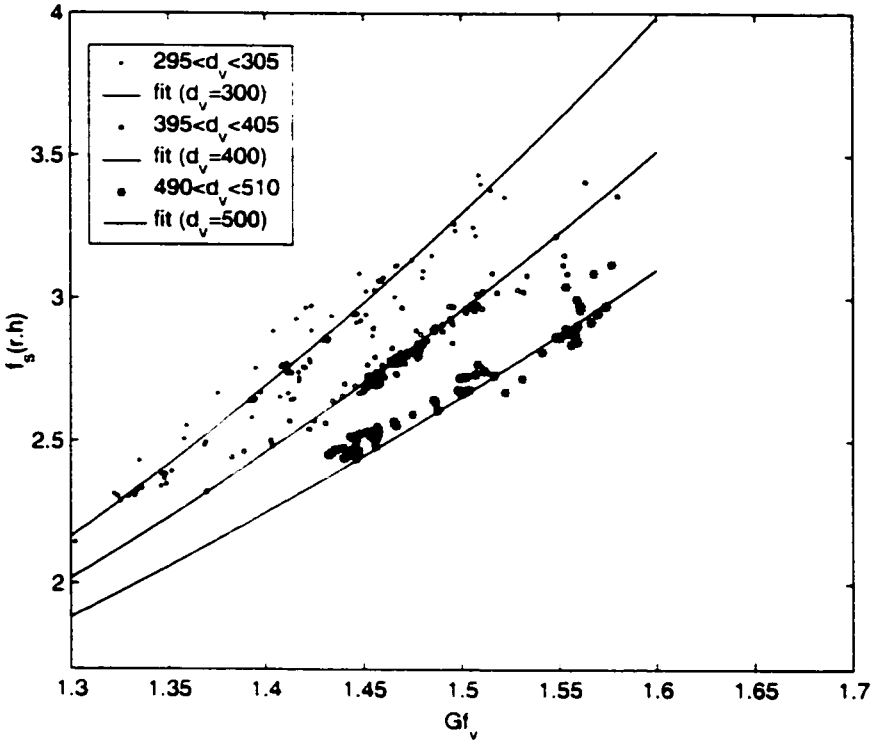

Figure 6.15: Dependence of f_s(r.h.)on Gf_v for volume mean diameters of 300nm, 400nm and 500nm. The data points are shown as symbols. The parameterization $f_s(r.h.)=Gf_v^{3.74-0.0027 \cdot d_v}$ are shown as solid lines

on d_v at constant Gf_v is not as clear as the dependence of f_s(r.h.) on Gf_v at constant d_v shown in the previous figure. There is considerable scatter in the data.

6.5 Summary

The scattering consistency study attempted in this work shows that the scattering coefficient of dry particles measured by a nephelometer can be modeled using measured particle size distributions and a refractive index consistent with particle chemical composition. However at 82% humidity is the calculated scattering coeffi-

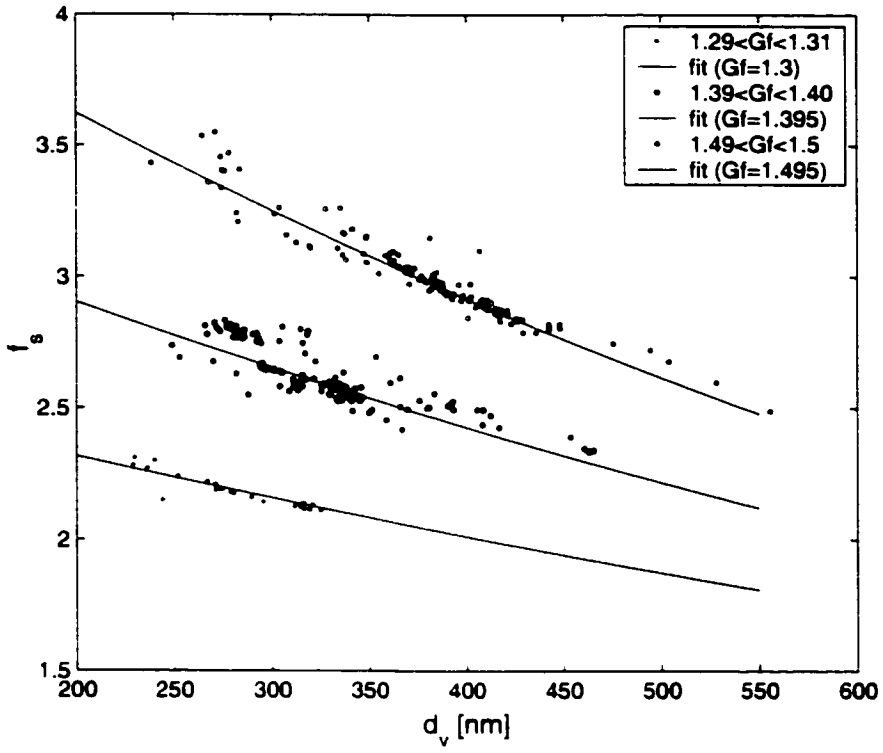

Figure 6.16: Dependence of f_s(r.h.)on d_v for Gf_v near 1.3, 1.4, and 1.5. The data points are shown as symbols. The parameterizations $f_s(r.h.)=Gf_v^{3.74-0.0027 \cdot d_v}$ for different values Gf_v of are shown as solid lines

cient is higher than the measured scattering coefficient by a factor of 1.4-1.8. The discrepancy cannot be completely explained in this work and must remain subject to further study. However it seems likely that the humidity dependence of the scattering coefficient was underestimated by the nephelometer.

A parameterization of the calculated f_s(r.h.) in terms of the volume mean diameter of the dry size distribution (d_v) and the volume weighted mean diameter growth factor (Gf_v) is proposed in this section. The parameterization has the simple form of $f_s(r.h.)=Gf_v(r.h.)^{a+b \cdot d_v}$, with a=3.74 and b=-0.0027 if d_v is given in nm. The empirical

parameters a and b are valid for the whole ACE-2 measurement period. As already noted by Hegg et al. (1993) the shape of the dry size distribution (represented here by the volume mean diameter) has a significant influence on f_s(r.h.).

Chapter 7

SUMMARY AND CONCLUSIONS

Aerosol physical properties and climate forcing parameters in the North-East Atlantic Ocean were clearly affected by pollution outbreaks from Europe. The aerosol in Sagres was never truly characteristic of marine background aerosol even in clean air mass conditions. Coastal land and maritime sources impose some anthropogenic signature on the aerosol even if air mass back trajectories indicate that it has been transported from remote areas. Despite this fact there is a significant change in some aerosol properties when air mass back indicate that pollution from Northern Europe or the Iberian Peninsula was transported to Sagres. The submicron particle volume increased by a factor of 5 in polluted conditions, the light scattering coefficient of dry particles increased on average by a factor of up to 10, CCN concentrations at supersaturations of 0.2% increased by a factor of 3-5. Other aerosol properties were less affected by European pollution outbreaks. These were mostly intensive properties, that are independent of the total number of particles present, such as particle chemical composition, hygroscopic growth, or number to volume ratios. The hygroscopic growth factors and the number to volume ratios are similar in Arctic and Atlantic marine conditions and aged pollution. Only in recent pollution that originates over the Iberian Peninsula and had no aging time and was not subjected to cloud processing over the ocean before reaching Sagres, intensive aerosol properties changed compared to other air mass conditions. The hygroscopic growth factors in recent pollution were slightly lower and the number to volume ratios were significantly higher

than in the other air mass conditions. This indicates that given some aging time the intensive aerosol properties relax more quickly to background conditions than extensive properties such as the particle volume.

Some aerosol physical properties such as the concentration of fine particles below 40nm or the hygroscopic growth factors have most of their variability on time and spatial scales shorter than the change in air mass conditions. A significant amount of this variability occurs on a diurnal scale. The diurnal change in hygroscopic growth factors is most closely related to the intensity of incoming solar radiation. On average the hygroscopic growth factors increase in the morning hours reach a maximum around 1pm and decrease during the afternoon, consistent with the solar elevation angle. The diurnal change in fine particle concentration can be explained by particle nucleation events in the morning hours and subsequent particle growth. Ultrafine particles with sizes smaller than 10nm are measured almost every day and appear in small quantities at any time during daylight hours. However high concentrations of ultrafine particles are measured almost exclusively during the morning hours shortly after sunrise. This seems to indicate that in addition to solar radiation the formation of small particles is controlled by at least one other meteorological factor such as temperature, or relative humidity. However the data base in Sagres is not sufficient to draw final conclusions on this subject.

Three consistency studies have been made in context of this thesis to test current theory and aerosol measurement techniques. The hygroscopic study showed that effective ions estimated based on hygroscopic growth factors were consistent with the actual ions that were chemically analyzed in impactor samples. This is an important result because it indicates that at least in this area of the globe hygroscopic growth factors can be predicted from particle chemical composition using a relatively simple model. It also indicates that at Sagres during ACE-2 there is no indication that

organic compounds contribute to the particle water uptake at 90% r.h.. The calculated effective ions were further used to estimate critical supersaturations and CCN spectra. These calculated CCN spectra were compared to actually measured CCN spectra in a second consistency study. As a result of this consistency study a dilution problem due to errors in flows could be identified in the CCN instrument. The calculations overestimate the measurements by about 30% on average. This overestimate cannot be fully explained with data available in Sagres during ACE-2. Since in many studies modeled CCN concentrations tend to be higher than measured CCN concentrations, further research is needed to address this subject. However the fact that the calculations overestimate the measurements is an indication that neither surfactant species nor the dissolution of soluble gases had a strong influence on CCN activation in Sagres during ACE-2. The third consistency study showed that the scattering coefficient of the submicron aerosol measured by a nephelometer is consistent with the calculated scattering coefficient at dry conditions (r.h.=28%), but not at elevated humidities (r.h.=82%). The reasons for this difference could not be identified, but it indicates that measured scattering coefficients might be too low by approximately 50%.

A simple parameterization of the humidity dependence of the submicron aerosol scattering coefficient has been derived, depending only on a volume weighted average diameter growth factor and the volume mean diameter of the dry size distribution. One set of empirical parameters can be used to parameterize all aerosol types characterized during the ACE-2 measurement period.

BIBLIOGRAPHY

Ackermann, A. S., Toon, O. B., Stevens, D. E., Heymsfield, A. J., Ramanathan, V. and Welton, E. J. 2000. Reduction of tropical cloudiness by soot. *Science* **288**, 1042–1047.

Anderson, T. L., Covert, D. S., Marshall, S. F., Laucks, M. L., Charlson, R. J., Waggoner, A. P., Ogren, J. A., Caldow, R., Holm, R. L., Quant, F. R., Sem, G. J., Wiedensohler, A., Ahlquist, N. A. and Bates, T. S. 1996. Performance characteristics of a high sensitivity, three wavelength, total scatter/backscatter nephelometer. *J. Atmos. Oceanic Technol.* **13**, 967–986.

Andreae, M. O., Andreae, T. W., Annegarn, H., Beer, J., Cachier, H., le Canut, P., Elbert, W., Maenhaut, W., Salma, I., Wienhold, F. G. and Zenker, T. 1998. Chemical composition of aerosol emissions from savanna fires in southern Africa: 2. Aerosol chemical composition. *J. Geophys. Res.* **103**, D24, 32119–32128.

Ayers, G. P. 2001. Comment on regression analysis of air quality data. *Atmos. Environ.* **35**, 2423–2425.

Baker, M. B. and Charlson, R. J. 1990. Bistability of CCN concentrations and thermodynamics in the cloud topped boundary layer. *Nature* **345**, 142–145.

Bates, T. S., Huebert, B. J., J. L. Gras, F. B. G. and Durkee, P. A. 1998. International Global Atmospheric Chemistry (igac) project's first Aerosol Characterization Experiment (ACE-1): Overview. *J. Geophys. Res.* **D13**, 16,297–16,318.

Berg, O. H., Swietlicki, E., Frank, G., Martinsson, B. G., Cederfelt, S.-I., Laj, P., Ricci, L., Berner, A., Dusek, U., Galambos, Z., Mesfin, N. S., Yuskiewics, B., Wiedensohler, A., Stratmann, F. and Orsini, D. 1998a. Observed and modeled hygroscopic behavior of atmospheric particles. *Contr. Atmos. Phys.* **71**, 47–65.

Berg, O. H., Swietlicki, E. and Krejci, R. 1998b. Hygroscopic growth of aerosol particles in the marine boundary layer over the Pacific and Southern Oceans during the first Aerosol Characterization Experiment (ACE 1). *J. Geophys. Res.* **103**, D13, 16535–16545.

Berner, A. and Lürzer, C. 1980. Mass size distributions of traffic aerosols at Vienna. *Journal of Physical Chemistry* **84**, 2079–2083.

Birmili, W. 1998. Ph.D. thesis Institut für Troposphärenforschung.

Birmili, W., Stratmann, F. and Wiedensohler, A. 1999. Design of a DMA-based size spectrometer for a large particle size range and stable operation. *J. Aerosol Sci.* **30**, 549–553.

Birmili, W., Stratmann, F. and Wiedensohler, A. 2000. Nwe particle formation in the continental boundary layer: Meteorological and gas phase parameter influence. *Geophys. Res. Lett.* **27**, 3325–3328.

Boers, R., Jenson, J. B. and Krummel, P. B. 1998. Microphysical and short-wave radiative structure of stratocumulus clouds over the Southern Ocean: Summer results and seasonal differences. *Quarterly Journal of the Royal Meteorological Society* **124**, 151–168.

Boucher, O. and Anderson, T. L. 1995. General circulation model assessment of the sensitivity of direct climate forcing by anthropogenic sulfate aerosols to aerosol size and chemistry. *J. Geophys. Res.* **100**, D12, 26117–26134.

Boy, M. and Kulmala, M. 2001. Nucleation events in the continental boundary layer: Influenec of physical and meteorological parameters. *Atmos. Chem. Phys. Discuss.* **1**, 239–276.

Brenguier, J. L., Chuang, P. Y., Fouquart, Y., Johnson, D. W., Parol, F., Pawlowska, H., Pelon, J., Schueller, L., Schroeder, F. and Snider, J. 2000. An overview of the ACE-2 CLOUDYCOLUMN closure experiment. *Tellus* **52B**, 815–827.

Bruggeman, D. 1935. Berechnung verschiedener physikalischer Konstanten von heterogenen Substanzen I. Dielektrizitätskonstanten und Leitfähigkeiten der Mischkörper aus isotropen Subtstanzen. *Ann. Phys.* **24**, 636–679.

Cantrell, W., Shaw, G. and Benner, R. 1999. Cloud properties inferred from bimodal aerosol number distributions. *J. Geophys. Res.* **104**, D22, 27615–27624.

Carrico, C. M., Rood, M. J. and Ogren, J. A. 1998. Aerosol light scattering properties at Cape Grim, tasmania, during the First Aerosol Characterization Experiment (ACE-1). *J. Geophys. Res.* **103**, D13, 16,565–16,574.

Carrico, C. M., Rood, M. J., Ogren, J. A., Neusuess, C., Wiedensohler, A. and Heintzenberg, J. 2000. Aerosol optical properties at Sagres, Portugal during ACE2. *Tellus* **52B**, 694–715.

Charlson, R. J., Langer, J., Rohde, H., Leovy, C. B. and Warren, S. G. 1991. Perturbation of the northern hemisphere radiative balance by backscattering from anthropogenic sulfate aerosols. *Tellus* **43AB**, 152–143.

Charlson, R. J., Schwartz, S. E., Hales, J. M., Cess, R. D., Coakley, J. A., Hansen, J. E. and Hofmann, D. J. 1992. Climate forcing by anthropogenic aerosols. *Science* **255**, 423–430.

Chuang, P. Y., Charlson, R. J. and Seinfeld, J. H. 1997. Kinetic limitations on droplet formation in clouds. *Nature* **390**, 594–596.

Chuang, P. Y., Collins, D. R., Pawlowski, H., Snider, J. R., Jonsson, H. H., Brenguier, J. L., Flagan, R. C. and Seinfeld, J. H. 2000. CCN measurements during ACE-2 and their relationship to cloud microphysical properties. *Tellus* **52B**, 843–867.

Chylek, P. and Wong, J. 1995. Effect of absorbing aerosols on global radiation budget. *Geophys. Res. Lett.* **22**, 929–931.

Clegg, S. L., Brimblecombe, P. and Wexler, A. S. 1998. A thermodynamic model of the system h-nh_4-na-so_4-no_3cl-h_2o at 298.15k. *J. Phys. Chem.* **102A**, 2155–2171.

Coakley, J. A., Bernstein, R. L. and Durkee, P. A. 1987. Effect of ship-track effluents on cloud reflectivity. *Science* **255**, 423–430.

Covert, D. S., Gras, J. L., Wiedensohler, A. and Stratman, F. 1998. Comparison of directly measured CCN with CCN modeled from the number-size distribution in the marine boundary layer during ACE1 at Cape Grim, Tasmania. *J. Geophys. Res.* **103**, 16597–16608.

Covert, D. S. and Heintzenberg, J. 1993. Size distributions and chemical properties of aerosol at Ny Alesund, Svalbard. *Atmos. Environ.* **27**, 2989–2997.

Covert, D. S., Kapustin, V. N., Bates, T. S. and Quinn, P. K. 1996a. Physical properties of marine boundary layer aerosol particles of the mid-Pacific in relation to sources and meterological transport. *J. Geophys. Res.* **101**, 6919–6930.

Covert, D. S., Wiedensohler, A., Aalto, P., Heintzenberg, J., McMurry, P. H. and Leck, C. 1996b. Aerosol number size distributions from 3 to 500 nm diameter in the arctic marine boundary layer during summer and autumn. *Tellus* **48B**, 197–212.

Cruz, C. N. and Pandis, S. N. 1998. The effect of organic coatings on the cloud condensation nuclei activation of inorganic atmospheric aerosol. *J. Geophys. Res.* **103**, D11, 13111–13123.

Dick, W. D., Saxeena, P. and McMurry, P. H. 2000. Estimation of water uptake by organic compounds in submicron aerosols measured during the Southeastern aerosol and visibility study. *J. Geophys. Res.* **105**, 1471–1479.

Faccini, M. C., Decesari, S., Mirea, M., Fuzzi, S. and Loglio, S. 2000. Surface tension of atmospheric wet aerosol and cloud/fog droplets in relation to their organic carbon content and chemical composition. *Atmos. Environ.* **34**, 4853–4857.

Ferek, R. J., Hegg, D. A., Hobbs, P. V., Durkee, P. and Nielsen, K. 1998. Measurements of ship induced tracks in clouds off the Washington coast. *J. Geophys. Res.* **103**, D18, 23199–23206.

Hansen, J. E., Sato, M., Lacis, A., Ruedy, R., Tegen, I. and Matthews, E. 1998. Climate forcings in the industrial era. *Proc. Natl. Acad. Sci.* **95**, 12,753–12,758.

Haywood, J. M. and Boucher, O. 2000. Estimates of the direct and indirect radiative forcings of due to tropospheric aerosols: A review. *Rev. Geophys.* **38**, 513–543.

Haywood, J. M. and Ramaswany, V. 1998. Globel sensitivity studies of the direct radiative forcing due to anthropogenic sulfate and black carbon aerosols. *J. Geophys. Res.* **103**, 6043–6058.

Haywood, J. M. and Shine, K. P. 1995. The effect of anthropogenic sulfate and soot aerosol on the clear sky planetary radiation budget. *J. Geophys. Res.* **22**, 5, 603–606.

Haywood, J. M. and Shine, K. P. 1997. Multispectral calculations of the direct radiative forcing of tropospheric sulfate and soot aerosols using a column model. *Quarterly Journal of the Royal Meteorological Scociety* **123**, 1907–1930.

Hegg, D. A. and Jonsson, H. 2000. Aerosol number-to-volume relationship and relative humidity in the eastern Atlantic. *J. Geophys. Res.* **105**, 1987–1995.

Hegg, D. A. and Kaufman, Y. J. 1998. Measurements of the relationship between submicron aerosol number and volume concentration. *J. Geophys. Res.* **103**, 5671–5678.

Hegg, D. A., Larson, T. and Yuen, P. F. 1993. A theoretical study of the effect of relative humidity on light scattering by tropospheric aerosols. *J. Geophys. Res.* pp. 18,435–18,439.

Hegg, D. A. and Russel, L. M. 2000. An analysis of processes determining the number to volume relationship for submicron aerosol in the eastern Atlantic. *J. Geophys. Res.* **105**, 15,321–15,328.

Heintzenberg, J. and Charlson, R. J. 1996. Design and applications of the integrating nephelometer: A review. *J. Atmos. Oceanic Technol.* **13**, 987–1000.

Hitzenberger, R. M., Berner, A., Dusek, U. and Alabashi, R. 1997. Humidity dependent growth of size-segregated aerosol samples. *Aerosol Sci. Technol.* **27**, 116–130.

Hobbs, P. V., Garrett, T. J., Ferek, R. J., Strader, S. R., Hegg, D. A., Frick, G. M., Hoppel, W. A., Gasparovic, R. F., Russel, L. M., Johnson, D. W., O'Dowwd, C., Durkee, P. A., Nielsen, K. E. and Innis, G. 2000. Emissions from ships with respect to their effect on clouds. *J. Atmos. Sci.* **57**, 2570–2590.

Hoppel, W. A., Frick, G. M., Fitzgerald, J. W. and Larson, R. E. 1994. Marine boundary layer measurements of new particle formation and the effects nonpercipitating clouds have on aerosol size distribution. *J. Geophys. Res.* **99**, 14,443–14,459.

Hudson, J. G. 1989. An instantaneous CCN spectrometer. *J. Atmos. Oceanic Technol.* **6**, 1055–1065.

Hudson, J. G. and Clarke, A. D. 1992. Aerosol and cloud condensation nuclei measurements in the Kuwait plume. *J. Geophys. Res.* **97**, 14533–14536.

Hudson, J. G., Xie, Y. and Yum, S. S. 1998. Vertical distribution of cloud condensation nuclei spectra over the summertime Southern Ocean. *J. Geophys. Res.* **103**, D13, 16609–16624.

Ji, Q. and Shaw, G. E. 1998. On supersaturation spectrum and size distributions of cloud condensation nuclei. *Geophys. Res. Lett.* **25**, 1903–1906.

Ji, Q., Shaw, G. E. and Cantrell, W. 1998. A new instrument for measuring cloud condensation nuclei: Cloud condensation nucleus remover. *J. Geophys. Res.* **103**, D21, 28013–28019.

Kiehl, J. T. and Briegleb, B. P. 1993. The relative roles of sulfate aerosols and greenhouse gases in climate forcing. *Science* **260**, 311–314.

Knutson, E. O. and Whitby, K. T. 1975. Aerosol classification by electric mobility: Apperatus,theory and applications. *J. Aerosol Sci.* **6**, 443–451.

Kulmala, M., Laaksonen, A., Charlson, R. J. and Korhonen, P. 1997. Clouds without supersaturation. *Nature* **388**, 336–337.

Kulmala, M., Pirjola, L. and Mäkelä, J. 2000. Stable sulphate clusters as a source of new atmospheric particles. *Nature* **404**, 66–69.

Laaksonen, A., Korhonen, P., Kulmala, M. and Charlson, R. J. 1998. Modification of the Koehler equation to include soluble trace gases and slightly soluble substances. *J. Atmos. Sci.* **55**, 853–862.

Lacis, A. A. and Mishchenko, M. I. 1995. Climate forcing, climate sensitivity and climate response: A radiative modeling perspective on atmospheric aerosols. in R. J. Charlson and J. Heintzenberg, editors, *Aerosol Forcing of Climate* pp. 11–42. John Wiley and Sons.

Li-Jones, X., Maring, H. B. and Prospero, J. M. 1998. Effect of relative humidity on light scattering by mineral dust aerosol as measured in the marine boundary layer over the tropical Atlantic Ocean. *J. Geophys. Res.* **D23**, 31,113–31,121.

Malm, W. C., Day, D. E. and Kreidenweis, S. M. 2000. Light scattering characteristics of aerosols as a function of relative humidity: PartI-A comparison of measured scattering and aerosol concentrations using the theoretical models. *J. Air Waste Manage. Assoc.* **50**, 686–700.

Martinsson, B. G., Frank, G., Cederfelt, S. I., Berg, O. H., Mentes, B., Papaspiropoulos, G., Swietlicki, E., Zhou, J. C., Flynn, M., Bower, K. N., Choularton, T. W., Mäkelä, J., Virkkula, A. and VanDingenen, R. 2000. Validation of very high cloud droplet number concetrations in air masses transported thousands of kilometers over the ocean. *Tellus* **52B**, 801–814.

Martinsson, B. G., Karlsson, M. N. A. and Frank, G. 2001. Methodology to estimate the transfer function of individual differential mobility analyzers. *Aerosol Sci. Technol.* **35**, 815–823.

Nenes, A., Ghan, S., Abdul-Razzak, H., Chuang, P. Y. and Seinfeld, J. H. 2001.

Kinetic limitations on cloud droplet formation and impact on cloud albedo. *Tellus* **53**, 133–149.

Neusüß, C., Weise, D., Birmili, W., Wex, H., Wiedensohler, A. and Covert, D. S. 2000. Size-segregated chemical mass closure and number-derived mass closure of the marine aerosol in Sagres, Portugal. *Tellus* **52B**, 169–184.

Novakov, T. and Corrigan, C. E. 1996. Cloud condensation nucleus activity of the organic component of biomass burning smoke. *Geophys. Res. Lett.* **23**, 2141–2144.

Novakov, T. and Penner, J. E. 1993. Large contribution of organic aerosols to cloud-condensation nuclei concentrations. *Nature* **365**, 823–826.

Penner, J. E. 1995. Carbonaceous aerosols influencing atmospheric radiation: Black and organic carbon. in R. J. Charlson and J. Heintzenberg, editors, *Aerosol Forcing of Climate* pp. 91–107. John Wiley and Sons.

Penner, J. E., Dickinson, R. and O'Neill, C. 1992. Effects of aerosols from biomass burning on the global radiation budget. *Science* **256**, 1432–1434.

Pilinis, C., Pandis, S. N. and Seinfeld, J. H. 1995. Sensitivity of direct climate forcing by atmospheric aerosols to aerosol size and composition. *J. Geophys. Res.* **100**, 18739–18754.

Potukuchi, S. and Wexler, A. S. 1995. Identifying solid-aqueous phase transitions in atmospheric aerosols - I. neutral-acidity solutions. *Atmos. Environ.* **29**, 1663–1676.

Pruppbacher, H. R. and Klett, J. D. 1997. *Microphysics of clouds and precipitation.* Kluwer Academic.

Putaud, J.-P., van Dingenen, R., Mangoni, M., Virkkula, A., Raes, F., Maring, H., Prospero, J. M., Swietlicki, E., Berg, O. H., Hillamo, R. and Mäkelä, T. 2000.

Chemical closure and assessment of the origin of the submicron aerosol in the marine boundary layer and the free troposphere during ACE-2. *Tellus* **52B**, 141–168.

Quinn, P. K., Anderson, T. L., Bates, T. S., Dlugi, R., Heintzenberg, J., von Hoyningen-Huene, W., Kulmala, M., Russel, P. B. and Swietlicki, E. 1996. Closure in tropospheric aerosol-climate research: A review and future needs for addressing aerosol direct shortwave radiative forcing. *Contr. Atmos. Phys.* **69**, 547–577.

Quinn, P. K. and Coffmann, D. J. 1998. Local closure during the first Aerosol Characterization Experiment (ACE-1): Aerosol mass concentration and backscattering coefficients. *J. Geophys. Res.* **103**, 16,609–16,624.

Quinn, P. K., Coffmann, D. J., Kapustin, V. N., Bates, T. S. and Covert, D. S. 1998. Aerosol optical properties in the marine boundary layer during the first Aerosol Characterization Experiment(ACE-1) and the underlying chemical and phsyical aerosol properties. *J. Geophys. Res.* **103**, D13, 16,547–16,565.

Rader, D. J. and McMurry, P. H. 1986. Application of the Tandem Differential Mobility Analyzer to studies of droplet grwoth or evaporation. *J. Aerosol Sci.* **17**, 771–787.

Raes, F. 1995. Entrainment of free tropospheric aerosol as a regulating meachanism for cloud condensation nuclei in the remote marine boundary layer. *J. Geophys. Res.* **100**, 2893–2903.

Raes, F., Bates, T., McGovern, F. and Liedekerke, M. V. 2000. The 2nd Aerosol Characterization Experiment (ACE-2): General overview and main results. *Tellus* **52B**, 111–125.

Raes, F., VanDingenen, R., Cuevas, E., VanVelthofen, P. F. J. and Prospero, J. M. 1997. Observations of aerosols in the free troposphere and marine boundary layer of the subtropical North East Atlantic: Discussion of processes determinig their size distribution. *J. Geophys. Res.* **102**, 21,315–21,328.

Rogge, W. F., Mazurek, M. A., Hildemann, L. M., Cass, G. R. and Simoneit, B. R. T. 1993. Quantification of urban organic aerosols at a molecular level: Identification, abundance and seasonal variation. *Atmos. Environ.* **A27**, 1309–1330.

Saxena, P. and Hildemann, L. M. 1996. Water-soluble organics in atmospheric particles: A critical review of the literature and application of thermodynamics to identify candidate compounds. *Journal of Atmospheric Chemistry* **24**, 57–109.

Saxena, P., Hildemann, L. M., McMurry, P. H. and Seinfeld, J. H. 1995. Organics alter the hygroscopic behavior of atmospheric particles. *J. Geophys. Res.* **100**, 18755–18770.

Seinfeld, J. H. and Pandis, S. N. 1998. *Atmospheric Chemistry and Physics.* John Wiley & Sons.

Shulman, M. L., Jacobson, M. C., Charlson, R. J., Syncovec, R. E. and Young, T. E. 1996. Dissolution behavior and surface tension effects of organic compounds in nucleating cloud droplets. *Geophys. Res. Lett.* **23**, 277–280.

Snider, J. R. and Brenguier, J.-L. 2000. Cloud condensation nuclei and cloud droplet measurements during ACE-2. *Tellus* **52B**, 828–842.

Stolzenburg, M. R. and McMurry, P. H. 1988. *TDMAFIT user's manual.* PTL Publications N0. 653, Particle Technology Laboratory Department of Mechanical Eng., University of Minnesota, Minneapolis, USA.

Stratmann, F. and Wiedensohler, A. 1996. A new data inversion algorithm for dmps measurements. *J. Aerosol Sci.* **27**, S1, S339–340.

Swietlicki, E., Zhou, J., Berg, O. H., Martinsson, B. G., Frank, G., Cederfelt, S. I., Dusek, U., Berner, A., Birmili, W., Wiedensohler, A., Yuskiewicz, B. and Bower, K. N. 1999. A closure study of sub-micrometer aerosol particle hygroscopic behavior. *Atmospheric Research* **50**, 205–240.

Swietlicki, E., Zhou, J., Covert, D. S., Hämeri, K., Busch, B., Väkeva, M., Dusek, U., Berg, O. H., Wiedensohler, A., Aalto, P., Mäkelä, J., Martinsson, B. G., Papaspiropoulos, G., Mentes, B., Frank, G. and Stratmann, F. 2000. Hygroscopic properties of aerosol particles in the northeastern Atlantic during ACE2. *Tellus* **52B**, 201–227.

Tang, I. N. 1997. Thermodynamic and optical properties of mixed-salt aerosols of atmospheric importance. *J. Geophys. Res.* **102**, D2, 1883–1893.

Tang, I. N. and Munkelwitz, H. R. 1994. Water activities, densities and refractive indices of aqueous sulfate and sodium nitrate droplets of atmospheric importance. *J. Geophys. Res.* **99**, 18801–18808.

Taylor, K. E. and Penner, J. E. 1994. Response of the climate system to atmospheric aerosols and greenhouse gases. *Nature* **369**, 734–737.

Tegen, I., Lacis, A. A. and Fung, I. 1996. The influence on climate forcing of mineral dust aerosols from disturbed soils. *Nature* **380**, 419–422.

Twomey, S. 1959. The nuclei of natural cloud formation, Part II: the supersaturation in natural clouds and variation of cloud droplet concentration. *Geofis. Pura Appl.*

Twomey, S. 1991. Aerosols, clouds and radiation. *Atmos. Environ.* **25**, 2435–2442.

Twomey, S., Gall, R. and Leuthold, M. 1987. Pollution and cloud reflectance. *Boundary-Layer Meteorology* **41**, 335–348.

VanDingenen, R., Virkkula, A. O., Raes, F., Bates, T. S. and Wiedensohler, A. 2000. A simple non-linear analytical relationship between aerosol accumulation number and sub-micron volume, explaining their observed ratio in the clean and polluted marine boundary layer. *Tellus* **52B**, 439–451.

Verver, G., Raes, F., Vogelzang, D. and Johnson, D. 2000. The 2nd Aerosol Characterization Experiment (ACE-2): Meteoroogical and chemical context. *Tellus* **52B**, 126–140.

Vong, R. J. and Covert, D. S. 1998. Simultaneous observations of aerosol and cloud droplet size spectra in marine stratocumulus. *J. Atmos. Sci.* **55**, 2180–2192.

Weingartner, E., Burtscher, H. and Baltensberger, U. 1997. Hygroscopic properties of carbon and doesel soot particles. *Atmos. Environ.* **31**, 15, 2311–2327.

Winklmayr, W., Reischel, G. P., Lindner, A. O. and Berner, A. 1991. A new electromobility spectrometer for the measurement of aerosol size distributions in the size range from 1 to 1000nm. *J. Aerosol Sci.* **22**, 289–296.

Wiscombe, W. J. 1980. Improved mie scattering algorithms. *Applied Optics* **19**, 1505–1509.

Wood, R., Johnson, D., Osborne, S., Andreae, M. O., Bandy, B., Bates, T. S., O'Dowd, C., Glantz, P., Noone, K. J. and Quinn, P. K. 2000. Boundary layer and aerosol evolution during the 3rd lagrangian experiment of ACE-2. *Tellus* **52B**, 401–422.

Yamasoe, M. A., Artaxo, P., Miguel, A. H. and Allen, G. 2000. Chemical composition of aerosol particles from direct emissions of vegetation fires in the Amazon Basin: water-soluble species and trace elements. *Atmos. Environ.* **34**, 1641–1653.

Zhang, X. Q., McMurry, P. H., Hering, S. V. and Casuccio, G. S. 1993. Mixing characteristics and water content of submicron aerosols measured in Los Angeles and at the Grand Canyon. *Atmos. Environ.* **27A**, 1593–1607.

Zhou, J. 2001. *Hygroscopic properties of Atmospheric Particles in various environments.* Ph.D. thesis Lund University.

VITA

Ulrike Dusek got a Masters degree in physics in 1997 from the University of Vienna. In 1997 she was awarded a Fulbright scholarship. In the summer 200 she was a participant in the IIASA summer program and was awarded a Peccei scholarship for her work on secondary organic aerosol formation. In 2001 she received a Ford fellowship for environmental sciences.